REPUBLIC OF TURKEY

YILDIZ TECHNICAL UNIVERSITY

GRADUATE SCHOOL OF NATURAL AND APPLIED SCIENCES

INVESTIGATION THE EFFECT OF WEATHERING ON CHEMICALLY STRENGTHENED THIN FLAT GLASSES

Yekta Ateş GÖSTERİŞLİOĞLU

MASTER OF SCIENCE THESIS

Department of Metallurgical and Materials Engineering

Material Program

Advisor

Assoc. Prof. Dr. Ali Erçin ERSUNDU

July, 2020

REPUBLIC OF TURKEY

YILDIZ TECHNICAL UNIVERSITY

GRADUATE SCHOOL OF NATURAL AND APPLIED SCIENCES

INVESTIGATION THE EFFECT OF WEATHERING ON CHEMICALLY STRENGTHENED THIN FLAT GLASSES

A thesis submitted by Yekta Ateş GÖSTERİŞLİOĞLU in partial fulfillment of the requirements for the degree of **MASTER OF SCIENCE** is approved by the committee on 17.07.2020 in Department of Metallurgical and Materials Engineering, Material Program.

Assoc. Prof. Dr. Ali Erçin ERSUNDU
Yıldız Technical University
Advisor

Approved by the Examining Committee

Assoc. Prof. Dr. Ali Erçin ERSUNDU, Advisor
Yıldız Technical University _____

Assoc. Prof. Dr. Metin GENÇTEN, Member
Yıldız Technical University _____

Assoc. Prof. Dr. Aziz GENÇ, Member
İzmir Institute of Technology _____

I hereby declare that I have obtained the required legal permissions during data collection and exploitation procedures, that I have made the in-text citations and cited the references properly, that I haven't falsified and/or fabricated research data and results of the study and that I have abided by the principles of the scientific research and ethics during my Thesis Study under the title of Investigation the Effect of Weathering on Chemical Strengthening of Thin Glasses supervised by my supervisor, Assoc. Prof. Dr. Ali Erçin ERSUNDU. In the case of a discovery of false statement, I am to acknowledge any legal consequence.

Yekta Ateş GÖSTERİŞLİOĞLU

Signature

This study was supported by the Scientific and Technological Research Council of Turkey (TUBITAK) 2210-D funding program under application number 1649B021807051 and Yildiz Technical University Scientific Research Fund under the project numbered FYL-2019-3577.

When you look at a piece of delicately spun glass you think of two things:

how beautiful it is and how easily it can be broken.

Tennessee Williams

ACKNOWLEDGEMENTS

First and foremost, I am grateful to my supervisor Assoc. Prof. Dr. Ali Erçin ERSUNDU for his valuable guidance and encouragement for the accomplishment of this work. I will always be proud of being his student. I am also thankful to Assoc. Prof. Dr. Miray Çelikbilek ERSUNDU for her endless help for the entire period of my studentship. Their supporting, caring and hardworking approach during my bachelor and master studies will always be a guideline for me.

I am gratefully thanking to Şişecam Science, Technology and Design Center managers Dr. İlkay SÖKMEN and Hande SESİGÜR who gave life to this field of study and providing me the opportunity of being part of this big family. This study would not be possible without their guidance, support, and trust.

I would like to express my deepest thanks to Surface Technologies Group for their valuable friendship during my studies. I would especially like to thank my dear friends Bengü GÜLDALI and Gülcan TERZİ for their pleasant accompany, with whom we carry out our laboratory studies with great devotion, dedication, and commitment.

My thanks also belong to YTU Glass Research Group for their hospitality in KMC106 laboratory and for their collaboration on many topics.

Finally, many thanks to my family for always encouraging and supporting me in every step I take. Especially to my brother, for walking by me for his entire life to this point where we are.

I also acknowledge The Scientific and Technological Research Council of Turkey (TÜBİTAK) for their financial support to this work under 2210-D funding program.

Yekta Ateş GÖSTERİŞLİOĞLU

TABLE OF CONTENTS

LIST OF SYMBOLS ix

LIST OF ABBREVIATIONS x

LIST OF FIGURES xi

LIST OF TABLES xiv

ABSTRACT xv

ÖZET xvii

1 INTRODUCTION 1

1.1 Literature Review 1

1.2 Objective of Thesis 2

1.3 Hypothesis 2

2 THEORETICAL INFORMATION 4

2.1 Glass and Its Structure 4

2.2 Flat Glass Manufacturing 8

2.3 Glass Strengthening Techniques 12

2.4 Chemical Strengthening 15

2.5 Weathering and Aqueous Corrosion of Glass 18

2.5.1 Leaching Reactions 18

2.5.2 Dissolution Reactions 19

3 EXPERIMENTAL STUDIES 20

3.1 Sample Preparation 20

3.1.1 Chemical Strengthening Procedure 22

3.1.2 Weathering Test Procedure 23

3.1.3 Experimental Conditions 24

3.2 Tests and Characterizations 25
3.2.1 Macroscopic and Microscopic Investigations 26
3.2.2 Topographical Analysis 26
3.2.3 Depth Profiling 27
3.2.4 Optical Analysis 27
3.2.5 Structural Analysis 27
3.2.6 Stress Profile Generation 27
3.2.7 Mechanical Analysis 28
4 RESULTS AND DISCUSSION **31**
4.1 Results 31
4.1.1 Macro Examination Results of L-SLS Glasses 31
4.1.2 Macro Examination Results of H-SLS Glasses 32
4.1.3 Macro Examination Results of AS Glasses 32
4.1.4 Micrographs of L-SLS Glasses 33
4.1.5 Micrographs of H-SLS Glasses 34
4.1.6 Micrographs of AS Glasses 35
4.1.7 Surface Roughness of L-SLS Glasses 35
4.1.8 Surface Roughness of H-SLS Glasses 36
4.1.9 Surface Roughness of AS Glasses 37
4.1.10 Depth Profiles of Pristine and Weathered L-SLS Glasses 38
4.1.11 Depth Profiles of Chemically Strengthened L-SLS Glasses 38
4.1.12 Transmittance Spectra of L-SLS Glasses 40
4.1.13 Transmittance Spectra of H-SLS Glasses 40
4.1.14 Transmittance Spectra of AS Glasses 41
4.1.15 Infrared Spectra of L-SLS Glasses 42

4.1.16 Infrared Spectra of H-SLS Glasses 42
4.1.17 Infrared Spectra of AS Glasses 43
4.1.18 Stress Profiles of L-SLS Glasses 44
4.1.19 Stress Profiles of H-SLS Glasses 44
4.1.20 Stress Profile of AS Glasses 45
4.1.21 Ring-on-Ring Test Results of L-SLS Glasses 46
4.1.22 Ring-on-Ring Test Results of H-SLS Glasses 46
4.1.23 Ring-on-Ring Test Results of AS Glasses 47
4.1.24 Hardness and Crack Formation Results of L-SLS Glasses 48
4.1.25 Hardness and Crack Formation Results of H-SLS Glasses 51
4.1.26 Hardness and Crack Formation Results of AS Glasses 53
4.2 Discussion 55
4.2.1 Evaluation of Visual Appearance of Glasses 55
4.2.2 Interpretation of Topographical Changes 57
4.2.3 Evaluation of Optical Changes 60
4.2.4 Assessment of Depth Profiles 62
4.2.5 Fourier Transform Infrared Spectra 65
4.2.6 Generation of Stress Profiles 68
4.2.7 Determination of Fracture Probability 70
4.2.8 Determination of Surface Hardness 72
4.2.9 Determination of Cracking Probability 74
4.3 General Results and Future Outlook 78
5 REFERENCES **81**
6 PUBLICATIONS FROM THE THESIS **89**

LIST OF SYMBOLS

Å	Angstrom
a.u.	Arbitrary units
R_a	Arithmetic average
cm	Centimeter
°C	Degree Celsius
F	Force
P	Fracture Load
GPa	Gigapascal
g	Gram
MPa	Megapascal
µm	Micrometer
mm	Millimeter
nm	Nanometer
N	Newton
Pa	Pascal
P	Poise
ν	Poisson's ratio
P_f	Probability of failure
σ	Strength
η	Viscosity
λ	Wavelength
m	Weibull modulus

LIST OF ABBREVIATIONS

AFM	Atomic force microscopy
AS	Aluminosilicate glass
CS	Chemical strengthening process
DOL	Depth of layer
FTIR	Fourier transform infrared spectroscopy
H-SLS	Soda-lime silicate glass with mid Al_2O_3 content
HV	Vickers hardness
L-SLS	Soda-lime silicate glass with low Al_2O_3 content
NBO	Non-bridging oxygen bonds
NIR	Near infrared
PR	Pristine
PVB	Polyvinyl butyral
RH	Relative humidity
SCL	Super cooled liquids
T_g	Glass transition temperature
T_M	Melting temperature
TOF-SIMS	Time of flight – secondary ion mass spectroscopy
UV	Ultraviolet
VIS	Visible
W	Weathering process
WLI	White light interferometry
XRF	X-Ray fluorescence spectrometer

LIST OF FIGURES

Figure 2.1 Specific volume change difference of a material between crystal and glass structure upon cooling [17] 5

Figure 2.2 A representative image of the disordered structure of a silicate glass (continious worm-like lines represent the glass network and colored spheres represent the modifier ions) [21] 6

Figure 2.3 Effect of Al_2O_3 substitution on the structure of silicate glass [25] 8

Figure 2.4 Producing of flat glass by a) crown process [29] and b) cylinder blown process [30] 9

Figure 2.5 Representative images of a) glass melt is being poured on the molten tin from tweel [31] b) glass ribbon being drawn in the tin bath by rollers [32] 10

Figure 2.6 Forming vessel of the fusion draw process [33] 11

Figure 2.7 Distribution of glass market with specific focus on flat glass market [35] 12

Figure 2.8 a) Representative flaw at the glass surface with stress vectors and b) strength of as a function of effective flaw depth [35] 13

Figure 2.9 Illustration of exchange of alkali ions between salt and the glass through diffusion process and healing of already existent flaws on the surface (alkali earth ions are excluded in the representation) 16

Figure 2.10 Comparison of stress profiles between thermal and chemical strengthened glass (magnitude and the depth of stress may vary depending on the glass composition and the process parameters) [47] 17

Figure 3.1 Image of cut samples ready for further processing 21

Figure 3.2 a) LEMA TC 804A chemical tempering furnace and b) tray placement 23

Figure 3.3 a) Weathering test cabinet, b) interior of the cabinet and sample placement 24

Figure 3.4 a) ring-on-ring testing equipment and b) technical drawing of the equipment 28

Figure 4.1 Macro images of L-SLS samples 31

Figure 4.2 Macro images of H-SLS samples 32

Figure 4.3 Macro images of AS samples 33

Figure 4.4 Micrographs of L-SLS samples (scale bar shows 40 μm for all captures) 34

Figure 4.5 Micrographs of H-SLS samples (scale bar shows 40 μm for all captures)..... 35

Figure 4.6 Micrographs of AS samples (scale bar shows 40 μm for all captures).. 35

Figure 4.7 Surface roughness chart of L-SLS glasses..... 36

Figure 4.8 Surface roughness chart of H-SLS glasses..... 37

Figure 4.9 Surface roughness chart of AS glasses..... 37

Figure 4.10 Depth profiles of a) PR condition and b)W condition of L-SLS glasses..... 38

Figure 4.11 Depth profiles of a) CS condition, b) W+CS condition and c) CS+W condition of L-SLS glasses..... 39

Figure 4.12 Transmittance spectra of L-SLS glasses..... 40

Figure 4.13 Transmittance spectra of H-SLS glasses..... 41

Figure 4.14 Transmittance spectra of AS glasses..... 41

Figure 4.15 Infrared spectra of L-SLS glasses..... 42

Figure 4.16 Infrared spectra of H-SLS glasses..... 43

Figure 4.17 Infrared spectra of AS glasses..... 43

Figure 4.18 Stress profiles of L-SLS glasses..... 44

Figure 4.19 Stress profiles of H-SLS glasses..... 45

Figure 4.20 Stress profiles of AS glasses..... 45

Figure 4.21 Raw data obtained from ring-on-ring tests for L-SLS glasses..... 46

Figure 4.22 Raw data obtained from ring-on-ring tests for H-SLS glasses..... 47

Figure 4.23 Raw data obtained from ring-on-ring tests for AS glasses..... 48

Figure 4.24 Vickers hardness results of L-SLS glasses..... 49

Figure 4.25 Vickers hardness results of H-SLS glasses..... 51

Figure 4.26 Vickers hardness results of AS glasses..... 53

Figure 4.27 Optical microscope images of glass surfaces under 500X magnification for different experimental conditions..... 56

Figure 4.28 Illustration of alteration layer on the weathered glass surface..... 57

Figure 4.29 Comparison of surface roughness values of investigated glass types under different experimental conditions..... 58

Figure 4.30 Comparison of surface topographical images obtained by WLI for investigated glass types under combinational processing conditions 59

Figure 4.31 Surface topographical maps obtained by AFM for a) L-SLS-CS+W sample and b) L-SLS-W+CS+W sample 60

Figure 4.32 Transmittance spectra of L-SLS glass in the visible range of the spectrum 61

Figure 4.33 Transmittance spectra of H-SLS glass in the visible range of the spectrum 61

Figure 4.34 Transmittance spectra of AS glass in the visible range of the spectrum 62

Figure 4.35 Alkali ion profiles of a) L-SLS-PR sample and b) L-SLS-CS sample 63

Figure 4.36 Comparison of K^{+} profiles of chemically strengthened L-SLS glasses. 64

Figure 4.37 Alkali-earth ion profiles of chemically strengthened L-SLS glasses a) Mg^{+2} profiles and b) Ca^{+2} profiles 64

Figure 4.38 Representation of a glass network containing different Q^{n} structure units 65

Figure 4.39 IR spectrum of soda-lime-silicate glass demonstrating the main vibration modes and related wavenumbers 66

Figure 4.40 Comparison of main vibrational peak positions and intensities of a) L-SLS glasses, b) H-SLS glasses and c) AS glasses 67

Figure 4.41 Comparison of stress profiles of a) L-SLS glasses, b) H-SLS glasses and c) AS glasses 69

Figure 4.42 Weibull plot of L-SLS glasses under different experimental conditions 70

Figure 4.43 Weibull plot of H-SLS glasses under different experimental conditions 71

Figure 4.44 Weibull plot of AS glasses with different experimental conditions 72

Figure 4.45 Comparison of surface hardness values for three different glass types under different experimental conditions 73

Figure 4.46 Crack formation probability of chemically strengthened glasses under 500g of load 74

Figure 4.47 Crack formation probability of chemically strengthened glasses under 1000g of load 75

Figure 4.48 Crack formation probability of chemically strengthened glasses under 2000g of load 76

LIST OF TABLES

Table 3.1 Chemical compositions, producer information and acronyms of glasses 21

Table 3.2 Impurities and pH of the KNO_3 salt used in experimental studies 22

Table 3.3 Description of experimental conditions along with sample names and process history 25

Table 4.1 Representative indentation images of L-SLS glasses for crack formation determination 50

Table 4.2 Representative indentation images of H-SLS glasses for crack formation determination 52

Table 4.3 Representative indentation images of AS glasses for crack formation determination 54

Table 4.4 FTIR band assignments for silicate glasses 66

ABSTRACT

Investigation the Effect of Weathering on Chemically Strengthened Thin Flat Glasses

Yekta Ateş GÖSTERİŞLİOĞLU

Department of Metallurgical and Materials Engineering

Master of Science Thesis

Assoc. Prof. Dr. Ali Erçin Ersundu

Thin glasses are increasingly being used in numerous industrial flat glass applications including touchscreens of mobile phones and tablets, cover screens of computers and televisions, laminated windshields of sports cars and airplanes, where lightness and high mechanical strength properties are sought together. Therefore, chemical strengthening method has recently become a crucial part for most of the thin flat glass manufacturing facilities to improve the mechanical properties of the glass product. In chemical strengthening technology — a novel method that is used to improve the mechanical strength of the glass by submerging the glass item into molten potassium nitrate salt bath at a temperature lower than the glass transition point — substitution of sodium ions in the glass surface with the potassium ions in the salt bath is ensured via diffusion mechanism. This leads to stress generation on the surface resulting an overall increase in glass strength.

Chemically strengthened glass products with increased mechanical strength are being used as complementary parts in multi-component products where high quality is offered for longer periods. These glasses are expected to be used in harmony with aforementioned multi-component products, therefore visual disturbances in the macro level caused by atmospheric effects such as weathering

are undesirable. Herein, it is crucial to investigate the atmospheric corrosion behavior of chemically strengthened products for determining their lifespan, product reliability and compliance with the standards. The weathering behavior of silica-based glasses has already been investigated in the literature from many perspectives. However, there is still a lack of information on the weathering behavior of chemically strengthened thin glasses.

The main objectives of this thesis are to enlighten the current knowledge on weathering behavior of chemically strengthened glasses, to propose some new approaches for the improvement of chemical strengthening process efficiency for industrial practices and to reveal how to increase the weathering resistance of chemically strengthened glasses for improving their lifespan and reliability. Therefore, in this work, flat glass samples with 1.1 mm thickness having three different compositions, i.e. soda-lime silicate glasses with low and mid Al_2O_3 content and aluminosilicate glasses, are subjected to weathering tests before and after chemical strengthening process to simulate possible processing sequence scenarios that toughened glass products face and the effect of weathering on topographical, optical, structural and mechanical properties are investigated. It is deduced from the experimental results that there is a strong correlation between the weathering behavior and the processing sequence as well as the Al_2O_3 content in glass compositions. Consequently, chemically strengthened soda-lime silicate glasses are found to be more prone to weathering after processed with chemical strengthening. Weathering has manifested itself in such cases as surface deterioration and decrease of strength which has a detrimental impact on the product quality. Compositional modification of glass by increasing Al_2O_3 content compensates this behavior as well as increasing the chemical strengthening efficiency.

Keywords: Thin flat glasses, chemical strengthening, weathering, soda-lime silicate glass, aluminosilicate glass

ÖZET

Yaşlandırmanın Kimyasal Temperli İnce Düzcamlara Etkisinin İncelenmesi

Yekta Ateş GÖSTERİŞLİOĞLU

Metalurji ve Malzeme Mühendisliği

Yüksek Lisans Tezi

Doç. Dr. Ali Erçin Ersundu

İnce camlar, özellikle bilgisayar, tablet, mobil telefon, televizyon ekranları, spor araba ve uçak camları gibi hafiflik ve yüksek mekanik mukavemet özelliklerinin birlikte arandığı endüstriyel düzcam uygulamalarında giderek artan oranlarda kullanılmaya başlanmıştır. Buna bağlı olarak ince camların mekanik dayanımlarının arttırılmasına yönelik olarak tercih edilen başlıca uygulamalardan biri olan kimyasal temperleme teknolojisi, ince düzcam üretim tesislerinin birçoğu için kritik bir uygulama haline gelmiştir. Kimyasal temperleme teknolojisinde, camın eriyik potasyum nitrat (KNO_3) tuz banyosu içinde, cam geçiş sıcaklığının altında belirli bir süre bekletilmesi sonucunda cam yüzeyindeki sodyum iyonlarının daha büyük iyonik yarıçaplı potasyum iyonlarıyla difüzyon mekanizması yolu ile yer değiştirmeleri sağlanır. Bu sayede cam yüzeyinde basma gerilimi oluşarak camın mekanik mukavemeti artar.

Mekanik mukavemetleri kimyasal temperleme yöntemi ile arttırılan ince düzcamların çok bileşenli uygulamalarda kullanılabilmesi için atmosferik korozyon dayanımlarının ve kullanım ömürlerinin yüksek olması beklenirken, atmosferik koşulların cam yüzeyinde olumsuz bir etkiye sebep olması da istenmemektedir. Dolayısıyla sıcaklık ve nem ile zamanla korozyona uğradığı bilinen cam ürünün

kullanım ömrünün, standartlara uygunluğunun ve ürünün güvenilirliğinin saptanması açısından atmosferik korozyon davranışının bilinmesi ve geliştirilmesi önem arz etmektedir. Literatürde camların yaşlandırma davranışı çeşitli perspektiflerden incelenmiş olsa da kimyasal temperli ince düzcamların yaşlanmaya karşı davranışları konusunda yapılmış herhangi bir çalışma bulunmamaktadır.

Bu çalışmanın amacı, kimyasal temperlenmiş camların yaşlandırma davranışlarına ait güncel bilgi birikimini genişletmek, endüstriyel uygulamalar için kimyasal temperleme prosesinin verimliliğini arttırmak ve kimyasal temperlenmiş camların yaşlandırma dayanımlarının geliştirilmesi ile ürün ömrü ve güvenilirliğinin iyileştirilmesine yönelik öneriler sunmaktır. Bu amaç doğrultusunda, atmosferik korozyon sürecinin kimyasal temperleme prosesine olan etkisinin incelenmesi ve iyileştirilmesi için, 1.1 mm eş kalınlığa ve farklı kompozisyonlara sahip ince düzcamların karşılabilecekleri olası proses sıralaması senaryolarının simüle edilmesi gözetilerek, camların kimyasal temperleme öncesi ve sonrası yaşlandırılması ve ardından topografik, optik, yapısal ve mekanik özelliklerinin incelenmesi gerçekleştirilmiştir. Deneysel sonuçlara göre camların yaşlandırma davranışlarının proses sıralaması ve kompozisyondaki Al_2O_3 miktarı ile güçlü bir ilişkisi olduğu saptanmıştır. Kimyasal temperleme sonrası soda-kireç silikat camların yaşlandırma dayanımlarının daha düşük olduğu görülmüştür. Yaşlandırma süreci sonrasında yüzeyde görsel bozunma ve mekanik mukavemette düşüş meydana gelmiş, kompozisyonda daha yüksek oranda Al_2O_3 kullanılması durumunda bu durumun önlenebildiği ve aynı zamanda kimyasal temperleme prosesinin verimliliğin arttığı görülmüştür.

Anahtar Kelimeler: İnce düzcamlar**,** kimyasal temperleme, yaşlandırma, soda-kireç silikat cam, alümina silikat cam

1 INTRODUCTION

1.1 Literature Review

Product design criteria are constantly being renewed to shape the current trends and product expectations. Currently, there is a growing demand for thinner, lighter and durable designs and glass also has its share from these expectations. As a result of this, new glass products, e.g. thinner but durable touch screens for consumer electronics or lighter windshields for automotive industry to reduce the total weight of the vehicle, have recently come into our lives.

Glass, which has a reputation of being fragile, is also an indispensable material for many applications that we use in almost every area of our daily life. Growing demand for use of thin flat glasses, where weight reduction and high mechanical strength is desired, pushes the glass industry to fulfill the market expectations. Herein, several methods can be listed that are being used in the glass technology to improve the mechanical properties of glass. Each of these methods has its pros and cons but in terms of applications where main criteria are high compressive stress, high strength, high scratch resistance and applicability to complex geometries, chemical strengthening steps forward. Chemical strengthening is one of the latest introduced method by Kistler [1] for the toughening of glass plates. The main advantage of chemical strengthening is that it can be applied to thin glasses and complex geometries, making it indispensable choice for strengthening of thin glasses.

Even though glass is known by its durability and long lifespan, it is also quite vulnerable to corrosion under specific stimulants such as temperature and humidity — also known as weathering. Therefore, it is important to investigate the corrosion behavior of chemically strengthened products under atmospheric conditions for determining their lifetime, product reliability and compliance with standards for the applications of today and tomorrow.

Numerous works have been realized so far to understand the weathering induced corrosion mechanism of silicate glasses mainly focusing on leaching and layer formation [2]–[4], corrosion induced structural changes [5]–[9] and influence on mechanical performance [10], [11]. However, the effect of weathering on chemically strengthened glasses has not been extensively studied to date and therefore, there is scarce information on weathering behavior of chemically strengthened glasses. As a consequence, it is of great importance to investigate the effect of weathering on chemically strengthened flat glasses.

1.2 Objective of Thesis

With increasing thin flat glass production rates, chemical strengthening process has recently become almost an inseparable part of glass production lines to meet the required mechanical properties. Although weathering behavior of silica-based glasses are already known in the literature, the effect of weathering on chemically strengthened silica-based glasses still remain unclear in the present situation. Hence, it is of significant importance to discover the weathering behavior of glasses processed by chemical strengthening to ensure and improve the optimization of stocking and usage conditions. Therefore, this dissertation study aims to shed a light on weathering behavior of chemically strengthened flat glasses and to describe how compositional differences in silica-based glasses alter this behavior. Within this aim, different glass samples with varying compositions, mainly in Al_2O_3 content, are subjected to weathering tests before and after chemical strengthening and the effect of weathering on topographical, optical, structural and mechanical properties of glasses are analyzed.

1.3 Hypothesis

Earlier works focusing on weathering behavior of glasses have not covered the chemically strengthened glasses. Therefore, as an original contribution to the field of study, this work reveals the effect of weathering on chemically strengthened glasses by investigating topographical, optical, structural and mechanical properties for the first time. Mechanisms and possible results of weathering on chemically strengthened glasses, its influence on the product quality and lifespan is presented.

Consequently, obtained results are evaluated in terms of processing sequence as well as glass composition and expressed in a comparative manner.

2
THEORETICAL INFORMATION

2.1 Glass and Its Structure

Glass is one of the oldest materials that served mankind. For centuries it has been used as a traditional material in many geometrical forms and compositions. As well as being a traditional material, glass has drawn the attention of scientists as also being a promising material for many high-tech applications. Glass has been redefined many times by scientists over the years, and yet today its definition has not gained a certainty. First definitions proposed for glass were mainly focused on the structure that is solidified by rapid cooling of a viscous melt [12], [13]. Later, scientists implemented the term amorphous to the definition of glass to clarify and emphasize the structure of the disordered state of matter. However, a proper definition for glass should also cover the kinetic and thermodynamic aspects during and after the cooling of melt [14]. Finally, as the structural and thermodynamic studies have advanced on glass transition, and liquid-like behavior of glass is well understood, novel definitions of glasses continue to be proposed. The latest definition of glass has been reported by Zanotto and Mauro [15] where they describe the glass as "Glass is a nonequilibrium, noncrystalline condensed state of matter that exhibits a glass transition. The structure of glasses is similar to that of their parent supercooled liquids (SCL), and they spontaneously relax toward the SCL state. Their ultimate fate, in the limit of infinite time, is to crystallize."

Difficulty of describing the glass arises from the glass formation process itself and the complexity of its amorphous structure. Even though the structure of most well-known oxide glasses is composed of continuous network of tetrahedra it is not always the case. There are other glass forming systems whose network is not composed of tetrahedra or structural units that can be different than oxide groups. [16]. The difference of structure between a crystal and a glass can be explained by their unique behavior of volume change upon cooling from their melts. Figure 2.1 compares the change of specific volume of a material between liquid, crystalline and

glass forms upon cooling from molten phase. When a material is heated up above its melting temperature, it becomes a liquid having a viscosity of η (Pa.s or Poise).

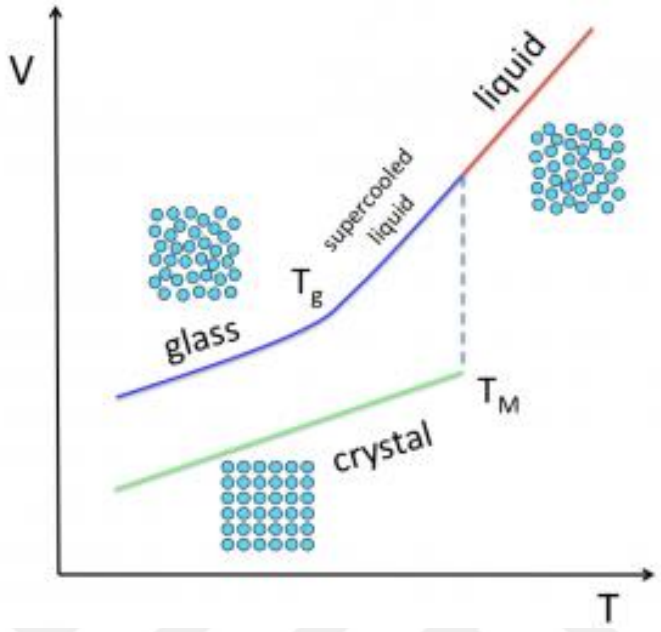


Figure 2.1 Specific volume change difference of a material between crystal and glass structure upon cooling [17]

Many compounds and elements have low viscosity in the molten phase. For instance, viscosities of some common liquids at the room temperature is given as follows: 10^{-5} Pa.s for air, 10^{-3} Pa.s for water, 10^{-1} Pa.s for olive oil and 10^{1} Pa.s for honey [18]. For compounds with a low viscosity, during slow cooling, volume of the melt decreases gradually, and at the melting temperature, T_M, first nucleation starts, and crystallization occurs with a dramatic decrease in the specific volume of the liquid. This cooling regime and crystallization satisfies the thermodynamic and kinetic rules and the final solid structure is called crystal and considered to be in thermodynamic equilibrium [19]. On the other hand, glassy state is known to be formed by rapid cooling of a viscous liquid from a temperature higher than its melting point [20]. Viscosity of molten silicate glass at approximately 1450°C is 10^{1} Pa.s (10^{2} Poise), similar with that of honey's viscosity at the room temperature.

The structure of the solidified matter is dependent on the arrangement of the material's structural units during cooling. For the melts with high viscosity, the

arrangement of the structural units into continuous long-range order is impeded by the high viscosity and thus resulting in low mobility of the structural units. This behavior is unique for materials that exhibit glass transition. For a material that exhibits glass transition behavior, with rapid cooling of the liquid the viscosity decreases proportional to the temperature and at some point where glass transition temperature, T_g, is reached volume change rate of the material decreases sharply and the obtained structure is considered to be frozen. This continuous frozen disordered structure is called the glass network. Therefore, a material is named as glass only if its temperature is lower than its T_g [14].

Formation of silicate glass structure is also realized by rapid cooling of its melt fast enough to suppress crystallization, thus freezing the viscous liquid with long-range disordered form into a solid amorphous structure. Structure of a commercial silicate glass is comprised of cross-linked long-range network of SiO_4 tetrahedral units and ionically bonded alkali and alkali-earth network modifier ions to the network for the modification of the melt and the glass properties. A representative image of a silicate glass structure is provided in Figure 2.2.

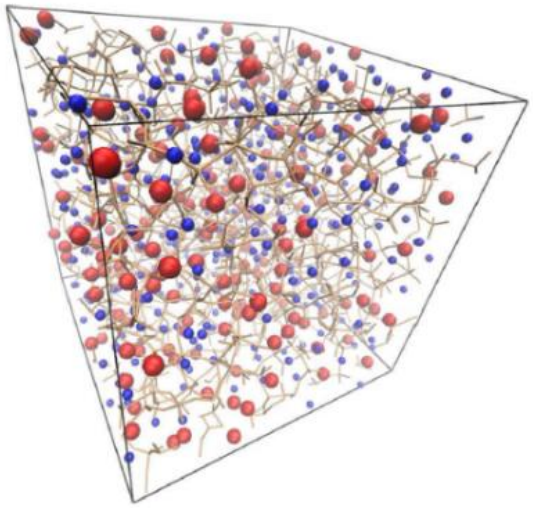


Figure 2.2 A representative image of the disordered structure of a silicate glass (continious worm-like lines represent the glass network and colored spheres represent the modifier ions) [21]

The glass forming melt might contain several oxides, namely SiO_2, Al_2O_3, Na_2O, K_2O, CaO, MgO, B_2O_3, BaO etc., each of them having a unique contribution to the properties of the final product. By varying the fractions of oxides in the melt, tailor-

made composition designing is possible. Thanks to the improvements in glass making; researchers, scientists and glass manufacturers are able to modify glass composition in industrial scale to alter the structure for obtaining desired physical, chemical and mechanical properties.

It is possible to obtain almost infinite number of different glass compositions. Among them, soda-lime-silicate glasses (SLS) are the most commercially produced and used glass types for numerous applications in the current situation. Windows, mirrors, windshields, containers, tableware, fibers glass and many more glass products that we are frequently using in our daily life are silica-based glasses, more precisely SLS glasses. SLS glass is comprised of silica as the network former and alkali/alkali earth ions, i.e. sodium, calcium, magnesium, as the network modifiers. Soda (Na_2CO_3) is used to decrease the melting temperature by forming non-bridging oxygen bonds and breaking the network connectivity. Thus, soda makes the glass making process more feasible. Calcium oxide (CaO) and magnesium oxide (MgO) are used mainly for increasing chemical durability but also to control working range and devitrification behavior of the melt. Also, there is a third type of ions whose behavior is in between the network formers and modifiers; thus, they are called intermediates. Al_2O_3, which is not a network former by itself, when added to the silicate glass composition forms the AlO_4 tetrahedra by replacing the SiO_4, acting as a network former. Al_2O_3 contributes to chemical, mechanical and thermal durability but also increases the melting temperature and the viscosity of the melt. Therefore, Al_2O_3 is added to almost all glass compositions in small amounts to improve glass performance but restricted to a certain amount due to it higher melting temperature[22]. For some applications though, where superior properties are required, Al_2O_3 is added in higher fractions to the glass composition. Such glasses are called alumina-silicate (AS) glasses. In general, AS glasses are composed of SiO_4 and AlO_4 tetrahedra. An AlO_4 tetrahedra with four bridging oxygen bonds can be thought of as a large anion with a valance of -1, and this valence covers the entire anion. This valence difference is compensated by an alkali ion with a valance of +1. The alkali ion otherwise leads to the formation of a non-bridging oxygen bond. Substitution of SiO_4 by AlO_4 or that is to say each Al^{3+} ion added to the composition, ensures network connectivity by eliminating the non-bridging oxygens (see Figure

2.3), so is the glass strength increases. This is not the case for (Al_2O_3/R_2O)> 1 conditions, since glasses with such a composition do not have enough alkali ions to compensate the -1 valence so in this case Al^{3+} ions are found in the structure as a modifier [23], [24].

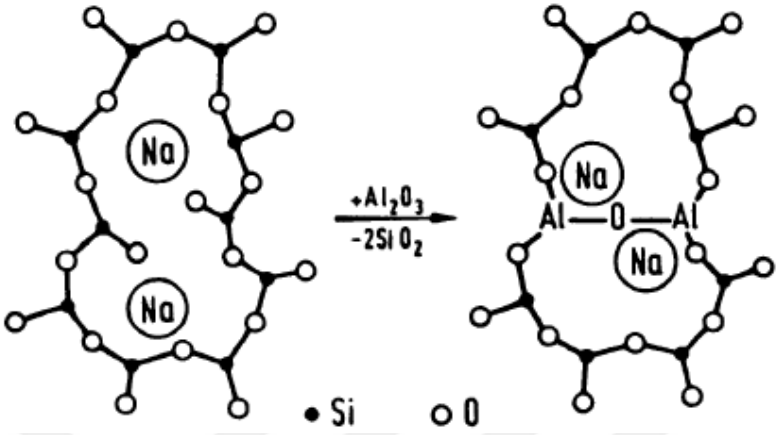


Figure 2.3 Effect of Al_2O_3 substitution on the structure of silicate glass [25]

Increasing Al_2O_3 content in glass composition has another beneficial role apart from ensuring the network connectivity. The bonding energy between the non-bridging oxygen and the alkali ion (NBO – Na^+) in silicate glass is greater than the energy between the $[AlO_4]^{-1}$ network forming unit and alkali ion ($[AlO_4]^{-1}$ – Na^+) resulting in higher ion diffusion capabilities of alumina-silicate glasses. Therefore, for diffusion-based processes, like chemical strengthening this feature becomes a benefit for alumina-silicate glasses [26].

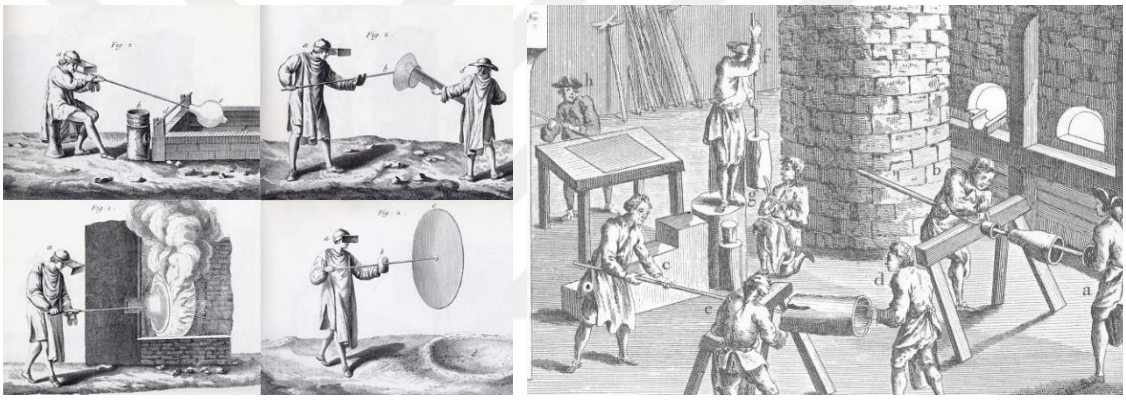
2.2 Flat Glass Manufacturing

Glass is a naturally occurring, i.e. obsidian, mineral produced by volcanic eruptions. First samples of man-made glass have been found near Egypt and Eastern Mesopotamia dating back to 1500 B.C [27]. For thousands of years glass has been used for several purposes such as, cutting tools, decorative applications, pottery and jewelry [28]. Invention of blow pipe by craftsmen in Syria around 650 B.C. contributed to glass making by enabling the production of thin walled, fine and variety of shaped glasses. The application of glass blowing pipe also opened a new

path for glass makers to produce flat glass. Through time applications of glass evolved and expanded to architectural, optical, and even electronics fields.

First methods to produce sheet glass plates such as crown process and cylinder blown process involved the use of a blow pipe to shape the glass melt into flat form. These processes required hard labor for spinning and blowing the melt on the pipe simultaneously. Therefore, glass was a quite expensive material and its surface was not good enough to be used as a transparent window. This is why it was usually used as stained windows for decorative purposes. Most of the historical stained glasses, present in the churches dating back up to 19th century, were shaped by these methods (see Figure 2.4).

.

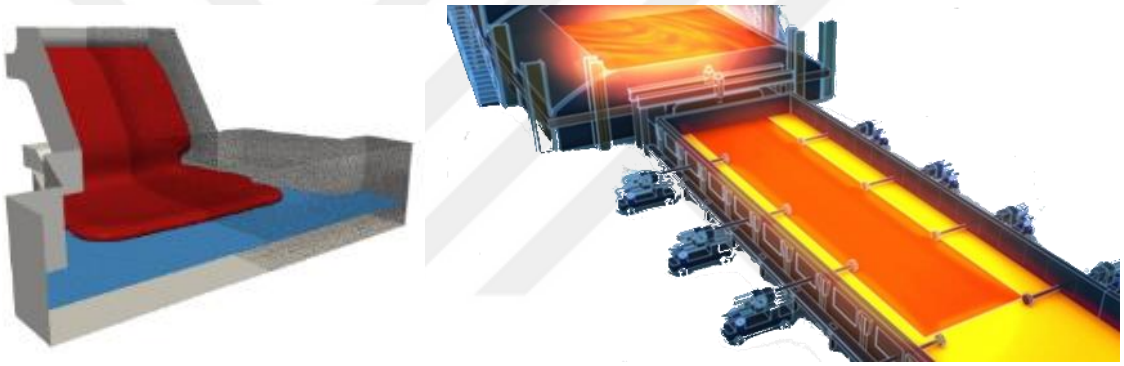


(a) (b)

Figure 2.4 Producing of flat glass by a) crown process [29] and b) cylinder blown process [30]

After industrial revolution and development of mechanization, glass making developed rapidly and this is followed by novel processes and shaping techniques such as polished plate glass. However, all these processes were discontinuous, not able to provide good quality due to operations applied on the glass surface or they were not capable of enabling feasible mass production. Construction of continuous tank furnaces with regenerators reduced the fuel consumption and skyrocketed the glass making in terms of daily production capacity in combination with development of Bessemer and Forcoult processes in the early stages of the flat glass industry. However, even shaping with these new processes leaved a distorted surface which limited the usage of the products for mirrors or automotive glasses. Later, along with

the announcement of a new process by Pilkington opened a new era for flat glass industry. A groundbreaking advancement of the flat glass industry is unarguably the invention of Float Process, in which the glass melt from the melting tank is poured into a bath containing molten tin (see Figure 2.5a) by a refractory brick called tweel to be shaped into flat sheet. The density difference between the glass melt and molten tin makes the glass melt float on the molten metal and the floating glass ribbon being continuously drawn vertically from its edges through the exit of the tin bath by the rollers while cooling (see Figure 2.5b). Hence the glass ribbon is shaped into a flat sheet by the high-density molten metal from the bottom surface (tin side) and upper surface (atmosphere side) is remained untouched, therefore better surface quality is achieved. After shaping, the sheet glass ribbon is rolled to cold section to be cut and stocked.



(a) (b)

Figure 2.5 Representative images of a) glass melt is being poured on the molten tin from tweel [31] b) glass ribbon being drawn in the tin bath by rollers [32]

Float process is mainly designed to produce soda-lime-silicate flat glass plates in high pull rates with high product quality. Design and operating parameters of float process furnace restricts the production of some glass compositions, and tin bath forming process restricts the production of thin glass plates. However, float process can be modified by changing the design parameters of the melting tank and subsequent step for forming the sheet plates which is tin bath, into small scale for producing thinner plates.

Lately an innovative approach emerged as a result of the need to produce ultra-thin glass plates with superior surface quality for special glass compositions that cannot be melted in the float furnace. This process is called fusion draw process and

invented by Corning Inc. As presented in Figure 2.6, in this process, the molten glass from the melting tank is poured into a forming vessel to be fused downwards due to overflow.



Figure 2.6 Forming vessel of the fusion draw process [33]

As the overflown glass flows downwards, its inner surface touches the vessel where some flaws might occur while outer surface remains untouched. Twin flows from both sides of the vessel come together at the bottom of the vessel to fuse and the inner surfaces are kept in the center during the fusion and solidification. Along the flat glass fabrication by fusion draw process, special care is taken to minimize the flaw formation. Since the glass is shaped downwards by gravitational pull, need for the rollers are completely eliminated [34].

Thanks to these improvements in flat glass making, amount of flat glass production has increased worldwide, and flat glass became a substitute material to concrete in meeting the needs of the developing construction sector. Today, the biggest portion of flat glass production is realized by float process. Figure 2.7 reveals that flat glass products constitute nearly a third of the worldwide glass market.

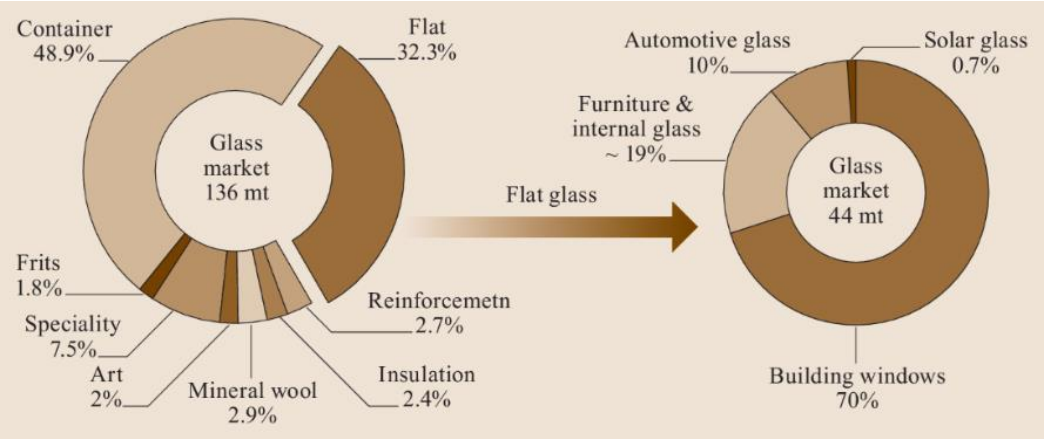


Figure 2.7 Distribution of glass market with specific focus on flat glass market [35]

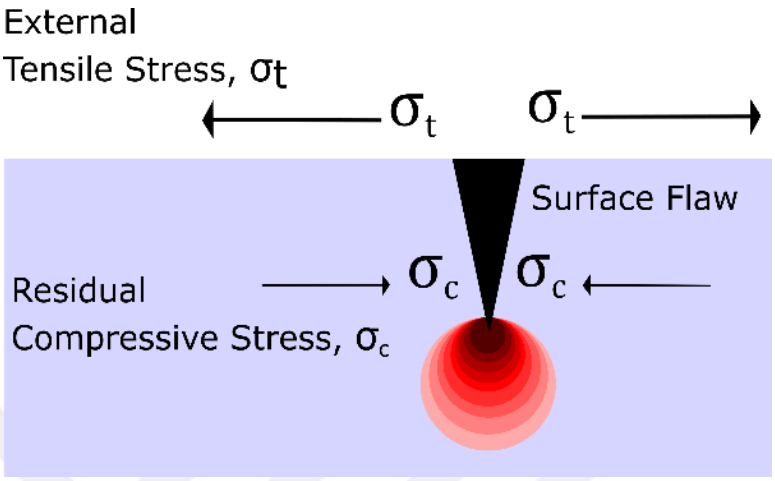
Flat glass products are mainly being used in architectural applications as well as furniture and internal designs. On the other hand, share of automotive and solar glass markets in the total consuption is lower but quality expectations are greater. Thin flat glass products have gained great attention over the last decade since they offer indispensable properties for several technological applications such as, display screens for consumer electronics, panels for solar energy cells, windshields for reduced weight vehicles. This interest led to process improvements and modifications for thin glass production. Therefore, some important advancements have been implemented to flat glass production technologies to meet the growing demand for much thinner products — for instance development of fusion draw process [36] to produce ultra-thin glasses and design of novel float lines [37] to achieve higher production capacity as explained before. Although there is a growing interest in thin flat glasses, their mechanical strength is still the major limitation for their use in various applications. Hence, increasing the mechanical strength of thin glasses has great importance in terms of expanding their usage area and converting them to high value-added products.

2.3 Glass Strengthening Techniques

In general, mechanical strength of a silica-based glass is determined by the energies of strongly bonded Si–O–Si bonds. Theoretical strength of glass calculated from the Si–O bond energies is approximately 20 GPa and this is almost 30 times higher than

its practical strength. However, presence of flaws such as microcracks on the surface decreases the overall strength of glass by causing formation of stress concentration points at the crack tips (see the red region in Figure 2.8a) which facilitates the growth and rapid propagation of a crack under applied external tensile stress.

a)



b)

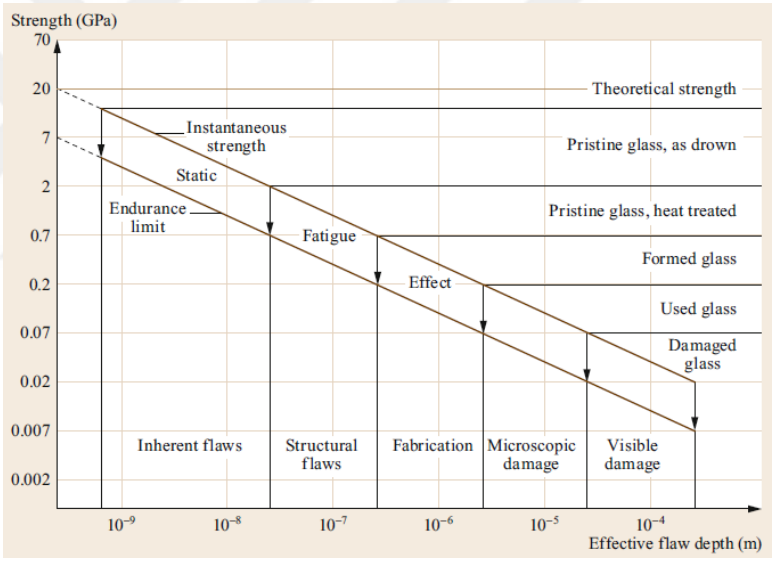


Figure 2.8 a) Representative flaw at the glass surface with stress vectors and b) strength of as a function of effective flaw depth [35]

Strength of the glass article is inversely proportional to the effective flaw depth (see Figure 2.8b) and visible flaws can decrease the glass strength by four orders of magnitude compared to its theoretical strength. Flaws can be originated during the fabrication by the rollers, during stacking or can be introduced after production during usage of the glass product [38].

Inherent flaws on the glass not just decreases the glass strength but also limits the strength increase by secondary applications [39]. There are several secondary processes that can be applied to a glass product for increasing its mechanical performance to meet the requirements for the desired application. One way to diminish these flaws is to polish the glass surface by a torch with high temperature flame or etching with strong acidic solutions [40]. However, these applications are neither so efficient nor feasible and quite costly. Another approach to make glass more resistant to mechanical stimulus is the lamination of two or more glass plates with a polyvinyl butyral (PVB) layer between the plates. This increases the total thickness and keeps the glass plates together in case of breakage, thus preventing the small and sharp pieces to be scattered around. This is why laminated glass is also known as security glass. However, lamination has no contribution to the prevention of crack formation or crack healing. Coating the surface with protective layer might prevent the formation of new flaws and cracks to some point but unfortunately not able to suppress the present flaws from growth. In addition, coating applications has other limitations that should be considered in terms of performance and lifespan [41].

Therefore, more effective solutions that both prevents the growth of present flaws and prevent the formation of new flaws are required to increase the strength of glass. It is known that, strength limiting surface flaws easily grow and thus lead to failure under applied tensile stress. Thereby, some glass strengthening processes focus on the generation of compression stress on glass surface that suppresses growth and propagation of microcracks as well as preventing the formation of new flaws [42]. The most common method for introducing compressive stress to glass surface is thermal tempering. Thermal tempering is realized by rapid cooling of the glass article which is heated above its glass transition temperature [43]. By doing so, the surface of the glass plate cools more rapidly than the bulk and setting up a temperature gradient accompanied by the instantaneous viscosity increase. If viscosity of the glass is relatively low, then thermal stress which is generated by the temperature gradient can be diminished quickly, in other words stress relaxation occurs. However, since the cooling of the glass plate is accomplished rapidly, increased viscosity forces the glass to behave as an elastic solid which restricts the

relaxation phenomena and the generated stresses are locked in the glass. In a thermal tempered glass, surface cools faster than the center of the glass plate which results compression stress generation on the surface and balancing tensile stress in the central layers of the plate [44].

Thermal tempering is based on uniform cooling rate difference between the surface and bulk which limits its implementation for complex geometries. In addition, thin glass plates having a thickness lower than 2 mm cannot be strengthened by thermal tempering without thermal shock driven failure. Therefore, the challenge to preserve and increase the mechanical strength of thin glass plates or products with complex geometries has been achieved to a great extent by the application of chemical strengthening process.

2.4 Chemical Strengthening

Chemical strengthening is a widely used process to improve the mechanical performance of thin glasses that cannot be accomplished by conventional thermal tempering process. In chemical strengthening process — which is based on the modification of the glass surface composition on the atomic scale — the glass article is immersed into a molten bath of alkali salt (KNO_3) below its transition temperature and subsequently diffusion driven ion-exchange reactions occur between the modifier Na^+ ions present in the glass matrix and K^+ ions in the molten salt [45]–[48]. A schematic illustration of chemical strengthening process is provided in Figure 2.9.

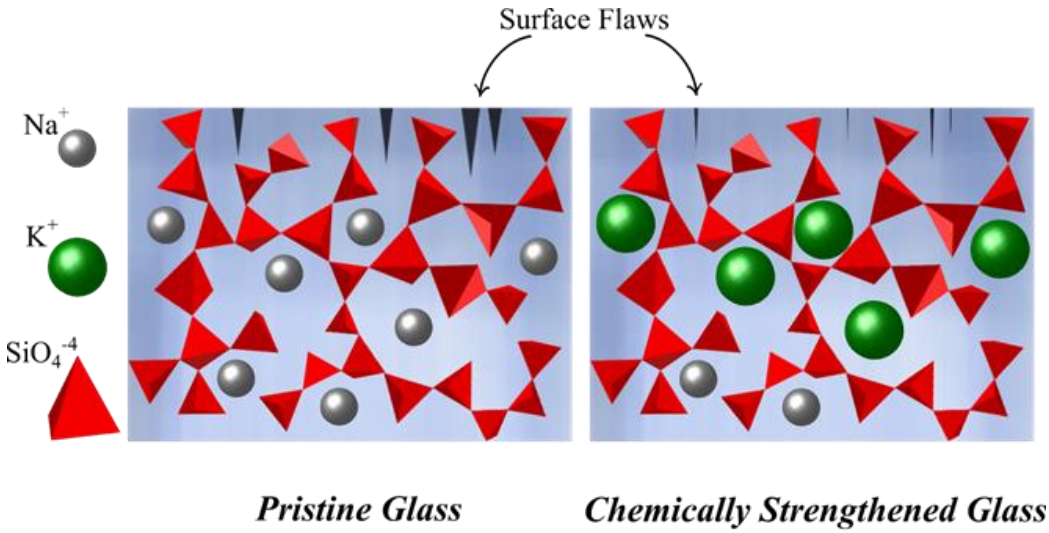


Figure 2.9 Illustration of exchange of alkali ions between salt and the glass through diffusion process and healing of already existent flaws on the surface (alkali earth ions are excluded in the representation)

According to Pauling's calculations, the ionic diameters of following alkali ions: Li^+, Na^+, K^+, Rb^+ and Cs^+ are 1.2 Å, 1.9 Å, 2.66 Å, 2.96 Å and 3.38 Å, respectively [1]. Diffusion of K^+ ions to the glass network, which is originally solidified to host Na^+ ions, results in rearrangement of the atomic structure and molar volume expansion (dilation). Although there are findings that both of these cases occur during ion exchange [49], [50], glass structure is not able modify itself due to its elastic behavior. Thus, guest K^+ ions are responsible of compression generation on the glass surface and this is expressed as compressive stress in MPa units. Compressive stress generation on the glass surface both suppresses the existing flaws and prevents the formation of new ones, ultimately leading to an increase in mechanical strength and hardness. With same approach for Li^+ containing glasses toughening can be done in Na^+ salts, or similarly for K^+ containing glasses can be toughened in Rb^+ salts.

The magnitude of obtained compressive stress values and depth of stress layer (depth of layer - DOL, or case depth on the basis of ASTM C-1422) mainly depend on several factors such as, glass composition [51]–[53], purity of molten salt [54]–[56], treatment temperature and duration [57], [58]. Another point that should be addressed here is that the application of chemical strengthening process is limited only for some alkali containing glass compositions, e.g. soda-lime silicate and alumina silicate glasses [59].

Since the compressive stress generation is accomplished by the introduction of guest ions in chemical strengthening process, depth of the stress layer can only reach to the effective diffusion depth. On the other hand, in thermal tempering process, stress generation is accomplished by the cooling rate difference between the surface and the bulk. Thus, the obtained depth of stress layer is considerably higher than chemical strengthening process (22% of the plate thickness). Stress profile comparison for chemically tempered and thermally tempered glasses are depicted in Figure 2.10.

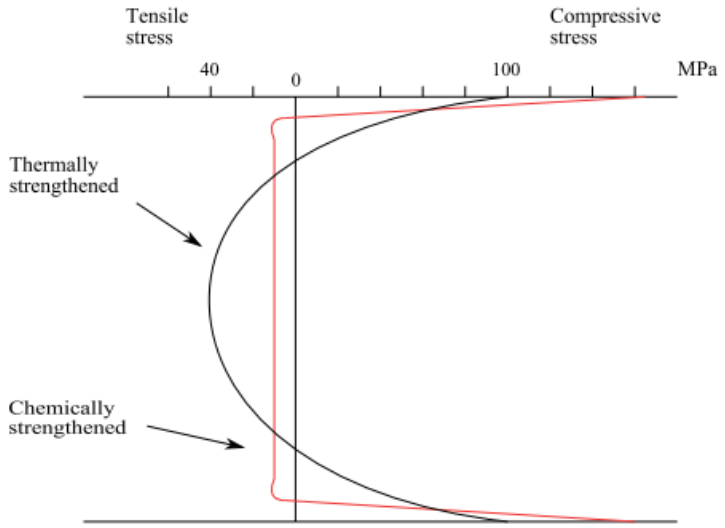


Figure 2.10 Comparison of stress profiles between thermal and chemical strengthened glass (magnitude and the depth of stress may vary depending on the glass composition and the process parameters) [47]

Figure 2.10 demonstrates that, apart from the depth and the magnitude of compressive stress layer, depth and the magnitude of the balancing tensile stress shows a great difference between chemically and thermally tempered glasses. Shattering to small pieces of thermally tempered glass in case of breakage is mainly realized by the high amount of tensile stress buried in the bulk. Since the tensile stress of chemically tempered glass is considerably low compared to thermally tempered glass, they do not shatter into small pieces and do not behave as a safety glass. Their breakage pattern is more similar to that of annealed glasses.

Chemically strengthened glass products have a broad range of applications, especially when the high strength is a must. Aircraft cockpit windshields are one of the first applications which benefit from this novel strengthening process, followed

by glasses for watches. Due to their complex geometries, yacht glasses are also being strengthened by this method. Additionally, ever-expanding of the usage of thin flat glasses lead to increase of alkali aluminosilicate glass production and subsequent toughening by chemical strengthening process for applications such as windshields for sport cars and cover screens for consumer electronics devices.

2.5 Weathering and Aqueous Corrosion of Glass

In many applications, glass products are exposed to warm and humid atmospheric conditions that shorten their lifetime and chemically strengthened glasses are not an exception. For assessment of the products' performance against such conditions, weathering — defines the response of a material to the surrounding atmosphere, usually encountered in the form of deterioration and premature failure [2], [5] — tests have been developed to simulate these warm and humid atmospheres.

Glass-vapor interactions occurring during static weathering test (described in detail in Section 3.1.2), in which the testing temperature is kept constant for the whole testing period, is reported to be similar with aqueous corrosion mechanism of glass [60]–[62]. Water vapor in weathering atmosphere enables water-glass reactions — expressed as alkali leaching and network dissolution reactions — to take place on the surface. In static conditions, there is no circulation of liquid water to drag away the accumulated corrosion products, thus pH level of the surface constantly increases during weathering tests and eventually leads to leaching and dissolution reactions to take place.

2.5.1 Leaching Reactions

Leaching is the first order reaction of the glass-water interactions and it describes the ion exchange phenomena between the glass network and the aqueous medium for the initial stages of the interaction.

Alkali ions of the glass network are ionically bonded to non-bridging oxygen sites (NBOs) and thus they can be easily mobilized while being in contact with water. Therefore, when silica-based glasses are exposed to aqueous medium, ion exchange

reaction takes place between the modifier ions of glass network and hydrous species of water. This mechanism is referred as leaching and it is accepted as the first step of silicate glass corrosion. The widely used model for rate determining step for leaching reactions of silicate glasses is explained using the following reaction [63]:

$$Si–O–M^{+} + H_2O = Si–OH + OH^{-} + M^{+} \quad (2.1)$$

where M represents the alkali ions present in silicate glass network. Leaching rate of alkali ions are governed by the ion type itself and the chemical composition of glass. As a result of leaching reaction, the OH^{-} concentration of condensed water vapor on glass surface increases and so is the pH level.

2.5.2 Dissolution Reactions

Subsequent stage of leaching is dissolution, which is the second order reactions of silicate glass corrosion. Dissolution describes the network hydrolysis and rupture of individual Si–O bonds by the hydrous medium. Even though the silicate glass corrosion reactions are explained to have stepped mechanisms, for complex glasses both of them can occur simultaneously [64]. Increase of pH as a result of first order reactions accelerates the second order reactions. Dissolution reactions are ensured where pH > 9 condition is met and molecular water breaks the Si–O bonds according to the following reaction [65]:

$$Si–O–Si + H_2O = 2SiOH \quad (2.2)$$

This reaction depicts the principle mechanism of strength decrease of silicate glasses in the presence of water molecules due to a hydrophilic attack [66] on Si–O–Si bonds, also known as stress corrosion [67]–[69] , thus resulting a breakage of these bonds [70], [71] and facilitating the crack growth and propagation. Time of exposure, temperature, humidity and pressure has a great influence on the rate of dissolution reactions. Moreover, severe dissolution might cause pitting and crater formation on the glass surface.

3
EXPERIMENTAL STUDIES

In this dissertation study, the effect of weathering on chemical strengthening behavior of thin flat glasses having different Al_2O_3 compositions is evaluated in terms of topographical, optical, structural, and mechanical properties. Surface images of samples are collected using optical microscopy technique. Optical transmittance properties are determined through UV-VIS-NIR spectrophotometry investigations. Surface roughness values and 3D surface images are obtained using white light interferometry and atomic force microscopy analysis, respectively. Structural changes of the glass network are investigated with FTIR spectroscopy. Compressive stress and compression depth resulting from chemical strengthening process are measured via surface stress meter and subsequently surface stress profiles are generated. Flexural strengths are determined with biaxial ring-on-ring tests and analyzed using Weibull distribution approach. Consequently, surface hardness and resistance to cracking behaviors are investigated through Vickers indentation technique.

3.1 Sample Preparation

In the experimental studies, sheet glass plates produced by float process are subjected to chemical strengthening and weathering processes. Therefore, three different glass compositions are chosen according to their Al_2O_3 content to investigate the effect of glass composition on weathering behavior of chemically strengthened glasses.

Pristine glass plates are received from commercial producers and cut from tin sides into square samples of 6 x 6 cm in size with 1.1 mm thickness by a diamond wheel (see Figure 3.1). Both weathering and chemical strengthening are diffusion-based processes. Therefore, surface conditions of samples used in experimental studies are of great importance considering the consistency and reliability of generated

data. For this reason, prior to the application of different experimental conditions, sample surfaces are cleaned in an ultrasonic bath under tap water, distilled water, and isopropyl alcohol, respectively for 5 minutes and subsequently dried under pressured N_2 gas flow.

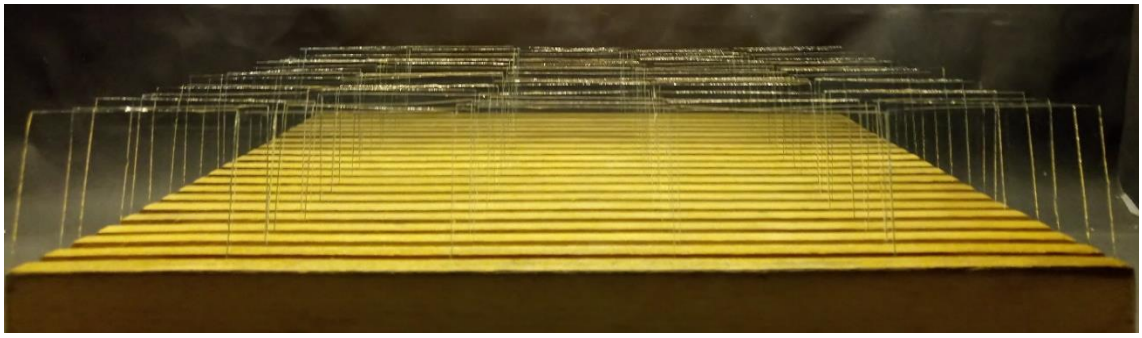


Figure 3.1 Image of cut samples ready for further processing

The elemental compositions of glasses are determined using a Rigaku Primus II X-Ray Fluorescence (XRF) spectrometer. Information on chemical compositions, glass producers and acronyms of glasses are presented in Table 3.1.

Table 3.1 Chemical compositions, producer information and acronyms of glasses

	SiO_2	**Al_2O_3**	**Na_2O**	**CaO**	**MgO**	**K_2O**	**Fe_2O_3**	**SO_3**	**Other**
L-SLS *Şişecam Düzcam*	72.3	0.99	13.5	8.43	4.4	0.06	0.09	0.2	0.03
H-SLS *Triumph Glass*	71.4	2.36	13.5	7.84	3.94	0.64	0.11	0.21	-
AS *Schott*	60.8	17.5	12.6	0.27	3.82	4.18	0.016	0.02	0.79

As seen from Table 3.1, chemical compositions of selected glasses mainly vary in Al_2O_3 content. L-SLS glasses have the lowest Al_2O_3 amount with 0.99%, followed by H-SLS glasses with 2.36%, whereas AS glasses have the highest Al_2O_3 amount with 17.5%. L-SLS and H-SLS samples are soda-lime silicate glasses, while AS samples are alkali aluminosilicate glasses.

3.1.1 Chemical Strengthening Procedure

Chemical strengthening process is used to improve the mechanical performance of the glass product by immersing the glass sample into a molten salt bath containing K^+ ions which have bigger ionic radius than Na^+ ions that are present in the glass structure. During immersion, interdiffusion between K^+ (salt) ↔ Na^+ (glass) ions takes place, thus introducing compression stress on the surface is accomplished. Chemical strengthening process is realized in a chemical tempering furnace (LEMA TC 804A) consisting of a stainless-steel tank for the conservation of the molten KNO_3 salt (see Figure 3.2.). The KNO_3 salt used in this study is supplied from LEMA company. The detected impurities by chemical analysis and the pH level of the salt is given in Table 3.2.

Table 3.2 Impurities and pH of the KNO_3 salt used in experimental studies

	Impurities (ppm)							**pH**
KNO_3	Na	Ca	Mg	Cr	Si	S	Cl	
	3582	NA*	NA*	< 5.00	< 5,00	< 5,00	NA*	10.2

**NA: Not available*

In chemical strengthening experiments, glass samples are placed into a tray having rids made of stainless-steel wires and then the tray is introduced into the chemical tempering furnace. Glass samples are pre-heated in the furnace just above the melting temperature of the salt at around 350°C for 1 hour and then post heat-treated under same conditions for 1 hour after completion of chemical strengthening process for preventing the thermal shock induced cracking during tempering. The temperature and duration for the chemical strengthening process is set to 425°C and 4 hours, respectively. These parameters are selected as a consequence of our previous experience for obtaining maximum compression stress on the surface without relaxation. Additionally, for the selection of chemical strengthening conditions, feasibility and operational expenses of the process are considered. It should be noted here that, the described salt has been used for a long period of time before this study. Therefore, increase in the alkalinity level and pH values are taken into consideration during interpretation of the results.



(a) (b)

Figure 3.2 a) LEMA TC 804A chemical tempering furnace and b) tray placement

3.1.2 Weathering Test Procedure

Weathering term describes the interaction of a material with the humid environment. Three main factors of weathering are solar radiation (high energy), temperature and water (moisture). Weathering tests of glassy materials usually cover the temperature and moisture stimulus. Therefore, weathering cabinets are used for realizing this controlled interaction in the laboratories. A weathering cabinet is a closed chamber that keeps the samples in a specific atmosphere containing artificially generated relative humidity (RH) at the desired temperature for the selected period. Weathering test could be employed under a static or a cycling condition depending on related standards. This study focuses on the automotive applications of chemically strengthened thin glasses, therefore specifications of the weathering test are obtained from the regulation no 43 of the Economic Commission for Europe of the United Nations about "uniform provisions concerning the approval of safety glazing materials and their installation on vehicles" [72]. Hence, Ascott weathering cabinet is used for the weathering test in static condition at 50°C and 95% relative humidity (RH) for 14 days (see Figure 3.3).



(a) (b)

Figure 3.3 a) Weathering test cabinet, b) interior of the cabinet and sample placement

Glass samples are placed in the cabinet in a declined position and air sides of glasses are faced towards the upper side of the cabinet. This sample placement enables water vapor to condensate homogenously on the air side of glasses. Finally, all prepared samples are rinsed under tap water to make sure no by-products are left on the glass surface and then all samples are sealed under vacuum to prevent any possible contamination on the surface until further tests and characterization studies are completed.

3.1.3 Experimental Conditions

For fulfilling the aims of this study, chemical strengthening and/or weathering processes are applied to glass samples individually or in combination and consequently six different experimental conditions are obtained for three different glass types having different chemical compositions. Different experimental conditions are applied to all glass compositions to investigate the weathering behavior of chemically strengthened glasses and to compare with the weathering behavior of pristine glasses. Details of experimental conditions are given in Table 3.3.

Table 3.3 Description of experimental conditions along with sample names and process history

Glass Composition	Sample Name	Process History
L-SLS H-SLS AS	PR	As Produced (Original)
	W	Weathering
	CS	Chemical Strengthening
	W+CS	Weathering + Chemical Strengthening
	CS+W	Chemical Strengthening + Weathering
	W+CS+W	Weathering + Chemical Strengthening + Weathering

Pristine (PR), weathered (W) and chemically strengthened (CS) samples are primarily used as reference sample sets. Afterwards, three different experimental conditions (W+CS, CS+W and W+CS+W) are tested by applying weathering in combination with chemical strengthening process in order to simulate possible scenarios that a strengthened glass product might face during its lifetime. After chemical strengthening process and weathering tests, all samples are inspected in terms of topographical, optical, structural, and mechanical properties by using various characterization techniques which are explained below.

3.2 Tests and Characterizations

Glass products manufactured by float process possess two different surfaces resulting from the tin diffusion to the bottom surface during floating on the molten tin — causing the upper and bottom surfaces of the glass product to exhibit different characteristics. In this study, all tests and characterizations are applied to the atmospheric surface of the samples to avoid unstable behavior of the tin surface and maintain the reliability of data.

3.2.1 Macroscopic and Microscopic Investigations

Macro images are taken by a digital camera and surface micrographs are collected with a LV100POL polarizing microscope equipped with Nikon H600L digital camera under 500X magnification to investigate the surface quality after chemical strengthening and weathering processes.

3.2.2 Topographical Analysis

It is well known that, when glass is exposed to corrosive environments its surface undergoes some topographical changes and this may affect the optical and strength characteristics of glass. Topographical changes may occur in the form of an increase or a decrease in the roughness of the glass surface. In this study, change in roughness can occur through leaching and dissolution reactions originating from weathering process or can be caused by the chemical strengthening process during immersion of the sample into the molten salt at high temperatures. Surface roughness measurements are realized by using white light interferometry (WLI) and atomic force microscopy (AFM) techniques. Therefore, Bruker Contour GT-X white Light Interferometer and Bruker Dimension 3100 Atomic Force Microscope are used to measure surface roughness and generate 3D surface maps. WLI is a non-contact optical method used to generate 3D maps and to measure roughness of the surface. This method utilizes an interferometer that splits the beam of white light and guides it to a flat reference and sample and collects the reflected beams. Phase difference of the collected beam is analyzed and converted into height difference to generate 3D map of the surface. In this study, WLI measurements are realized on ten different spots of glass surfaces under 20X magnification and each measurement covers an area of 0.2mmx0.3mm. Subsequently, the obtained data are processed for calculation of arithmetic average (R_a) values of roughness profiles by using Gwyddion data visualization and analysis software and error bars are generated from the standard deviation values. On the other hand, AFM is a more sophisticated surface mapping technique that could be operated in contact, tapping and non-contact modes. Very thin and sharp probe made of silicon or silicon nitride is guided through sample surface. Atomic forces between the probe and the sample repels the probe and this movement is observed with a photodiode stimulated by a laser beam.

In this work, AFM measurements are done in tapping mode at a frequency of 0.5 Hz using Bruker RTESP-525 probe with a coverage area of 50 μm^2.

3.2.3 Depth Profiling

Depth profiling of glass samples is carried out by means of time of flight secondary ion mass spectroscopy method (TOF-SIMS) using IONTOF 5 instrument.

3.2.4 Optical Analysis

Perkin Elmer Lambda 950 UV-VIS-NIR spectrophotometry is used for determining the optical transmittance properties of the samples in the spectral range 200-2500 nm with a spectral resolution of 1 nm.

3.2.5 Structural Analysis

Infrared radiations cover a portion of the electromagnetic spectrum between 0.8 – 1000 μm in wavelength (λ). Photon energies of this part of the spectrum are not large enough to excite electrons, however they are able to make interactions and cause vibrations to covalently bonded structures. IR reflectance spectroscopy is a surface sensitive technique which makes its usage convenient for the structural characterization of the glass surface and tracking even the smallest changes in the molecular bonds caused by chemical strengthening and weathering. Therefore, structural changes in the glass network are evaluated by Fourier transform infrared (FTIR) spectroscopy technique in the wavenumber range 400-4000 cm^{-1} with a resolution of 2 cm^{-1} using a Bruker Hyperion 3000 FTIR spectrometer. The equipment is operated in reflectance mode for realizing a surface sensitive measurement and background correction is made by a golden reference plate.

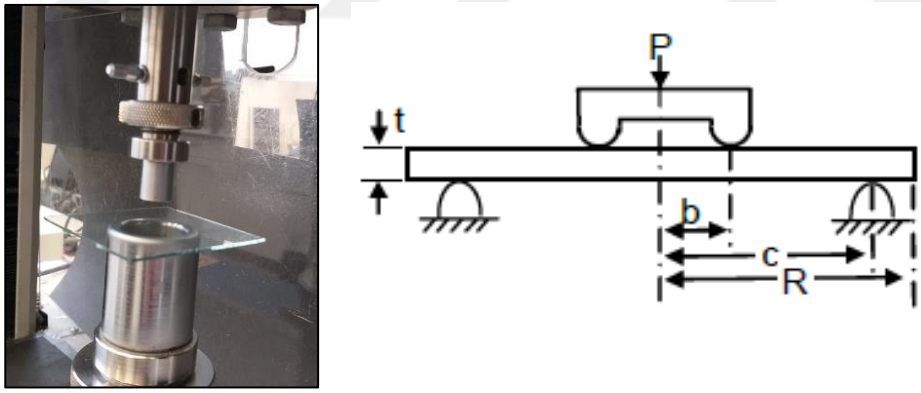
3.2.6 Stress Profile Generation

It is of great importance to quantitively measure the compressive stress and the depth of stress layer generated by chemical strengthening for process and quality control. Compressive stress and depth of layer measurements are realized by FSM-6000LE Surface Stress Meter (Orihara Ind., Japan) and subsequently stress profiles are generated. Surface stress meter is a sophisticated tool for analyzing the compressive stress (MPa) and depth of layer (μm) resulting from ion exchange

process [73]. Therefore, five measurements are taken for each sample and only atmosphere surface of the samples is taken into account for all measurements. Four corners and the center of the samples are determined as measurement points.

3.2.7 Mechanical Analysis

Strength evaluations of glass and ceramic materials are performed mainly under three groups: flexural tests, direct tensile tests and compressive loadings. Flexural strength testing is the most widely used technique for commercial glasses. There are several loading types for determining the flexural strength of glass and these types are categorized under two groups as uniaxial and biaxial loadings. Among these loading types, the mostly used testing methods are three-point bending, four-point bending and ring-on-ring tests. These tests can be applied to both rectangular and square shaped samples and each technique has its own pros and cons. In this study, ring-on-ring testing is chosen since this method allows minimizing the edge flaws and also provides reasonable results. Ring-on-ring method involves the application of a compressive load on the upper surface of sample until failure by a loading ring and the sample is situated on a supporting ring (see Figure 3.4).



(a) (b)

Figure 3.4 a) ring-on-ring testing equipment and b) technical drawing of the equipment

During ring-on-ring testing, displacement and applied load is monitored simultaneously and these values are recorded at the instant of failure. Since recorded fracture load is inversely proportional to the thickness of the glass sample, directly usage of this value is misleading. Hence, the result is incomparable with

glass samples having different thickness values. Therefore, conversion of fracture load into modulus of rupture is needed and it is accomplished by the following formula [74].

$$\sigma_f = 0.75 \left(\frac{P}{\pi t^2}\right)\left[2\,(1+v)\,ln\left(\frac{c}{b}\right) + \,(1-v)\left(\frac{c}{R}\right)^2\left\{1-\left(\frac{b}{c}\right)\right\}^2\right] \quad (3.1)$$

where P is fracture load, v Poisson's ratio of the material and t thickness of the sample. Instron 3366 testing system equipped with a supporting ring having 3 cm radius and loading ring having 1 cm radius is used for the ring-on-ring testing of the square samples with 6 cm edge length. The dimensions are provided from the national standard No. TS EN 1288-5 [75] and loading rate is kept constant for all tests as 1.1 mm/minutes. 30 samples for each condition are tested and Weibull distributions are applied to obtain raw data for a better interpretation and to increase the reliability of results.

Weibull distribution is a common statistical approach used to evaluate the mechanical strength values of brittle materials which utilizes linear regressions to correlate fracture load (N) or modulus of rupture (MPa) with the probability of failure (P_f) [76], [77]. Therefore, experimentally calculated modulus of rupture values are processed with Weibull cumulative distribution function for a better interpretation. Generation of Weibull plots in this work is accomplished using a series of equations. Cumulative probability of failure is related to the number of specimens which are subjected to mechanical tests and it can be explained by using probability estimators with different ranking methods. For this purpose, mean ranking method presented in below equation is used in this study since it provides the highest survival limit and regression coefficient [78].

$$P_f = \frac{j}{N+1} \quad (3.2)$$

In Equation 3.2, j is the rank of sample in ascending order strength distribution and N is the total number of specimens [54]. Correlation of the probability of failure with the mechanical strength is realized using the following equation [77].

$$P_f = 1 - \exp\left[-\left(\frac{\sigma}{\sigma_0}\right)^m\right] \quad (3.3)$$

Thus, a relation between the probability of failure, ring-on-ring test data and Weibull modulus (m) is obtained. Taking double natural logarithms of Equation 3.3 yields below given equation [79]:

$$\ln[\ln(1/1- P_f)] = m \ln\sigma - m \ln\sigma_0 \quad (3.4)$$

Equation 3.4 reveals that there is a linear correlation between failure probability and the modulus of rupture of test specimens where the slope of the linear plot is Weibull modulus (m).

As well as increasing the flexural strength, chemical strengthening process also contributes to an increase in surface hardness of the glass plate. Hardness measurements of the samples are determined by Vickers indentation technique. This method is realized by pressing a pyramid-shaped diamond tip on the sample surface with a constant load for a specific period. By examining the indentation made by a sharp diamond tip, applied force can be converted into hardness value by using the following formula [80]:

$$H_v = 1.854 \frac{F}{d^2} \quad (3.5)$$

where F is the applied force in Newton and d is the mean value of diagonal lengths (d_1 and d_2, mm) between edges of the indentation. Hardness measurements are done by Shimadzu HMV-G microhardness tester equipped with a Vickers indenter. The applied load is set to 50 g for 20 seconds. Ten indentations are made for each sample and mean values are considered. In addition, three different loads, i.e. 500 g, 1000 g and 2000 g, are used for crack resistance study. Crack resistance probability is calculated as follows [81]–[83]:

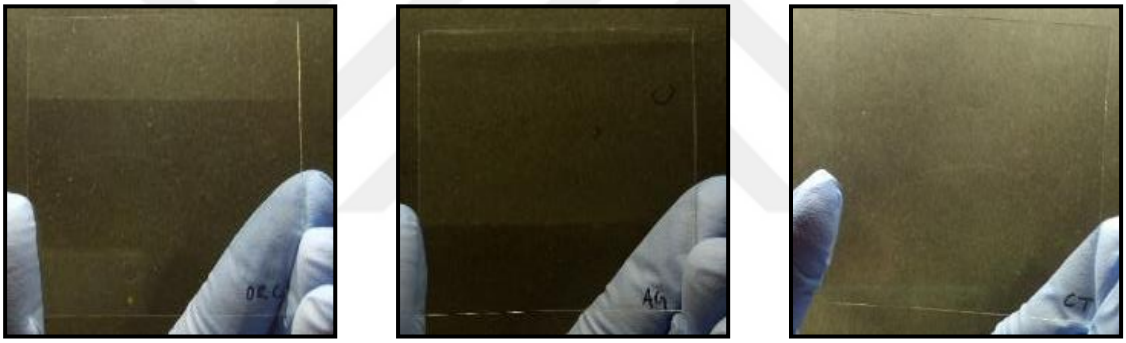
$$Crack\ resistance\% = \frac{\#\ \text{of}\ indentations - \#\ of\ cracked\ indentations}{\#\ \text{of}\ indentations}\ x\ 100 \quad (3.6)$$

4
RESULTS AND DISCUSSION

4.1 Results

4.1.1 Macro Examination Results of L-SLS Glasses

Macro images of L-SLS samples are demonstrated in Figure 4.1. The images show that weathering and chemical strengthening processes have no negative effect on glass surface in the macro scale for PR, W, CS and W+CS samples. However, iridescence pattern is observed for CS+W and WCS+W samples — that are exposed to weathering after chemical strengthening process. This pattern can be easily seen under a light source as in Figure 4.1e and Figure 4.1f.



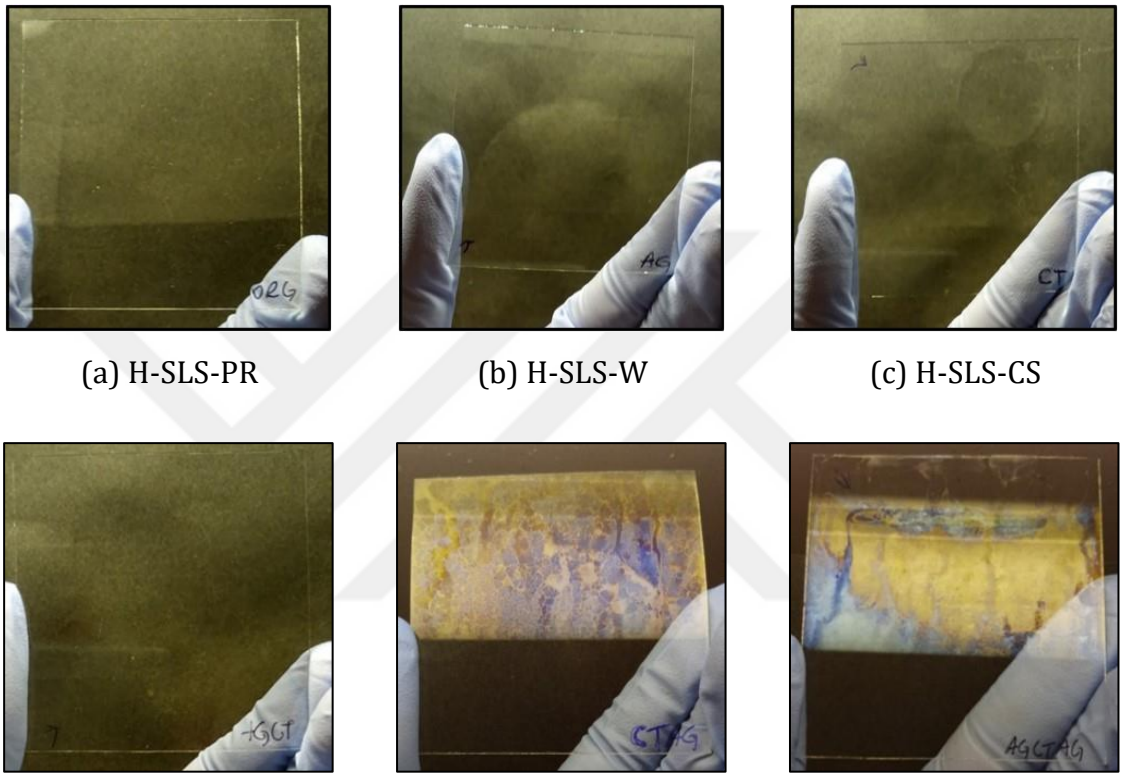
(a) L-SLS-PR (b) L-SLS-W (c) L-SLS-CS

(d) L-SLS-W+CS (e) L-SLS-CS+W (f) L-SLS-W+CS+W

Figure 4.1 Macro images of L-SLS samples

4.1.2 Macro Examination Results of H-SLS Glasses

Macro images of H-SLS samples are given in Figure 4.2. The appearance of H-SLS glasses revel that chemical strengthening or weathering processes do not cause a significant visual change for PR, W, CS and W+CS samples. However, similar to L-SLS samples, formation of an iridescence pattern is observed for CS+W and W+CS+W samples.



(a) H-SLS-PR (b) H-SLS-W (c) H-SLS-CS

(d) H-SLS-W+CS (e) H-SLS-CS+W (f) H-SLS-W+CS+W

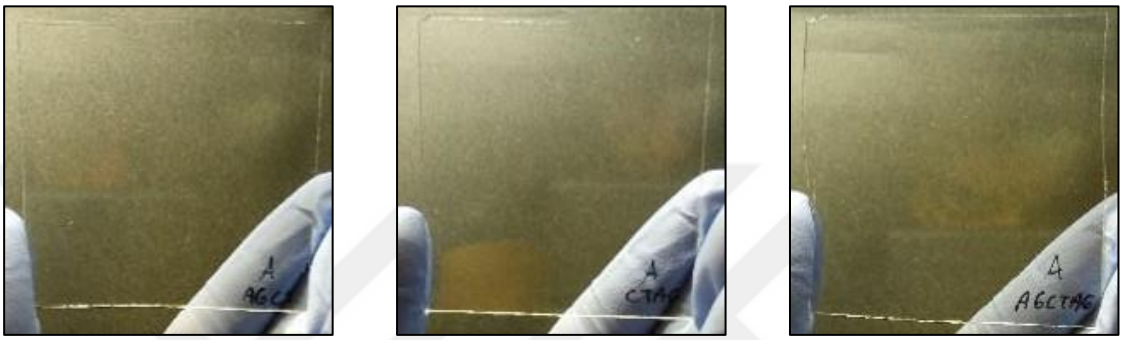
Figure 4.2 Macro images of H-SLS samples

4.1.3 Macro Examination Results of AS Glasses

Macro images of AS glasses are shown in Figure 4.3. All sample images indicate that weathering and chemical strengthening has no detectable effect on glass surface in the macro scale.



(a) AS-PR (b) AS-W (c) AS-CS

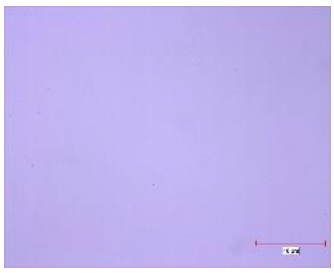


(d) AS-W+CS (e) AS-CS+W (f) AS-W+CS+W

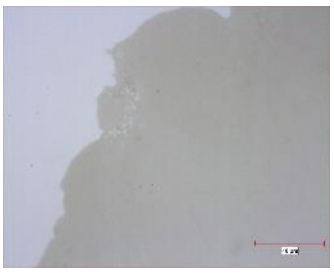
Figure 4.3 Macro images of AS samples

4.1.4 Micrographs of L-SLS Glasses

A detailed look on the glass surface is realized using a polarizing microscope and the obtained micrographs for L-SLS glasses are given in Figure 4.4. Surface images of CS and W+CS samples are identical with the PR condition revealing no change on the glass surface. On the other hand, stains caused by water interactions are detected for W sample at several points on the surface. Moreover, CS+W and W+CS+W samples manifest a significant change on the surface appearance. The formed iridescence pattern for these samples — also detected in the macro scale — is mainly comprised of dark-blue and brown color changes.



(a) L-SLS-PR



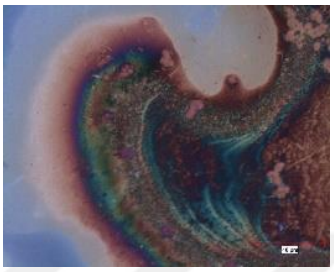
(b) L-SLS-W



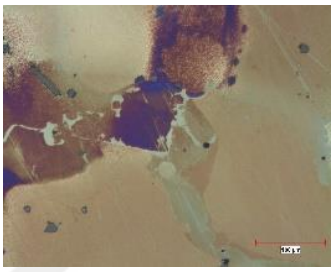
(c) L-SLS-CS



(d) L-SLS-W+CS



(e) L-SLS-CS+W



(f) L-SLS-W+CS+W

Figure 4.4 Micrographs of L-SLS samples (scale bar shows 40 μm for all captures)

4.1.5 Micrographs of H-SLS Glasses

Micrographs of H-SLS glass samples are illustrated in Figure 4.5. As seen from the given figures H-SLS glasses exhibit similar behavior with L-SLS glasses. Thereby, a water-related stain is spotted in W sample and no change on surface appearance is detected for CS and W+CS samples. Moreoever, formation of iridescence patterns is recorded on the surfaces of CS+W and W+CS+W samples.



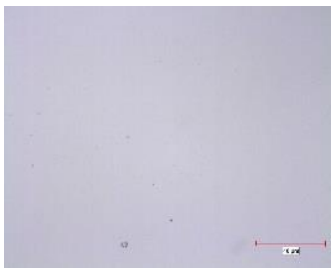
(a) H-SLS-PR



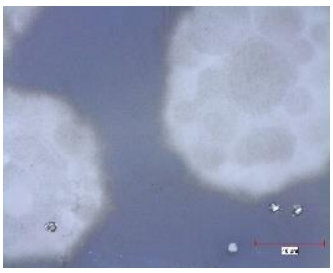
(b) H-SLS-W



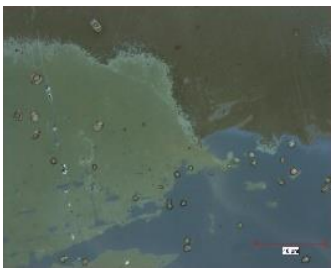
(c) H-SLS-CS



(d) H-SLS-W+CS



(e) H-SLS-CS+W



(f) H-SLS-W+CS+W

Figure 4.5 Micrographs of H-SLS samples (scale bar shows 40 µm for all captures)

4.1.6 Micrographs of AS Glasses

Micrographs of AS glasses that are given in Figure 4.6 show no sign of deterioration after secondary processes, i.e. weathering and chemical strengthening. All samples are found to be identical with the pristine condition and these findings correlate with the macro image results.



(a) AS-PR



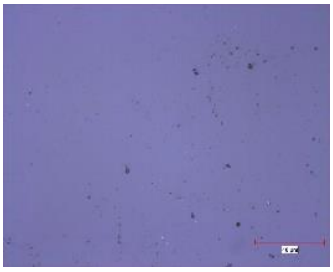
(b) AS-W



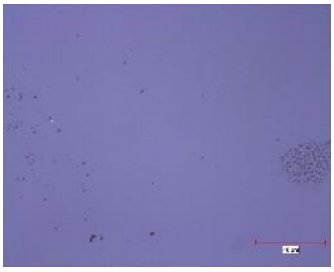
(c) AS-CS



(d) AS-W+CS



(e) AS-CS+W



(f) AS-W+CS+W

Figure 4.6 Micrographs of AS samples (scale bar shows 40 µm for all captures)

4.1.7 Surface Roughness of L-SLS Glasses

Surface roughness values of L-SLS glasses obtained by WLI measurements are given in Fig. 4.7. The roughness value for the pristine condition is found as 0.4 nm.

Furthermore, weathering process slightly increases the roughness values of W and W+CS samples, however CS sample does not experience any change in roughness values compared to pristine sample.

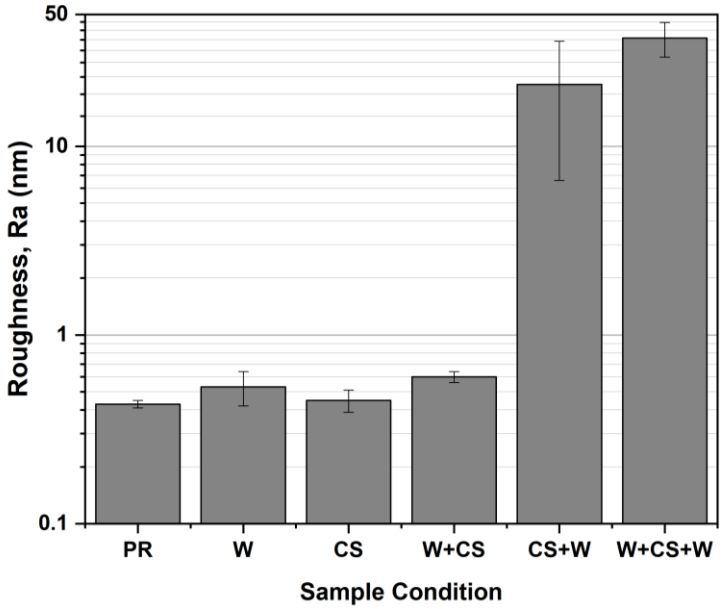


Figure 4.7 Surface roughness chart of L-SLS glasses

A dramatic increase in surface roughness is observed for CS+W and W+CS+W samples. In general, exposure of chemically strengthened L-SLS glasses to weathering increases the roughness values of glass surface approximately two orders of magnitude compared to pristine condition. Additionally, W+CS+W condition experiences a greater roughness increase than CS+W condition. A significant increase in roughness values for CS+W and W+CS+W samples indicates that these samples suffer from severe surface deterioration.

4.1.8 Surface Roughness of H-SLS Glasses

Similar to L-SLS glasses, surface roughness value of PR condition is measured as 0.4 nm for H-SLS glasses (see Figure 4.8). In addition, compared to PR condition, no significant change is observed in roughness values of CS, W, and W+CS samples. Chemically strengthened samples that are further exposed to weathering, i. e. CS+W and W+CS+W, exhibit surface roughness values of 10 nm and 30 nm, respectively, which is a sign of surface deterioration. Surface roughening of chemically strengthened H-SLS glasses after weathering is reduced compared to L-SLS glasses.

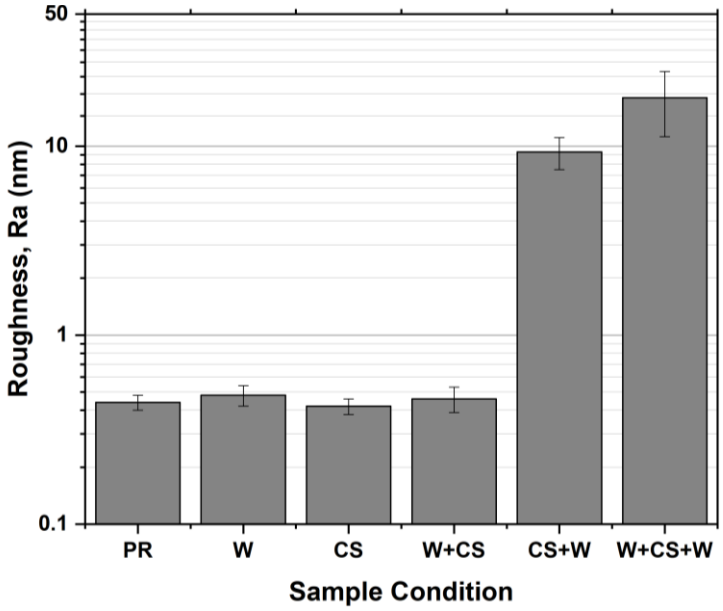


Figure 4.8 Surface roughness chart of H-SLS glasses

4.1.9 Surface Roughness of AS Glasses

Surface roughness values of AS glasses are depicted in Figure 4.8. Similar to the PR conditions of other glass compositions, AS-PR sample has a roughness value of 0.4 nm and surface roughness of AS glass samples is not affected significantly by the applied chemical strengthening and weathering processes.

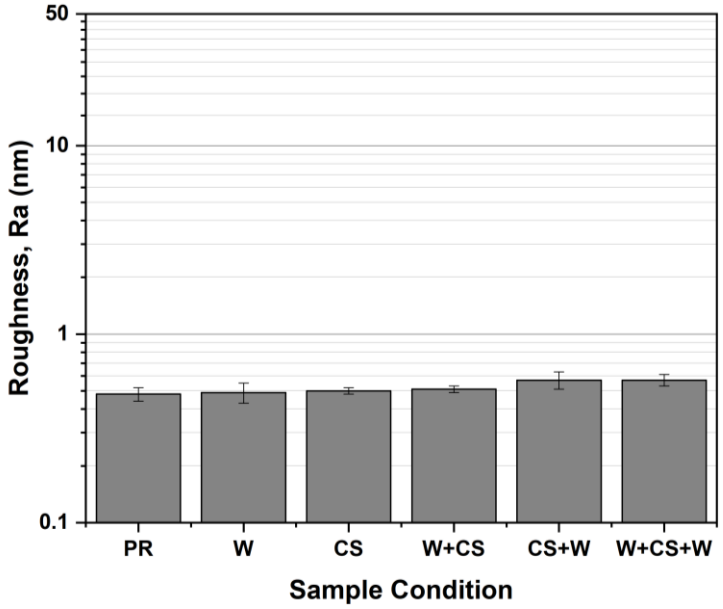


Figure 4.9 Surface roughness chart of AS glasses

4.1.10 Depth Profiles of Pristine and Weathered L-SLS Glasses

Elemental depth profiling data obtained by TOF-SIMS analysis is given in Figure 4.10 for L-SLS-PR and L-SLS-W samples up to a depth of 2000 nm. The y-axis is given as raw data of counts for each element. It should be noted here that depth profiling with TOF-SIMS does not provide information about the concentration of an element. Baseline of the intensity for the compared elements in both plots might be somewhat different depending on the background correction procedure applied before the analysis.

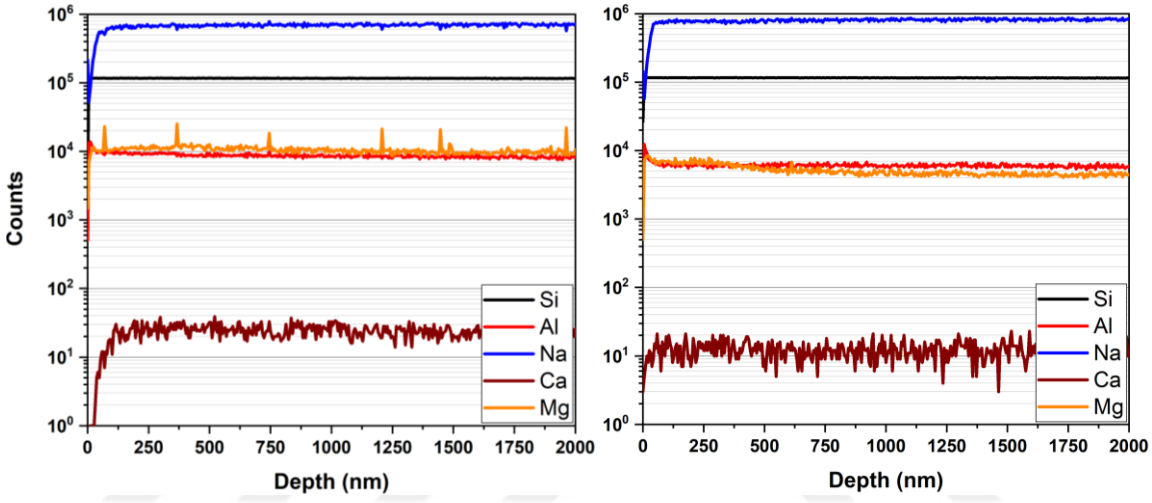


Figure 4.10 Depth profiles of a) PR condition and b)W condition of L-SLS glasses

Both plots given in Figure 4.10 present a constant signal for all interested elements since no ion exchange reactions occur in these samples. Even though a small amount of sodium depletion is expected in the weathered sample, it is not detected in depth profile analysis indicating that leaching reactions are not as severe as to influence the sodium profile.

4.1.11 Depth Profiles of Chemically Strengthened L-SLS Glasses

Elemental profile of chemically strengthened L-SLS glass samples shows different trends compared to pristine and weathered samples. Figure 4.11a-c indicate elemental depth profiling data up to a depth of 10000 nm. Interchange of Na^+ and K^+ ions due to treatment in the molten salt is observable for chemically strengthened

samples. Diffusion driven introduction of K^+ ions results an increase in K^+ signals in exchange of a decrease in Na^+ signals up to 8 microns.

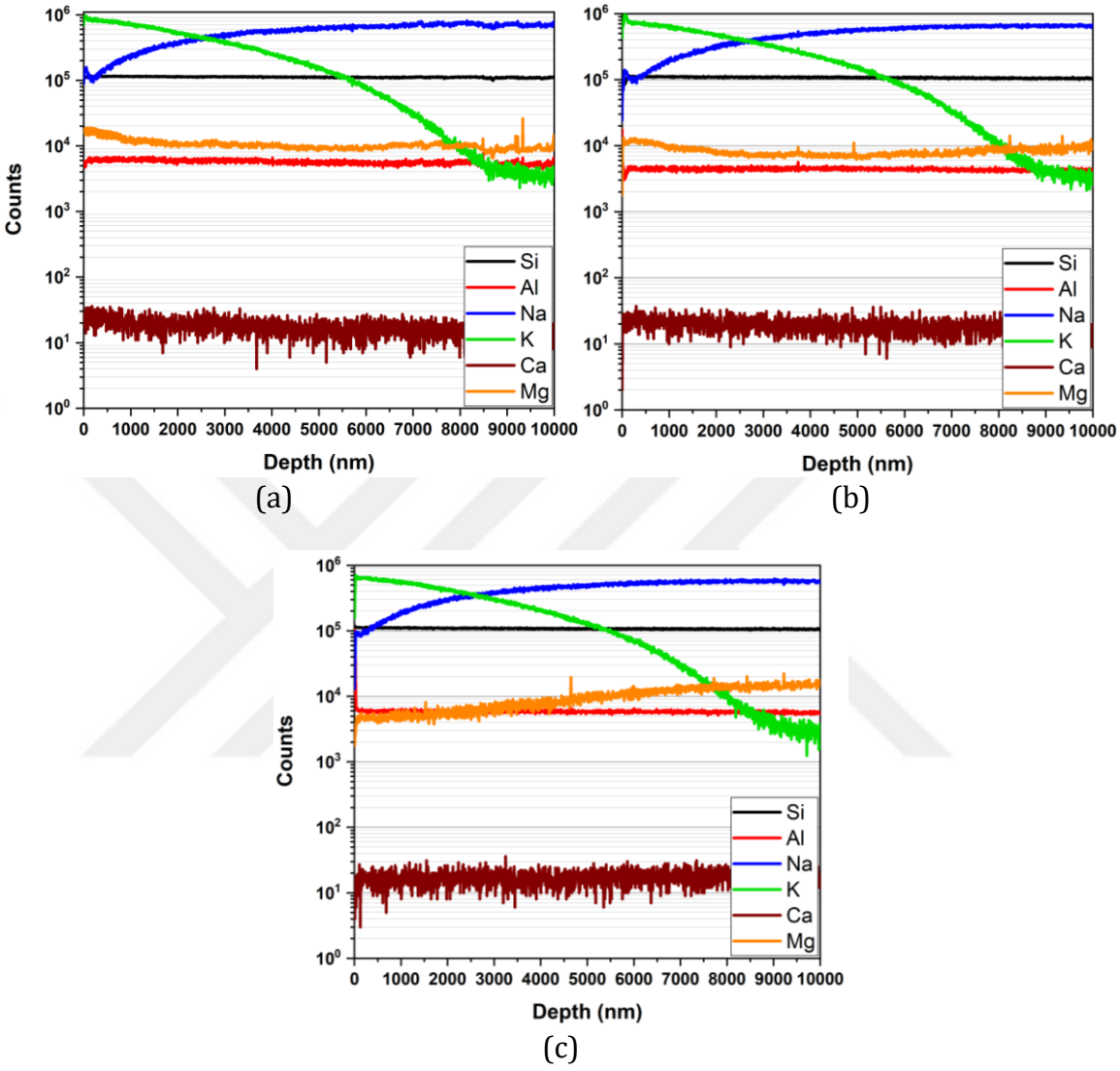


Figure 4.11 Depth profiles of a) CS condition, b) W+CS condition and c) CS+W condition of L-SLS glasses

Si and Al profiles of CS, W+CS, and CS+W samples are found to be identical for all three conditions. On the other hand, profiles of the alkali earth ions, i.e. Ca^{2+} and Mg^{2+}, for W+CS and C+W conditions differentiate up to a few microns from the surface compared to the CS condition.

4.1.12 Transmittance Spectra of L-SLS Glasses

Transmittance spectra of L-SLS glasses obtained by UV/VIS/NIR spectrophotometer measurements are demonstrated in Figure 4.12 between 200-2500 nm.

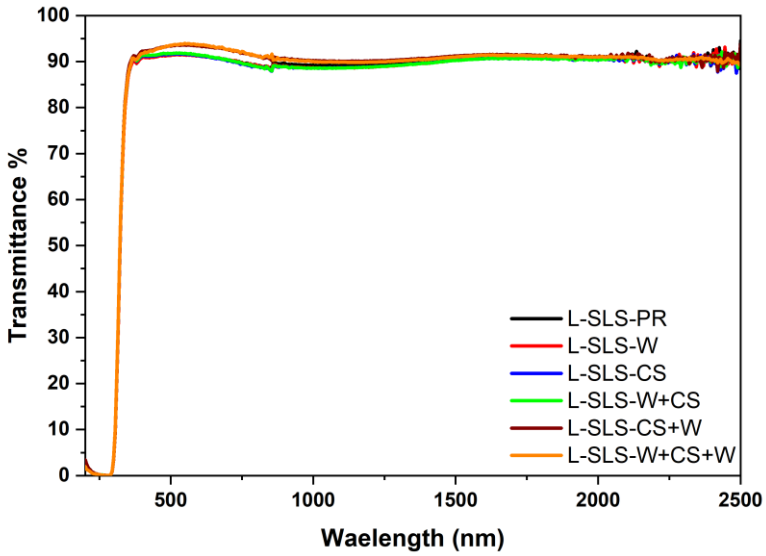


Figure 4.12 Transmittance spectra of L-SLS glasses

The transparency window of L-SLS glasses approximately starts from 255 nm and expands beyond 2500 nm. Average transmittance in the visible region is found as 92% and a slight decrease in transmittance is observed at around 1000 nm resulting from the impurities present in the glass composition. On the other hand, a slight increase of transmittance in the visible region is detected for CS+W and W+CS+W conditions.

4.1.13 Transmittance Spectra of H-SLS Glasses

Figure 4.13 depicts the transmittance spectra of H-SLS glasses. The transmittance of PR sample is detected as 91% in the visible region . A broad and weak absorption band is observed for all conditions and therefore, it is attributed to the impurities present in the glass. Compared to L-SLS glasses, a steeper increase of transmittance is detected for CS+W and W+CS+W conditions up to 1700 nm.

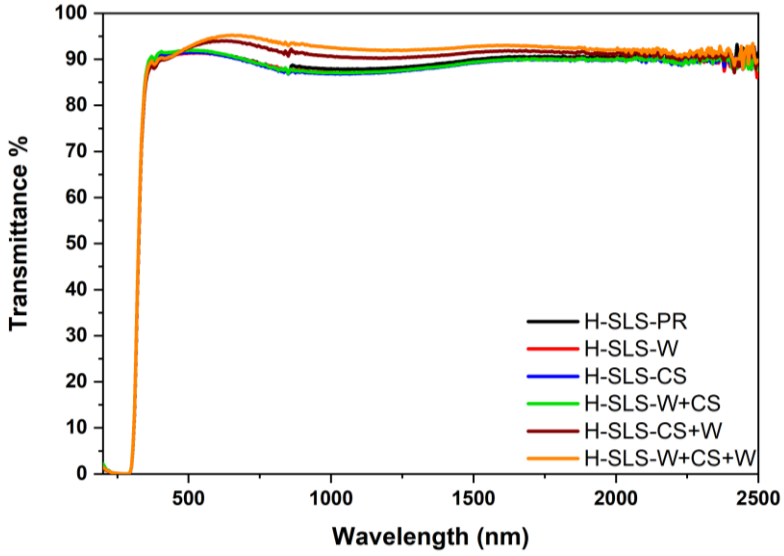


Figure 4.13 Transmittance spectra of H-SLS glasses

4.1.14 Transmittance Spectra of AS Glasses

Examination of the transmittance spectra of AS glasses given in Figure 4.14 reveal that all conditions has a constant transmittance of %92 between 250-2500 nm. Furthermore, no impurity related absorption bands are detected due to lower amount of impurities in AS glass composition.

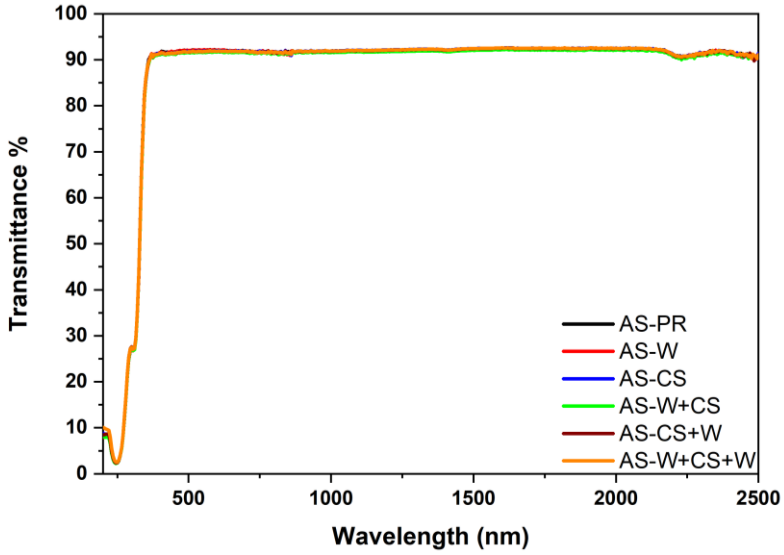


Figure 4.14 Transmittance spectra of AS glasses

4.1.15 Infrared Spectra of L-SLS Glasses

Infrared spectra of L-SLS glasses obtained by FTIR analysis are demonstrated in Figure 4.15 between 400-4000 cm^{-1} spectral range.

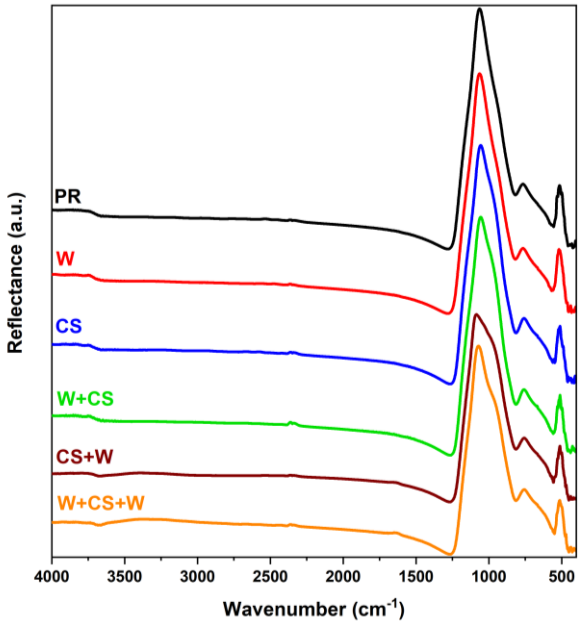


Figure 4.15 Infrared spectra of L-SLS glasses

Characteristic peak positions of silicate glasses that are asymmetric and symmetric stretching of Si–O–Si bonds are observed at around 1065 cm^{-1} and 765 cm^{-1}, respectively. A shoulder-like peak with low intensity at around 950 cm^{-1} which is assigned to Si–NBO stretching vibrations is also detected for L-SLS glasses. Intensity of this shoulder increases for C+W and W+CS+W samples. No peaks related to the glass structure is spotted between wavenumbers of 1250-4000 cm^{-1}.

4.1.16 Infrared Spectra of H-SLS Glasses

IR spectra of H-SLS glasses are depicted in Figure 4.16. Asymmetric and symmetric stretching vibration peaks of Si–O–Si bonds are detected at around 1060 cm^{-1} and 765 cm^{-1}, respectively. Formation of Si–NBO bands is observed as a shoulder at around 950 cm^{-1} in CS+W and W+CS+W samples.

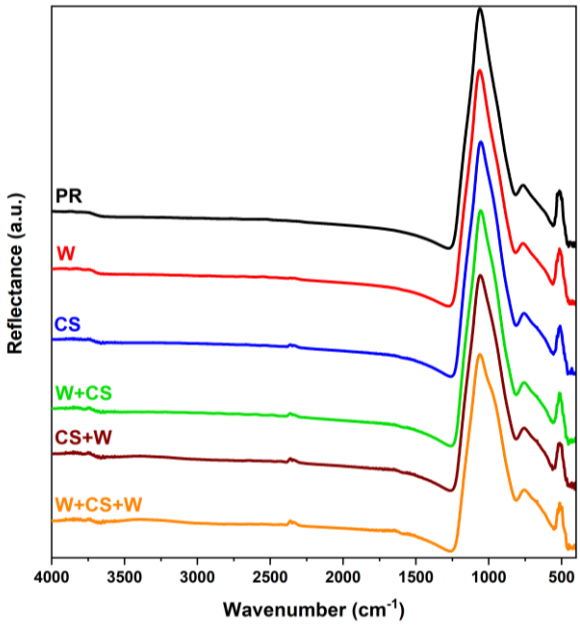


Figure 4.16 Infrared spectra of H-SLS glasses

4.1.17 Infrared Spectra of AS Glasses

Figure 4.17 exhibits the IR spectra of AS glasses with different conditions.

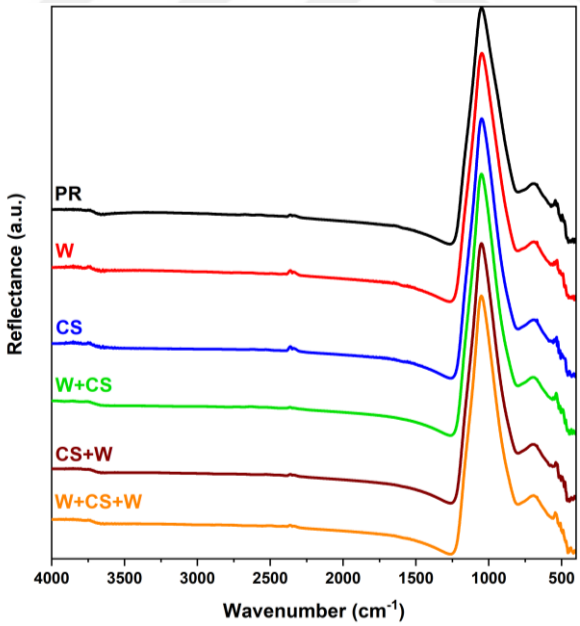


Figure 4.17 Infrared spectra of AS glasses

Asymmetric and symmetric stretching vibration peaks of Si–O–Si bonds are detected at around 1050 cm^{-1} and 690 cm^{-1}, respectively. For AS glasses, the asymmetric vibration peak is located at lower wavenumbers than SLS glasses with

higher intensity. Also, no Si–NBO related band or shoulder is detected for AS glasses.

4.1.18 Stress Profiles of L-SLS Glasses

Stress profile plots of chemically strengthened L-SLS glasses are given in Figure 4.18. Compressive stress value is found as 640 MPa on the glass surface for CS and CS+W samples where it reaches to its maximum value. The magnitude of stress shows a linear decrease and it reaches to zero at 6.7 μm depth. W+CS and W+CS+W samples — that are both weathered before chemical strengthening process — have somewhat lower compressive stress values in the level of 600 MPa on the surface. However, depth of layer values are found identical for all conditions.

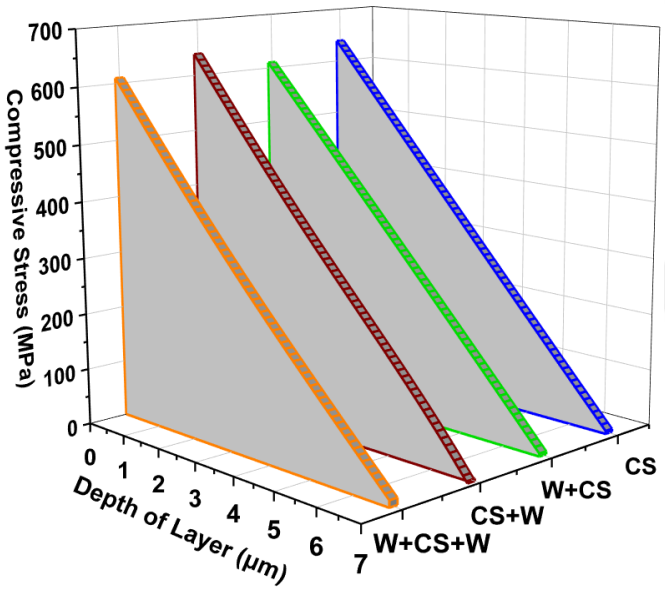


Figure 4.18 Stress profiles of L-SLS glasses

4.1.19 Stress Profiles of H-SLS Glasses

Stress profiles of chemically strengthened H-SLS glasses are demonstrated in Figure 4.19. In general, compressive stress values of chemically strengthened H-SLS glasses are found as 680 MPa for CS and W+CS conditions and 640 MPa for CS+W and W+CS+W conditions. Similar with L-SLS glasses, exposure to weathering prior to chemical strengthening process causes a mitigation on compressive stress generation for H-SLS glasses. Depth of layer values are found to be the same for all conditions around 9.5 μm.

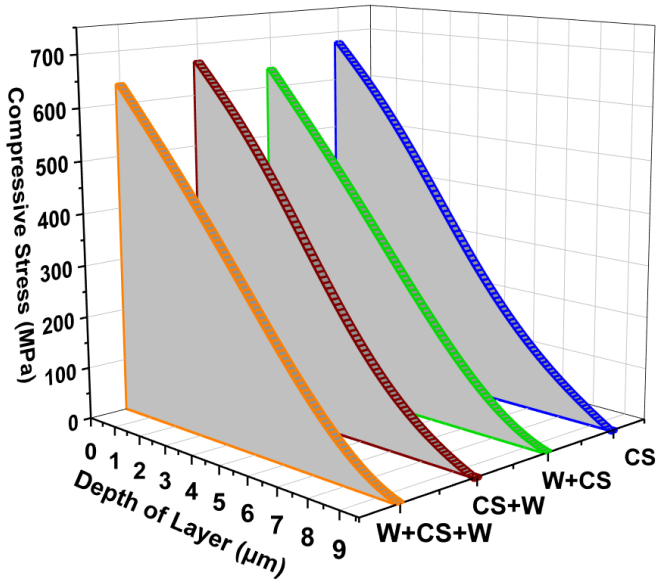


Figure 4.19 Stress profiles of H-SLS glasses

4.1.20 Stress Profile of AS Glasses

Examination of stress profile of chemically strengthened AS glasses from Figure 4.20 reveals that both compressive stress and depth of layer values of AS glasses are considerably higher than L-SLS and H-SLS glasses. In particular, compressive stress values are found as 900 MPa and depth of layer values are found as 40 μm.

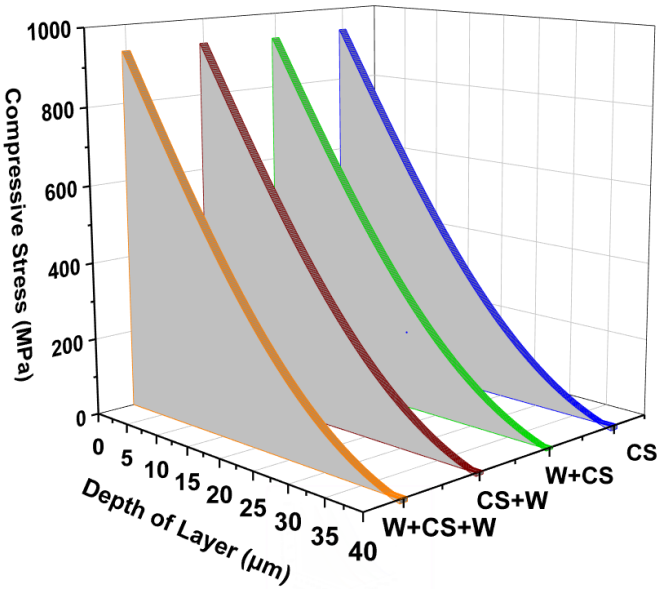


Figure 4.20 Stress profiles of AS glasses

4.1.21 Ring-on-Ring Test Results of L-SLS Glasses

The raw data obtained from the ring-on-ring strength measurements which are values of maximum displacement at failure point, fracture load and corresponding modulus of rupture are given in Figure 4.21 for L-SLS glasses.

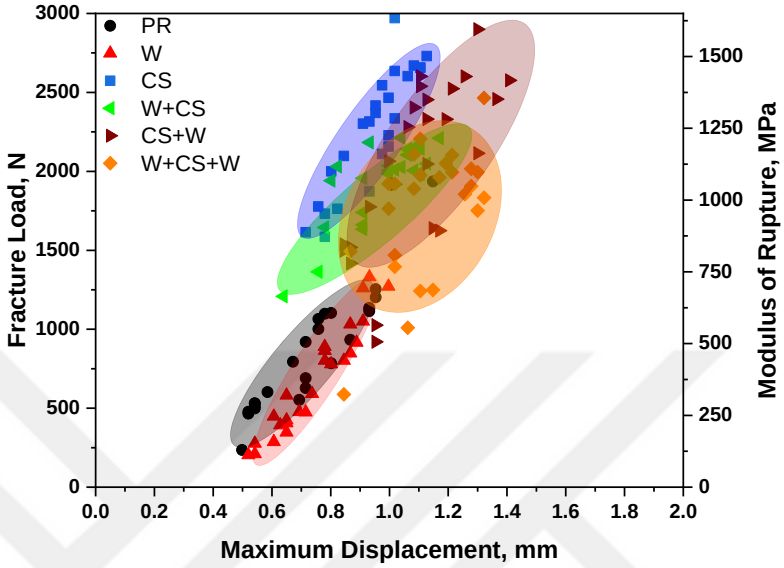


Figure 4.21 Raw data obtained from ring-on-ring tests for L-SLS glasses

Figure 4.21 shows that PR condition of L-SLS glasses have an average modulus of rupture value of 452 MPa. Among different conditioned samples, W sample has the lowest average modulus of rupture as 355 MPa, while CS and CS+W samples have the highest modulus of rupture as 1315 MPa and 1155 MPa, respectively. It is also observed from ring-on-ring tests that CS+W and W+CS+W samples have lower fracture load and modulus of rupture than CS sample.

4.1.22 Ring-on-Ring Test Results of H-SLS Glasses

Data collected at the instant of fracture of H-SLS glasses are plotted in Figure 4.22.

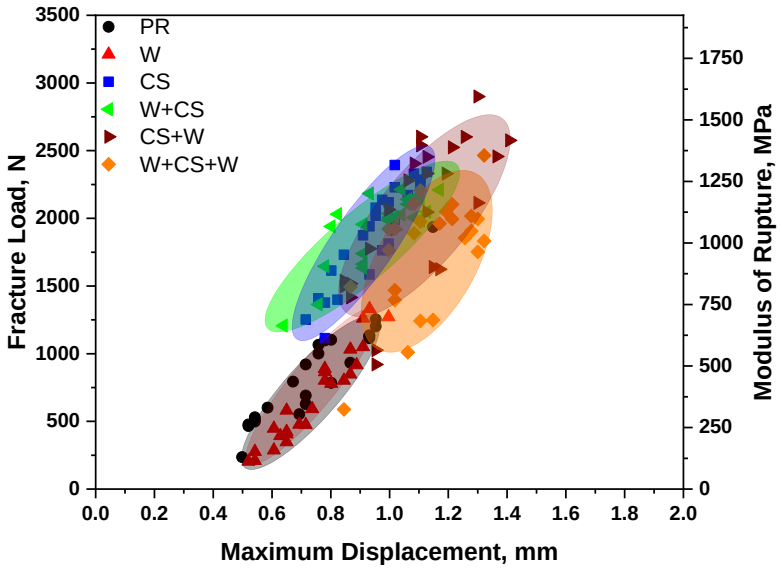


Figure 4.22 Raw data obtained from ring-on-ring tests for H-SLS glasses

Even though clusters of PR and W samples are overlapping, average modulus of rupture values for these conditions are found as 495 MPa and 378 MPa, respectively. This gap is mainly caused by the difference in distribution of individual samples' results. CS sample is found to have the highest average modulus of rupture value with 1327 MPa and followed by CS+W condition with 1227 MPa. When compared to CS condition, samples that are weathered prior to chemical strengthening, i.e. W+CS and W+CS+W, show a decrease in modulus of rupture values with 1170 MPa and 1045 MPa, respectively.

4.1.23 Ring-on-Ring Test Results of AS Glasses

Obtained ring-on-ring testing data for AS glasses are presented in Figure 4.23.

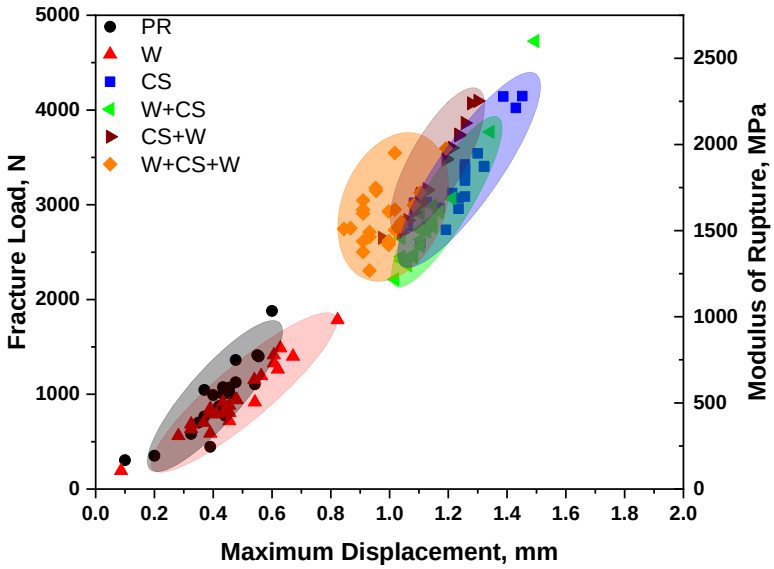


Figure 4.23 Raw data obtained from ring-on-ring tests for AS glasses

Data clusters for AS glasses formed by the individual samples corresponding to different process conditions are situated in two distinct regions. Compared to chemically strengthened conditions, PR and W conditions have lower mechanical strength values (619 MPa and 500 MPa, respectively) and also lower displacement values. A tremendous increase in both strength and displacement values is observed for chemically strengthened AS glasses. Average modulus of rupture values for CS, W+CS, CS+W and W+CS+W conditions are calculated as 1735, 1475, 1741 and 1566 MPa, respectively. Maximum displacements show an increase from 0.5 mm for PR and W conditions to 1.2 mm for chemically strengthened conditions.

4.1.24 Hardness and Crack Formation Results of L-SLS Glasses

Surface hardness values determined by Vickers indentation tests are given in Figure 4.24 for L-SLS glasses.

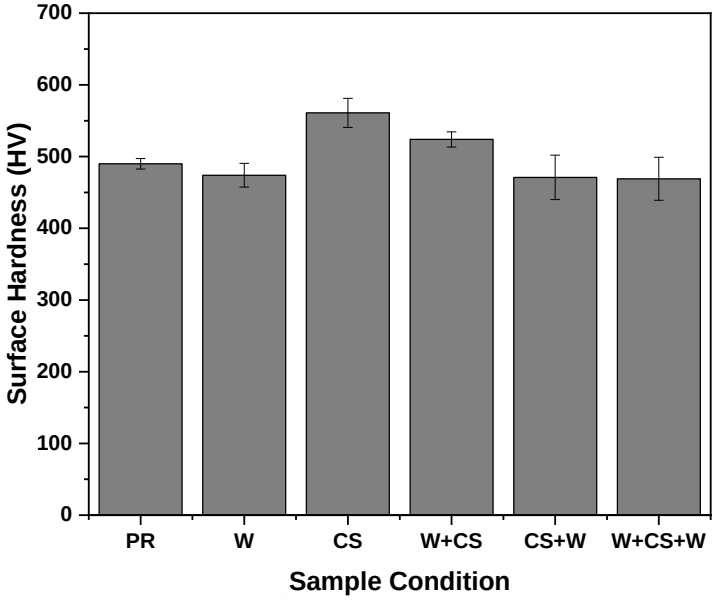
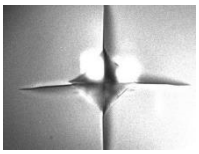
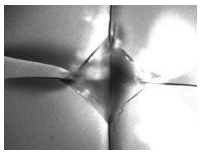
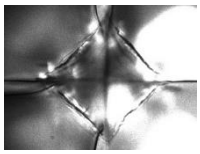
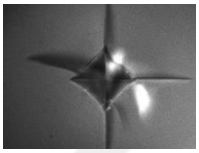
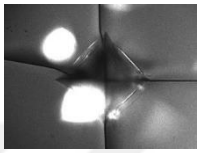
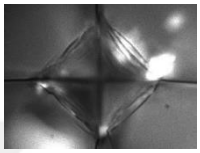
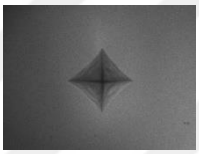
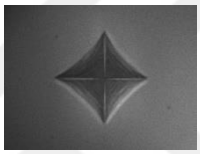
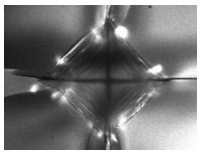
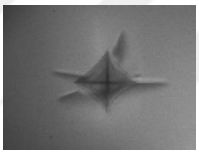
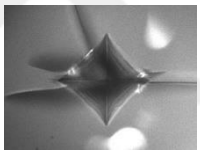
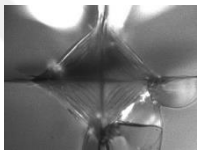
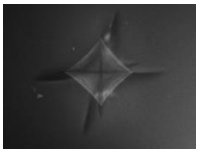
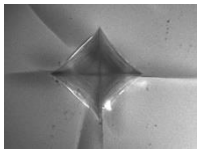
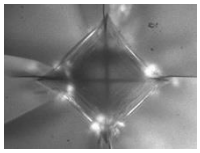
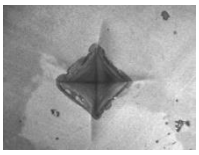
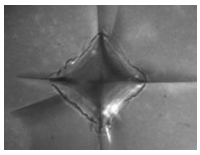
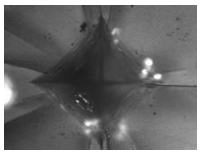


Figure 4.24 Vickers hardness results of L-SLS glasses

Hardness value of pristine L-SLS glass is found as 490±7 HV and for the weathered sample hardness value decreases to 474±16 HV. CS sample exhibits the maximum hardness value with 561±20 HV. However, exposure to weathering prior to or after chemical strengthening limits the hardness increase. In case of prior exposure to weathering, hardness of the glass surface is determined as 524±10 HV, while the post exposure leads to a decrease in hardness values to 470±30 HV. Figure 4.24 implies that the increased hardness of chemically strengthened L-SLS glasses shows a reduction after weathering and becomes almost similar with the hardness value of pristine condition. Also, increase in the standard deviation of collected data for CS+W and W+CS+W samples were observed.

Crack formation probabilities of L-SLS glasses are also evaluated by Vickers indentation technique. One representative image for each condition is given in Table 4.1 for different loads.

Table 4.1 Representative indentation images of L-SLS glasses for crack formation determination

Sample Name	Indentation Image (500g)	Indentation Image (1000g)	Indentation Image (2000g)
L-SLS-PR			
L-SLS-W			
L-SLS-CS			
L-SLS-W+CS			
L-SLS-CS+W			
L-SLS-W+CS+W			

Crack formation of PR condition starts at 500 g load, while the CS condition endures a 1000 g load with a low percentage of cracking. Regarding the other conditions, increase in crack formation probabilities is observed when the weathering is involved. All L-SLS glasses exhibit a high percentage of crack formation under 2000 g of indentation loading.

4.1.25 Hardness and Crack Formation Results of H-SLS Glasses

Vickers hardness values of H-SLS glasses are depicted in Figure 4.25. PR and W samples show very similar hardness values as 507±12 and 504±9 HV, respectively. Since hardness difference between PR and W samples falls within the deviations, surface hardness values of these two samples are considered to be the same.

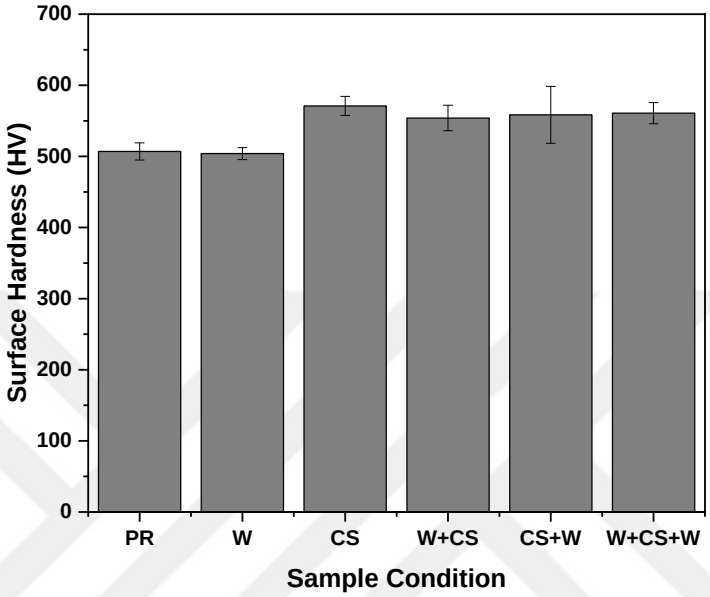
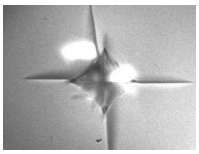
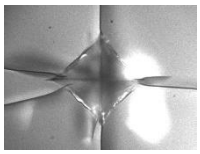
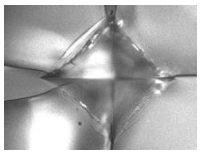
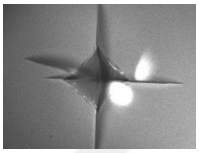
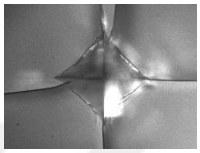
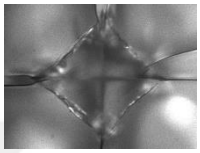
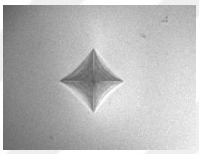
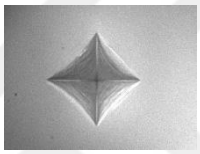
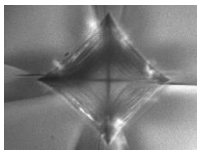
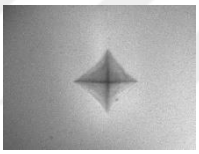
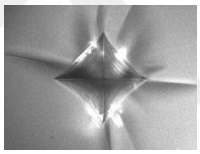
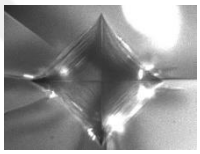
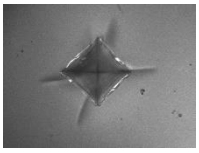
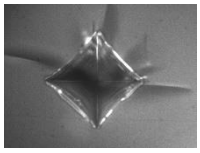
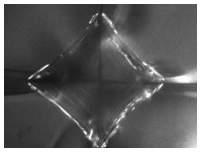
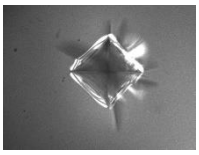
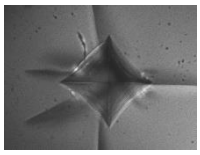
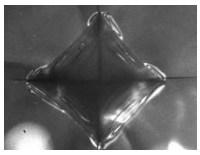


Figure 4.25 Vickers hardness results of H-SLS glasses

Hardness values of chemically strengthened samples which are CS, W+CS, CS+W and W+CS+W are found as 571±13, 554±18, 558±40 and 561±15 HV, respectively. Considering the hardness values of chemically strengthened samples, measured differences are found to be in the standard deviation range, therefore these samples are considered to have similar surface hardness values.

Captured images of indentation zones for six different conditions of H-SLS glasses under different loads are presented in Table 4.2.

Table 4.2 Representative indentation images of H-SLS glasses for crack formation determination

Sample Name	Indentation Image (500g)	Indentation Image (1000g)	Indentation Image (2000g)
H-SLS-PR			
H-SLS-W			
H-SLS-CS			
H-SLS-W+CS			
H-SLS-CS+W			
H-SLS-W+CS+W			

Indentation images of H-SLS glasses show that except for CS and W+CS conditions, crack formation starts under 500 g indentation loading. However, CS sample manages to survive 1000 g loading. Similar to L-SLS glasses, independent from the applied process conditions an overall increase in crack formation is observed under 2000 g loading for H-SLS glasses.

4.1.26 Hardness and Crack Formation Results of AS Glasses

Surface hardness of AS glasses are presented in Figure 4.26 and hardness values of PR and W conditions are found as 522 HV. Hardness value of pristine condition of AS glasses are higher than L-SLS glasses and H-SLS glasses. After chemical strengthening process, hardness values are found between 620-630 HV. Hardness increase of AS glasses after strengthening process is more efficient than L-SLS and H-SLS glasses. Also, decrease in surface hardness for chemically strengthened glasses is not observed after weathering test for AS glasses.

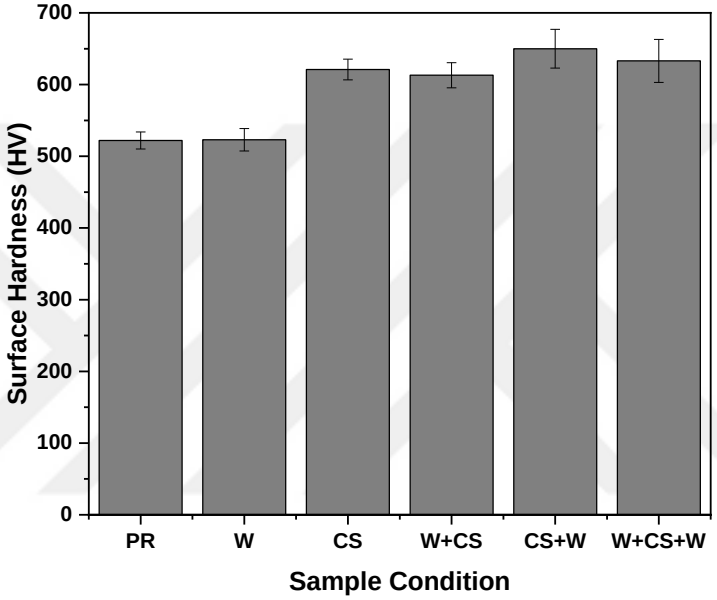
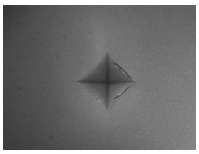
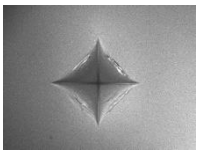
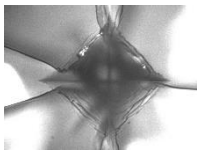
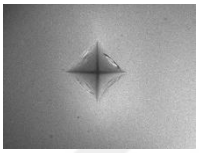
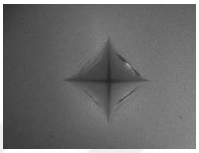
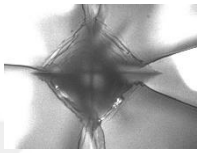
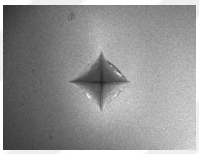
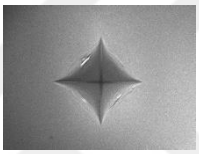
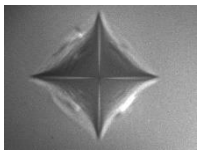
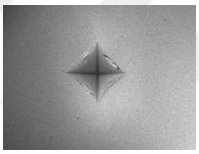
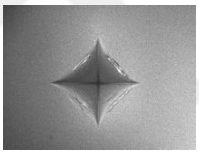
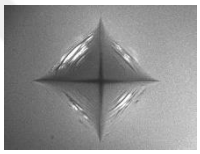
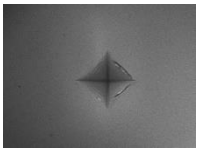
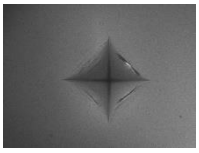
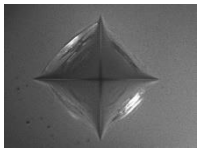
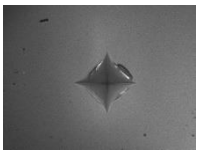
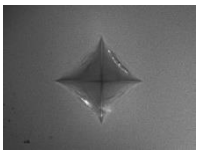
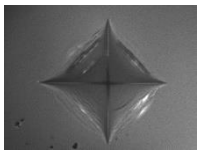


Figure 4.26 Vickers hardness results of AS glasses

Representative indentation images of AS glasses are demonstrated in Table 4.3. It is observed that AS glasses have superior cracking resistance compared to L-SLS and H-SLS glasses.

Table 4.3 Representative indentation images of AS glasses for crack formation determination

Sample Name	Indentation Image (500g)	Indentation Image (1000g)	Indentation Image (2000g)
AS-PR			
AS-W			
AS-CS			
AS-W+CS			
AS-CS+W			
AS-W+CS+W			

Representative images presented in Table 4.3 show that PR and W conditions of AS glasses are able to withstand cracking up to 1000 g loading and crack formation starts at 2000 g for these conditions. Images prove that chemically strengthened AS glasses are crack-resistant even under 2000 g of indentation loading, but severe chippings are detected on the edges of indentations.

4.2 Discussion

4.2.1 Evaluation of Visual Appearance of Glasses

Surface images obtained by polarizing microscope for L-SLS, H-SLS and AS glasses under different experimental conditions are demonstrated comparatively in Figure 4.27. Optical micrographs of AS glasses prove that weathering and chemical strengthening has no significant effect on appearance of samples no matter if applied individually or in combination. Comparison of micrographs of pristine (PR) soda-lime silicate glasses with weathered samples (W) reveals that weathering has a minor influence on the microscopic appearance of L-SLS and H-SLS samples. It is very well-known that when soda-lime silicate glasses are exposed to water vapor, sodium ions and some low amount of calcium and magnesium ions present in the glass matrix diffuse out from the surface and H^+ or H_3O^+ ions diffuse into the bulk. As a result of ion-exchange reactions, surface pH increases and this is followed by dissolution reactions which lead to deterioration of surface morphology and decrease in the optical quality [14], [84]. Similar to this phenomenon, formation of white stains is observed on weathered (W) soda-lime silicate glass surfaces. On the other hand, for chemically strengthened (CS) soda-lime silicate samples no significant change is observed on sample appearance. Furthermore, among different chemically strengthened L-SLS and H-SLS glasses, surface appearance of W+CS samples is not affected by weathering, while a major effect of weathering is observed from the micrographs for CS+W and W+CS+W samples that can also be easily detected by naked eye in the form of an iridescent pattern. The iridescence appearance due to the formation of alteration layer after weathering or corrosive attack is also reported in different studies [84]–[87], however this phenomenon is not fully understood or explained for chemically strengthened soda-lime silicate glasses.

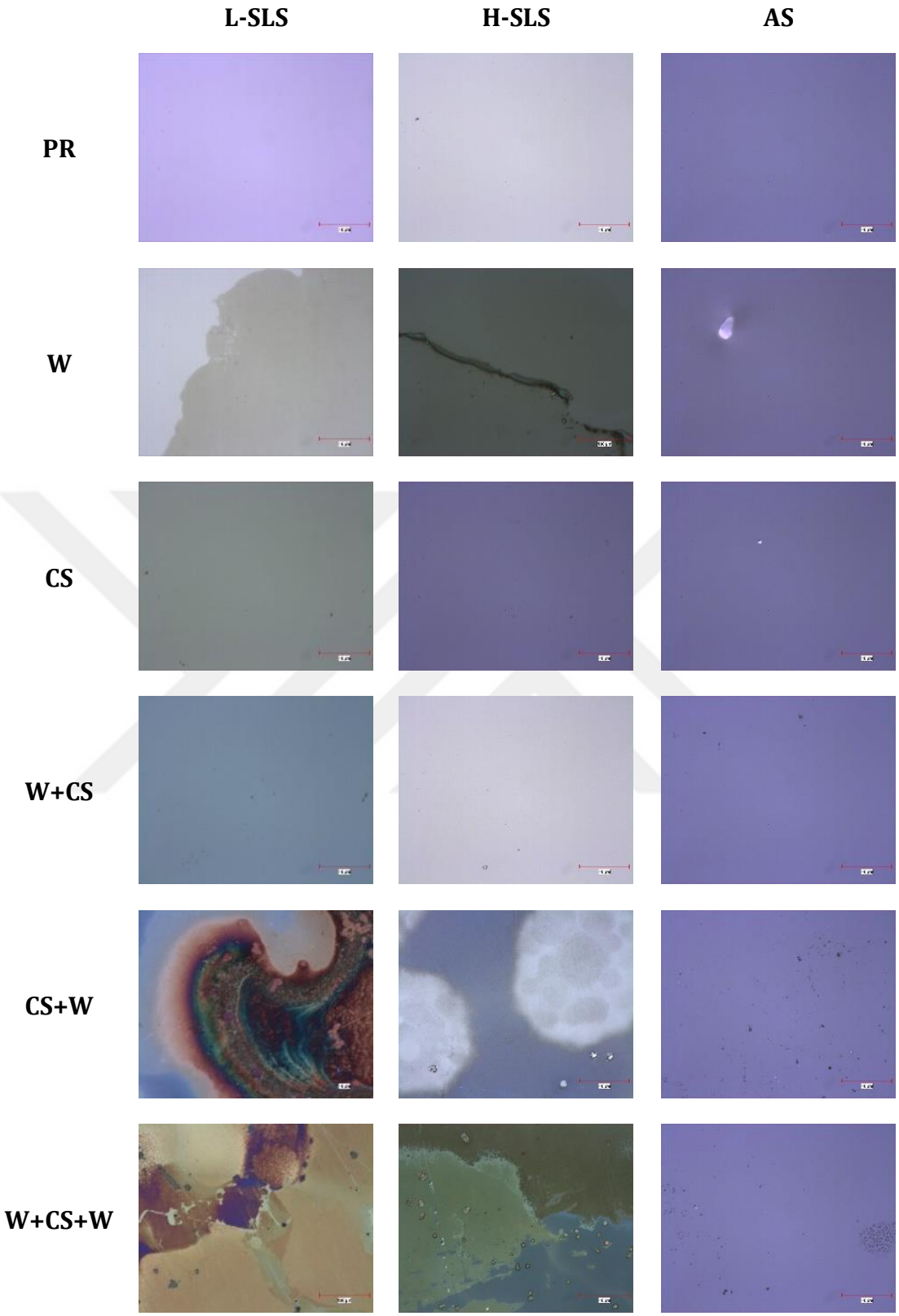


Figure 4.27 Optical microscope images of glass surfaces under 500X magnification for different experimental conditions

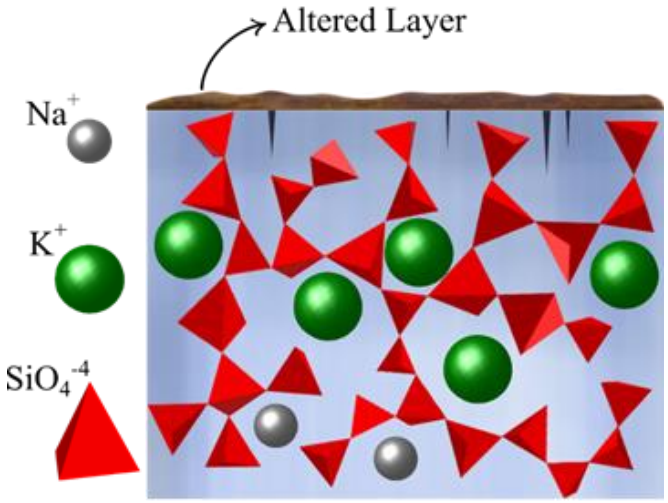


Figure 4.28 Illustration of alteration layer on the weathered glass surface

Common opinion is that, alteration layer formation due to weathering with nonuniform thickness and refractive index, causes interference effects which leads to an interplay of changing colors [87], [88] and shows itself in the macro scale, in our case as blue and brown colors (see Figure 4.28). The observed color change is thought to be dependent on the thickness of alteration layer and incident angle of light beam on the glass surface.

4.2.2 Interpretation of Topographical Changes

When glass is exposed to corrosive environments such as weathering, its surface undergoes some topographical changes that may influence the optical and mechanical characteristics of glass [89]. Therefore, it is quite crucial to observe the topographical changes of glasses operating under corrosive conditions. It is known that the topographical changes usually alter the roughness of glass surface. In this study, surface roughening can be caused by two possible scenarios: i) leaching and dissolution reactions originating from weathering process, ii) immersion of the glass sample into molten salt at high temperatures during chemical strengthening process. The measured surface roughness values of rinsed glass samples under different experimental conditions are presented in Figure 4.29.

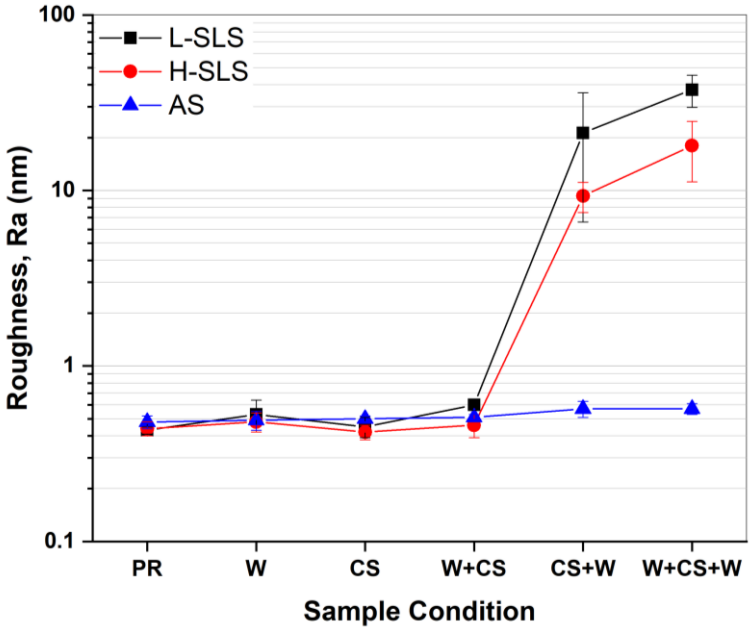


Figure 4.29 Comparison of surface roughness values of investigated glass types under different experimental conditions

It is evident from this plot that weathering or chemical strengthening do not cause a significant alteration on surface roughness if applied individually (for W and CS samples). Nonetheless, combinational processing of weathering and chemical strengthening leads to deterioration and roughening of the glass surface for L-SLS and H-SLS glasses. Roughness values of pristine conditions for all three glass types are found as 0.4 nm. However, due to weathering related roughening, roughness values reached up to 40 nm and 20 nm for L-SLS and H-SLS glasses, respectively. Roughness of AS glass surfaces does not experience an increase after exposure to weathering.

To better understand surface topographical changes of samples processed by applying weathering in combination with chemical strengthening, i.e. W+CS, CS+W and W+CS+W, images obtained by WLI analysis are given in Figure 4.30. For L-SLS glasses under W+CS condition, initial stage of alteration layer formation begins and dendritic (leaf-like) deposits are detected similar to some reports in the literature [90].

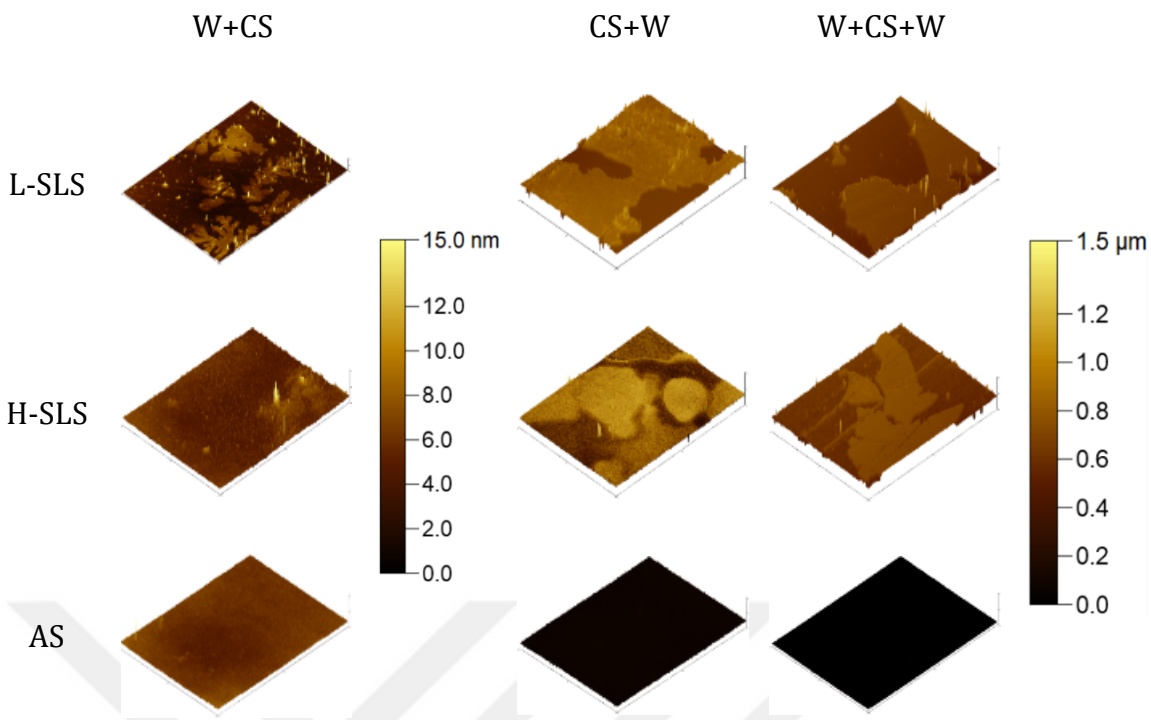


Figure 4.30 Comparison of surface topographical images obtained by WLI for investigated glass types under combinational processing conditions

Additionally, comparing with W+CS condition, if chemically strengthened samples are exposed to weathering afterwards, roughening of the glass surface appears to be more severe. The glass surface of PR samples has approximately 0.4 nm of Ra value, however for L-SLS and H-SLS glasses the Ra value reaches to an average of 20 nm especially for CS+W and W+CS+W conditions. This increase in roughness is attributed to leaching and dissolution related alteration layer formation in soda-lime silicate glasses, which also confirms the explanation of the iridescence pattern of some specific samples. Furthermore, it is observed that the increase in roughness is more pronounced for L-SLS glasses than H-SLS glasses. It should be also noted that W+CS+W condition shows a higher increase in roughness values than that of CS+W condition for both L-SLS and H-SLS glasses. As for AS glasses, no meaningful change in the surface roughness is detected since these glasses are chemically more stable and does not undergo leaching and dissolution reactions. Thus, for AS glasses no alteration layer occurs, and surface remains unchanged.

Further topographical studies are realized by AFM analysis for detailed and sensitive investigation of layer formation behavior of L-SLS glasses and obtained 3D

maps for CS+W and W+CS+W conditions are demonstrated in Figure 4.31. These two samples are selected for AFM investigations due to their significantly higher roughness values detected by WLI measurements.

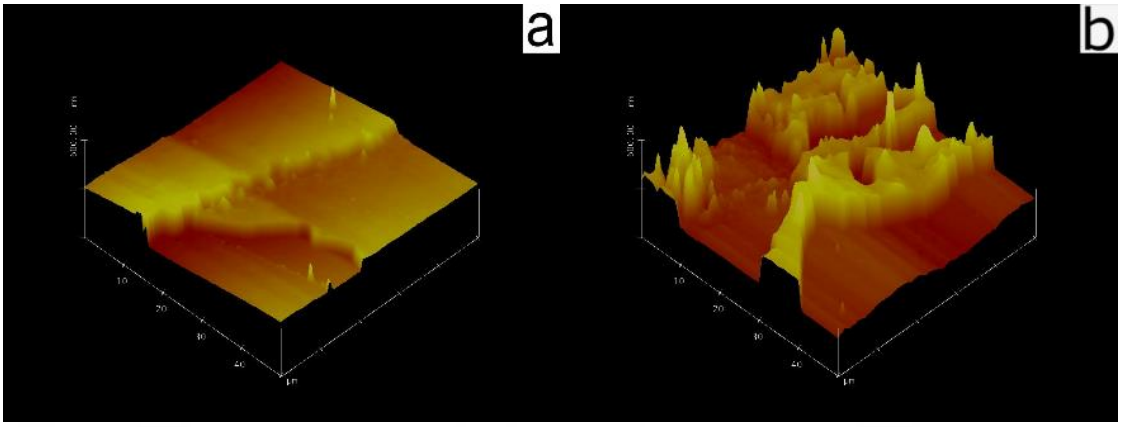


Figure 4.31 Surface topographical maps obtained by AFM for a) L-SLS-CS+W sample and b) L-SLS-W+CS+W sample

Post processing of AFM images given in Figure 4.31a and Figure 4.31b reveals that alteration layers may reach up to 100-400 nm of difference in altitude from the surface base point. Evaluating topographical findings together with optical microscopy images, it can be said that chemical strengthening has negative impact on the weathering resistance of L-SLS and H-SLS glasses (for CS+W and W+CS+W condition) and eases the formation of alteration layers caused by glass-water interaction. In the case of L-SLS glasses for CS+W and W+CS+W conditions, layer formation is accelerated, spreads to larger areas and layer thickness increases. The varying thickness of these several layers causes lustrous interplay of various colors on the sample surface (see Figure 4.1). On the other hand, surface topography of AS glasses remains unchanged even after combinational processing (for W+CS, CS+W and W+CS+W conditions) and no visible change is observed in the macro scale.

4.2.3 Evaluation of Optical Changes

Transmission spectra of L-SLS, H-SLS and AS glasses under different experimental conditions are given in the visible range in Figure 4.32, Figure 4.33 and Figure 4.34, respectively.

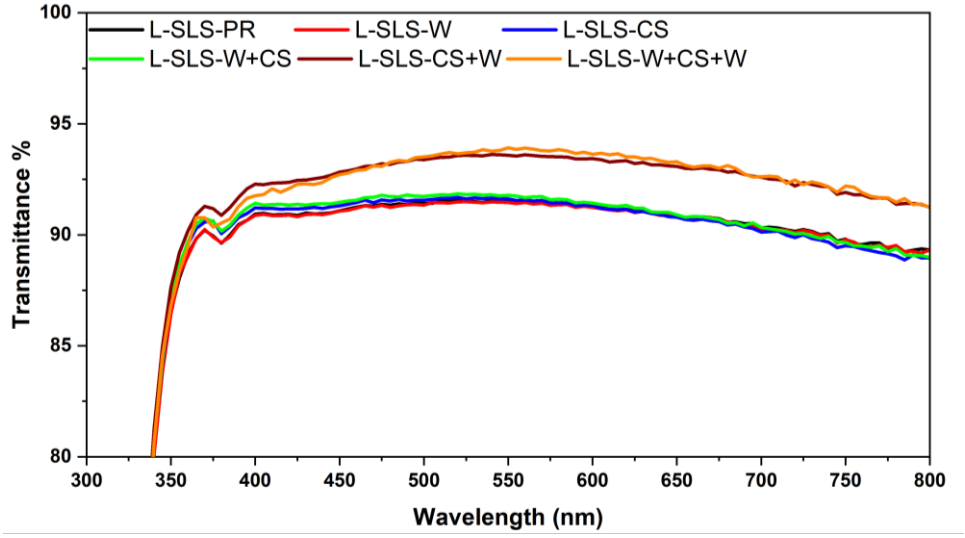


Figure 4.32 Transmittance spectra of L-SLS glass in the visible range of the spectrum

In general, transmittance values of pristine L-SLS, H-SLS and AS glasses are found to be quite similar. However, higher Fe_2O_3 impurities in the chemical compositions of L-SLS and H-SLS glasses (see Table 3.1) cause a broad absorption band towards 1050 nm which is absent for AS glasses because of their higher purity. Optical transmittance of L-SLS glasses for W, CS and W+CS conditions are found to be alike with the PR condition, whereas CS+W and W+CS+W samples show slightly higher transmittance values appearing as a 2-2.5% increase at 550 nm. In general, H-SLS glasses exhibit an equivalent optical transmittance behavior to L-SLS glasses.

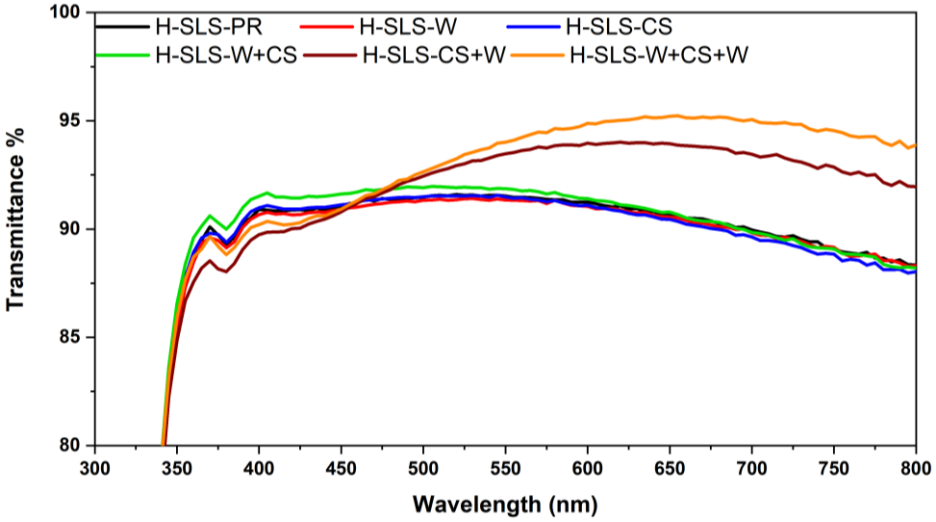


Figure 4.33 Transmittance spectra of H-SLS glass in the visible range of the spectrum

However, for AS glasses optical transmittance is not affected by weathering process for all experimental conditions.

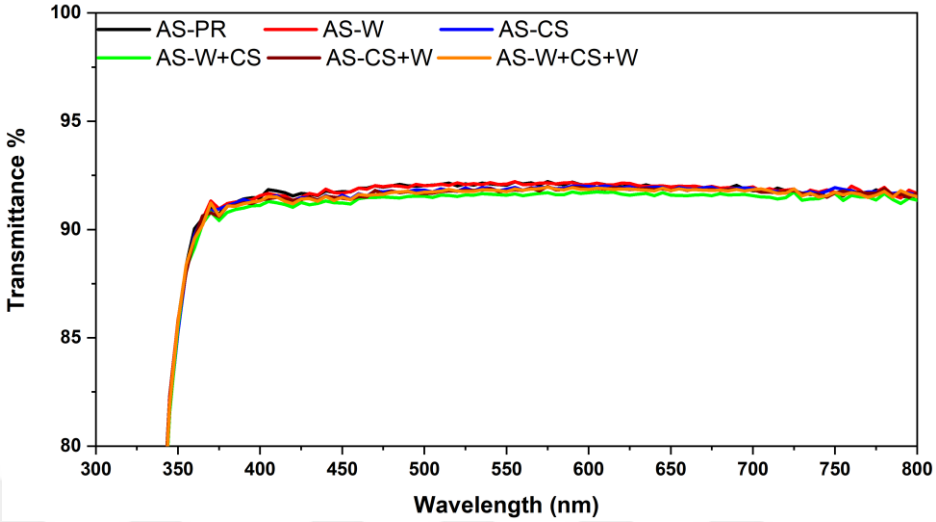


Figure 4.34 Transmittance spectra of AS glass in the visible range of the spectrum

Change in optical properties after secondary applications is mainly governed by the light-surface interaction. Therefore, increase of transmittance in the visible region for L-SLS and H-SLS glasses under CS+W and W+CS+W conditions is attributed to the modification of surface properties of the glass surface as a result of construction of an alteration layer. It is already reported in the literature that altered layers with lower refractive index and higher roughness than that of base glass act as antireflective coating and result a higher transmission in the visible region for such samples [84], [91]–[93].

4.2.4 Assessment of Depth Profiles

Weathering and chemical strengthening are both ion exchange reactions that alter the atomic concentrations of glass surface. Therefore, tracking the atomic concentration differences of the glass surface gives crucial information about the weathering behavior of chemically strengthened glasses. Since L-SLS glasses are more prone to water attack, weathering related ion exchange reactions are more intense and easily detectable. Therefore, TOF-SIMS analysis are conducted for pristine and chemically strengthened L-SLS glasses and comparison of alkali ion intensities are given in Figure 4.35.

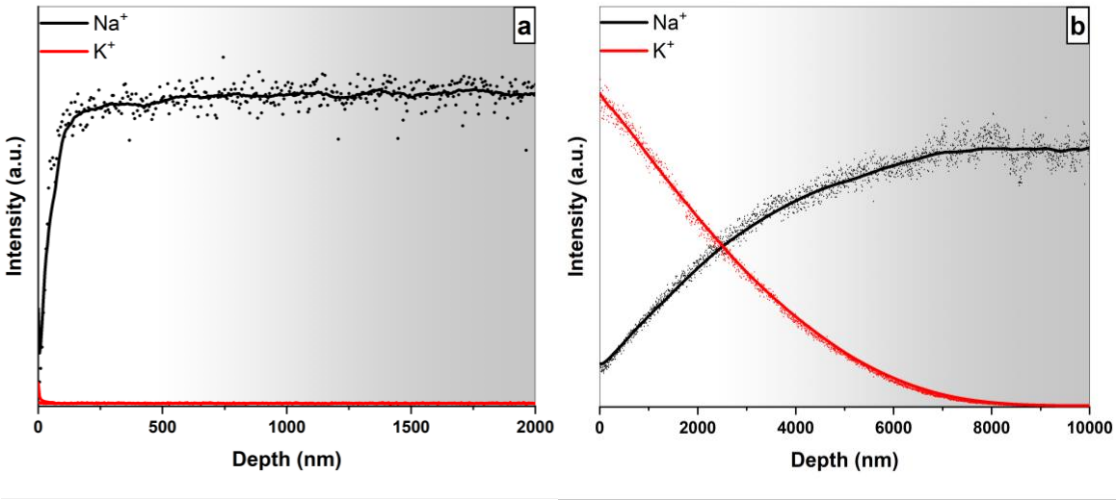


Figure 4.35 Alkali ion profiles of a) L-SLS-PR sample and b) L-SLS-CS sample

The depth profiles show that pristine L-SLS glass shows a constant signal of sodium ions along the bulk structure. Additionally, pristine L-SLS glass does not contain any potassium ions, therefore K^+ signal is not detected. After immersion into molten KNO_3 salt bath, potassium ions diffuse into the glass matrix, while sodium ions diffuse out from the bulk glass as a result of concentration difference of alkali ions between glass and salt. Therefore, potassium ions show maximum concentration on the glass surface and the concentration gradually decreases through the bulk. On the other hand, for sodium ions the concentration increases from surface through bulk. It can be seen from Figure 4.35b that potassium ions reach approximately a depth of 8 µm and simultaneously at this depth the increase of sodium concentration is concluded.

Surface alkali concentration comparisons, in this work given as K/Si intensity (see Figure 4.36), differentiate depending on the weathering condition of chemically strengthened samples. The sample that is not exposed to weathering (CS) shows the maximum K/Si intensity, while a decrease is observed for samples processed by applying weathering in combination with chemical strengthening (W+CS and CS+W). CS+W sample has the lowest concentration of K^+ among all weathered and chemically strengthened samples.

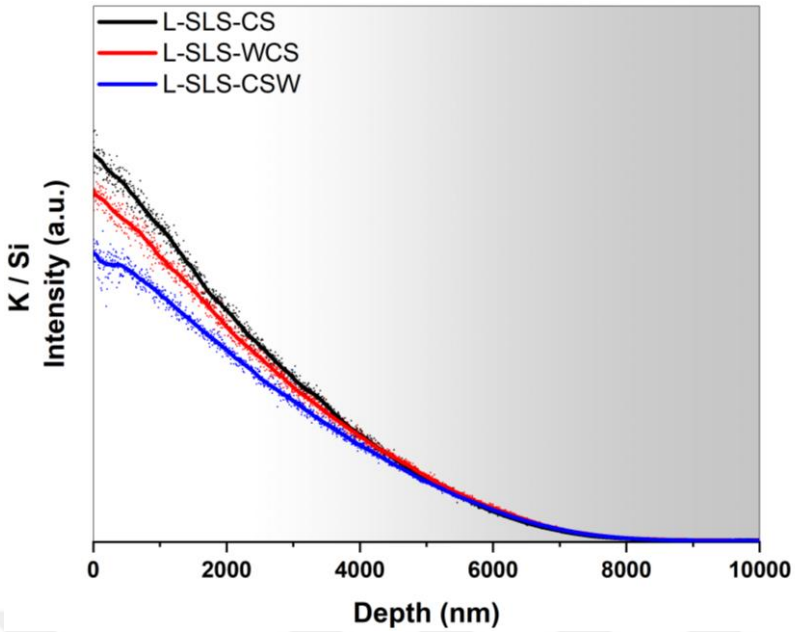


Figure 4.36 Comparison of K^+ profiles of chemically strengthened L-SLS glasses

A similar behavior is observed for relatively large and less mobile alkaline earth ions (see Figure 4.37a and Figure 4.37b), where Mg^{2+} and Ca^{2+} ion intensities of CS samples are compared with W+CS and CS+W samples. It can be seen that Mg^{2+} concentration profile changes for CS+W sample and a depletion of Mg^{2+} ions is observed to a depth of approximately 1.5 µm.

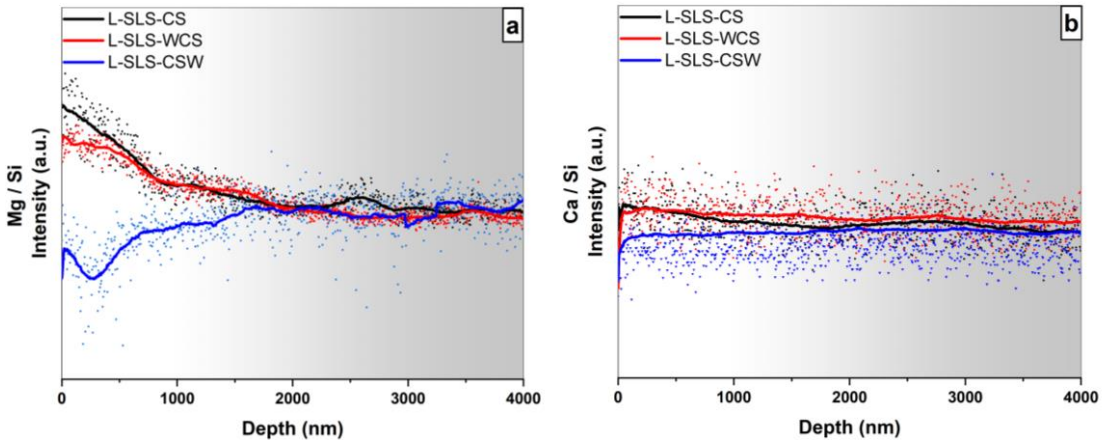


Figure 4.37 Alkali-earth ion profiles of chemically strengthened L-SLS glasses a) Mg^{+2} profiles and b) Ca^{+2} profiles

In addition, for Ca^{2+} ions a weak depletion is also noticed in CS+W sample. Therefore, it is concluded that, after chemical strengthening process larger K^+ ions dominate the glass surface and when these larger ions are leached-out from the network, they

leave larger voids behind than Na^+ depletion [94]. This facilitates the water diffusion and corrosion reactions, therefore affecting the weathering behavior of glass [95].

4.2.5 Fourier Transform Infrared Spectra

Silicate glass structure is made of central silicon ions surrounded by four coordinating oxygen ions, namely tetrahedral structural units [14], [23], [96], [97]. These tetrahedral units provide the structural integrity of silicate network that is comprised of Si–O–Si bonds. The oxygen anion here bonded to two network forming Si^{4+} ions is called bridging oxygen (BO). Q_n depicts the fraction of BO's in the silicate structure, where n (n = 0, 1, 2, 3, 4) represents the number of BO per tetrahedron (see Figure 4.38). Tetrahedral silicate units are consisting of four BO's and that is expressed as Q_4. Introducing network modifier ions to the glass network or penetration of water to glass structure (weathering) leads to breakage of these bonds and consequently formation of $Si–O^-$ bonds. The oxygen anion in these $Si–O^-$ bonds is called non-bridging oxygen (NBO) and this leads to decrease of number n.

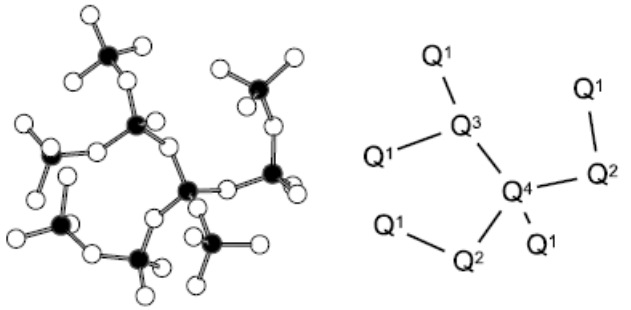


Figure 4.38 Representation of a glass network containing different Q^n structure units

Si–O–Si and $Si–O^-$ bonds have different absorption peaks in the IR region because of their different vibration energies. IR spectrum of a typical soda-lime-silicate glass is demonstrated in Figure 4.39 with main vibration modes and related wavenumbers. In addition, main vibrational peaks for silicate glasses are summarized in Table 4.4 [98]–[101].

Table 4.4 FTIR band assignments for silicate glasses

Wavenumber (cm^{-1})	Band	Assignment
930-950	ν_{Si-O^-}	Si–NBO stretching
1050-1100	$\nu_{Si-O-Si,as}$	Si–O–Si asymmetric stretching

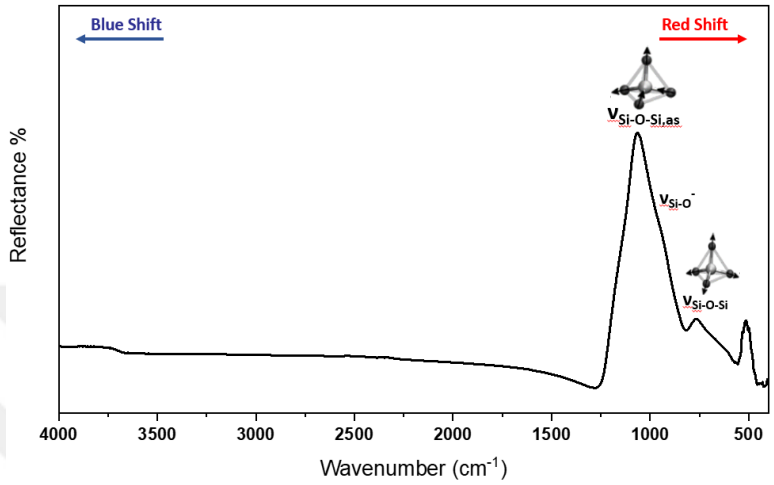


Figure 4.39 IR spectrum of soda-lime-silicate glass demonstrating the main vibration modes and related wavenumbers

Structural changes of the glass network arising from weathering and chemical strengthening processes are monitored by FTIR spectroscopy and the recorded reflectance spectra are given in Fig. 4.40a-c in the spectral range of 1300-700 cm^{-1} to observe the main vibrational peaks. Structural changes in the glass network are detected by the change of the peak intensities and shift in peak positions of the specific vibrations through red or blue region.

In this study, asymmetric stretching vibration peak of Si–O–Si bonds ($\boldsymbol{\upsilon}_{Si-O-Si,as}$) appears at 1064 cm^{-1}, 1060 cm^{-1} and 1048 cm^{-1} for pristine L-SLS, H-SLS and AS glasses, respectively.

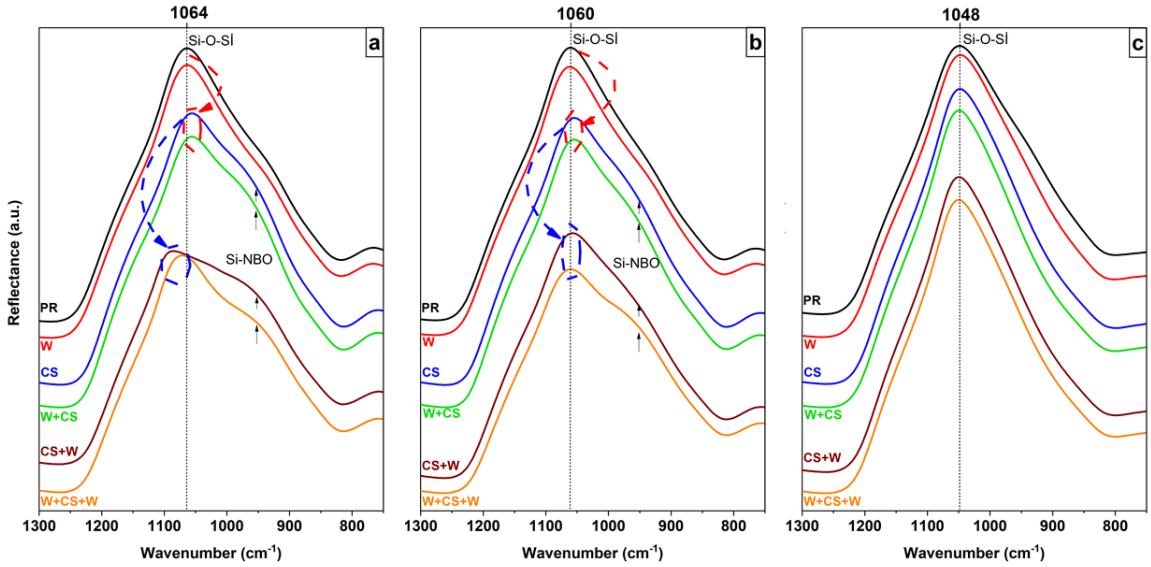


Figure 4.40 Comparison of main vibrational peak positions and intensities of a) L-SLS glasses, b) H-SLS glasses and c) AS glasses

Comparison of the FTIR spectra of L-SLS and H-SLS glasses for different experimental conditions reveal that main vibrational peak positions remain unchanged in W samples with respect to PR samples, indicating that weathering does not cause a detectable change in glass structure due to glass-water interactions. On the other hand, a red shift in $\boldsymbol{\upsilon}_{\text{Si-O-Si,as}}$ peak positions is detected for CS and W+CS samples which is thought to be induced by the increase of Si–O bond lengths surrounding the larger K^+ ions [102] and decrease of bond angles due to generated compressive stress [103]. Moreover, surface alkali concentration increase due to treatment in molten KNO_3 contributes to the clear appearance of the band at around 950 cm^{-1} for CS and W+CS samples [101]. It is also observed that, exposure to weathering after chemical strengthening causes striking structural changes. Comparing the $\boldsymbol{\upsilon}_{\text{Si–O–Si,as}}$ peak positions of CS+W and W+CS+W conditions with CS sample, a blue shift is observed and the peak intensities show a decrease. Along with peak shifting, the shoulder appeared at around 950 cm^{-1} increases in intensity for these conditions and it is assigned to Si–NBO vibrations in the glass network. Glass corrosion induced by leaching solutions, aqueous environments or humid environments have been reported to cause a blue shift of the IR spectrum and decrease the peak intensity of Si–O–Si stretching vibrations [2], [91], [104]–[107] and also peak intensity of Si–NBO vibrations increases in IR spectrum owing to

dissolution of Si–O–Si network by hydroxyl groups [108]. As reported by Hench and Clark [109], prominence of Si–NBO band and significant shifting in $\boldsymbol{\upsilon}_{\text{Si–O–Si,as}}$ peak indicates that accumulated leaching products lead to network dissolution as a result of second step reactions of the glass corrosion by increasing the pH level of the surface. It is known that K^+ can be detached easily than Na^+ because of its lower bonding energy originating from the higher ionic radii. Thus, leaching rate of the K^+ is reported to be faster than Na^+ [110]. In sodium aluminosilicate glasses, however, apart from the bonding energy differences, introduction of Al_2O_3 to the glass composition leads to formation of AlO^{4-} structural groups and some of the sodium ions are immobilized by being bonded to these groups [111]. Also compositional modification via substitution of Al_2O_3 by alkali/alkali earth oxides reduces the NBO sites of glass structure and results in an increased leaching and dissolution resistance [23], [25], [98], [112]. Therefore, peak positions of AS glasses are found to be almost identical for all conditions. It is known that glass corrosion is sensitive to the chemical composition of the glass, more precisely it is related to the amount of NBO sites in the network. It is reported that increase in NBO sites accelerates the weathering by facilitating the ion mobility. Therefore compared to SLS glasses weathering rate of AS glasses are expected to be rather slower due to reduced NBO sites [63]. Consequently, FTIR results show that, weathering affects the peak positions differently depending on the processing sequence. Application of weathering before chemical strengthening causes no detectable change on the peak positions, however when weathering is followed by chemical strengthening $\boldsymbol{\upsilon}_{\text{Si–O–Si,as}}$ band shifts towards higher wavenumbers and intensity of Si–NBO band shows an increase. Both changes occur as a result of weathering-induced alteration of surface.

4.2.6 Generation of Stress Profiles

Compressive stress and depth of layer values of L-SLS, H-SLS and AS glasses under different experimental conditions are given as stress profile plots in Figure 4.41a-c.

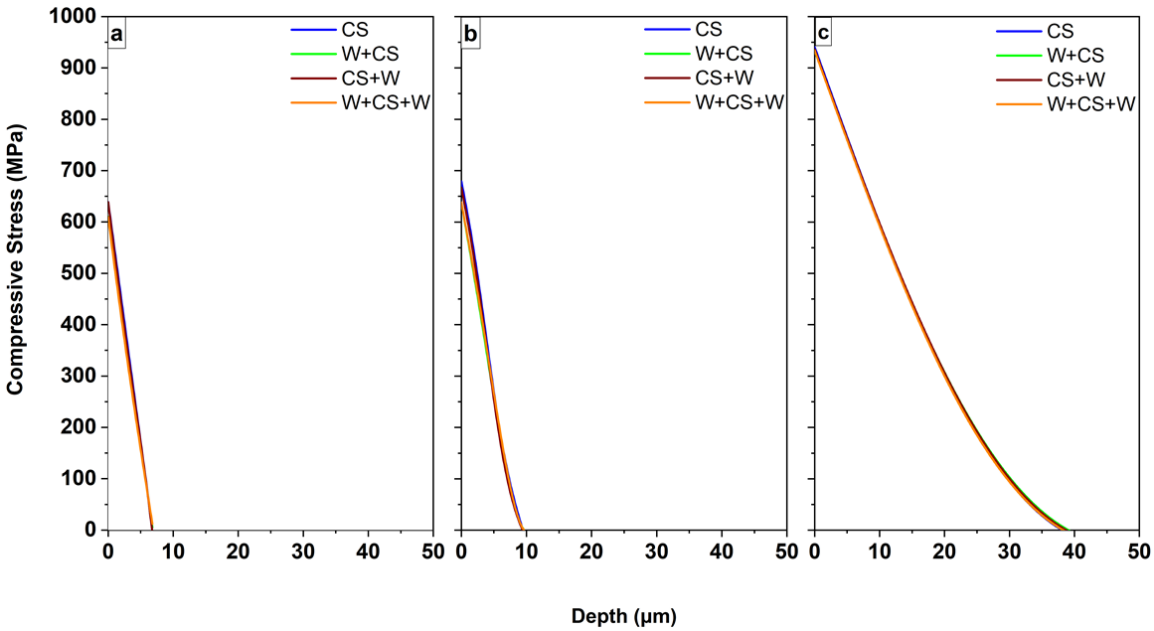


Figure 4.41 Comparison of stress profiles of a) L-SLS glasses, b) H-SLS glasses and c) AS glasses

In general, generated compressive stress values gradually decrease from surface to the bulk due to the nature of diffusion process. Stress profiles show that AS glasses have the highest values of compressive stress with 940 MPa and depth of layer (DOL) with 40 μm without being significantly affected by weathering due to improved Na^+ mobility and network connectivity by higher Al_2O_3 content [52], [113], [114]. The AS samples are followed by H-SLS and L-SLS samples, respectively both for compressive stress and DOL values. For L-SLS and H-SLS glasses, the maximum compressive stress reaches to 640 MPa and 680 MPa on the surface and depth of layer values are detected as 6.8 μm and 9.5 μm, respectively. For chemically strengthened soda-lime silicate glasses, stress decrease shows a linear path revealing that no structural relaxation occurs due to high temperature or extended tempering periods. In the presence of liquid water or water vapor atmosphere, surface flaws grow and require higher strength values for being suppressed. Therefore, when glass samples are exposed to weathering prior to chemical strengthening substitution of sodium ions by H^+/H_3O^+ ions confines stress generation via chemical strengthening [115]. It is observed that compressive stress values decrease to 610 MPa and 640 MPa for L-SLS and H-SLS glasses, respectively, whereas no decrease is detected in the DOL values.

4.2.7 Determination of Fracture Probability

The data collected from ring-on-ring tests are evaluated via Weibull distribution and generated Weibull plots are given in Figure 4.42, Figure 4.43 and Figure 4.44 with a 95% confidence interval for L-SLS, H-SLS and AS glasses, respectively. Each line in the Weibull plot presents the failure probability as a function modulus of rupture (MOR) or lnσ for a specific sample condition. The slope of the line is proportional with the reliability of the data series. Lower deviation in the data series increases the slope of the line. Weibull plots enables us to describe the fracture probability of the glass for a given load in MPa's, thus makes the interpretation of the data safer and more accurate than interpretation based on the average modulus of rupture and standard deviation values.

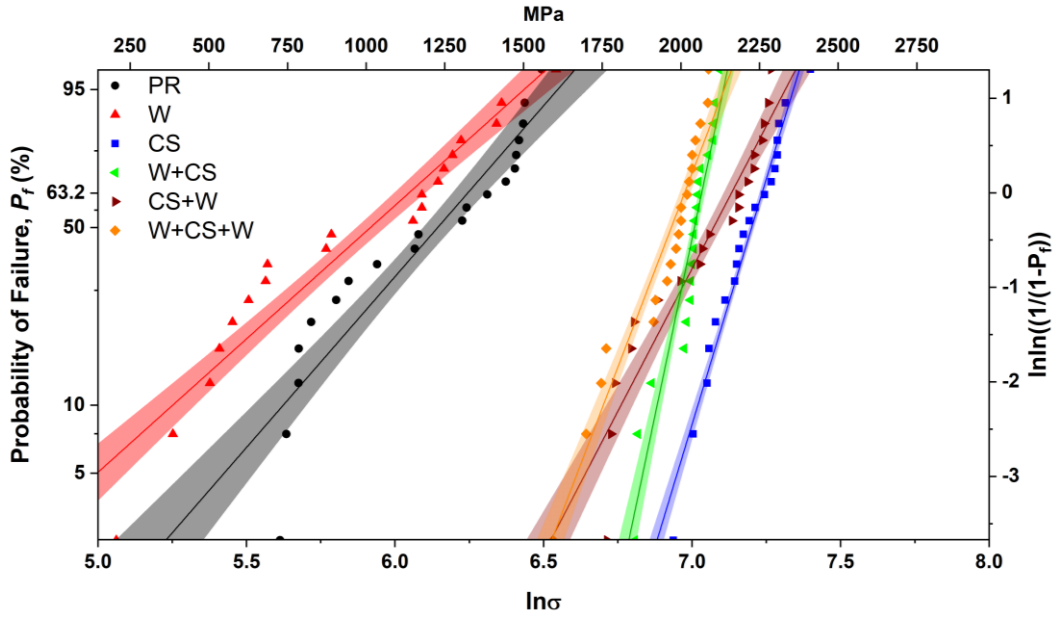


Figure 4.42 Weibull plot of L-SLS glasses under different experimental conditions

Weibull plots of SLS glasses reveal that W condition exhibits the lowest mechanical performance based on the 50% of failure probability, while CS condition exhibits the highest mechanical performance. Furthermore, pristine L-SLS and H-SLS glasses are considerably affected from the weathering process.

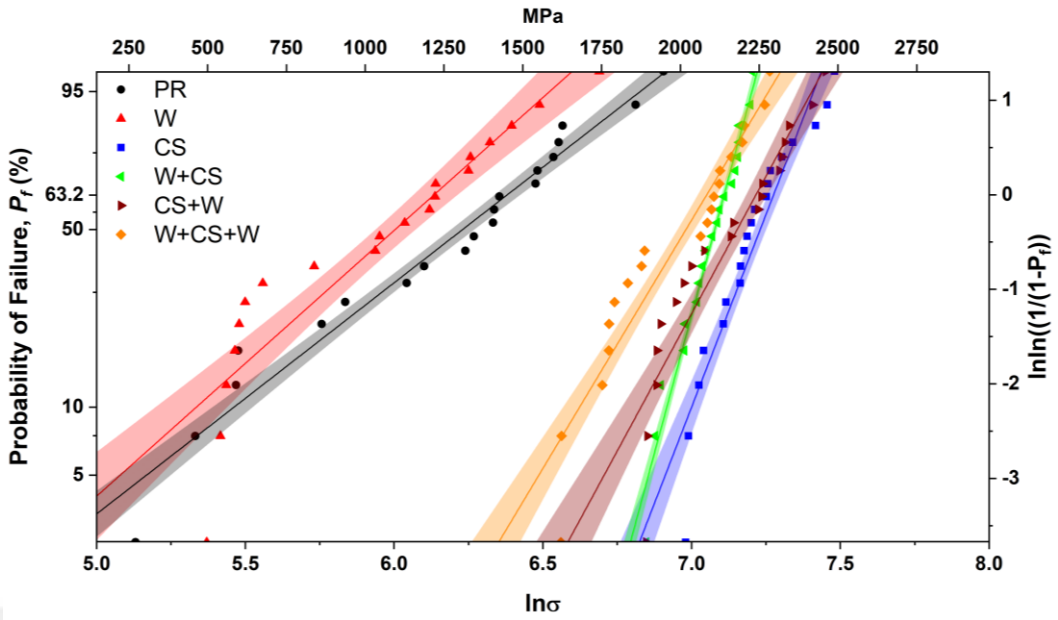


Figure 4.43 Weibull plot of H-SLS glasses under different experimental conditions

The degree of decrease in strength varies depending on the sequence of applied process condition: if weathering is applied before chemical strengthening the decrease in glass strength is more pronounced since a portion of the generated compressive stress is spent to heal already grown flaws. For L-SLS and H-SLS glasses, even though FTIR spectra of CS+W and W+CS+W samples indicate network dissolution which also contributes to crack growth, generated compressive stress tolerates the stress corrosion and results higher strength values than W+CS condition.

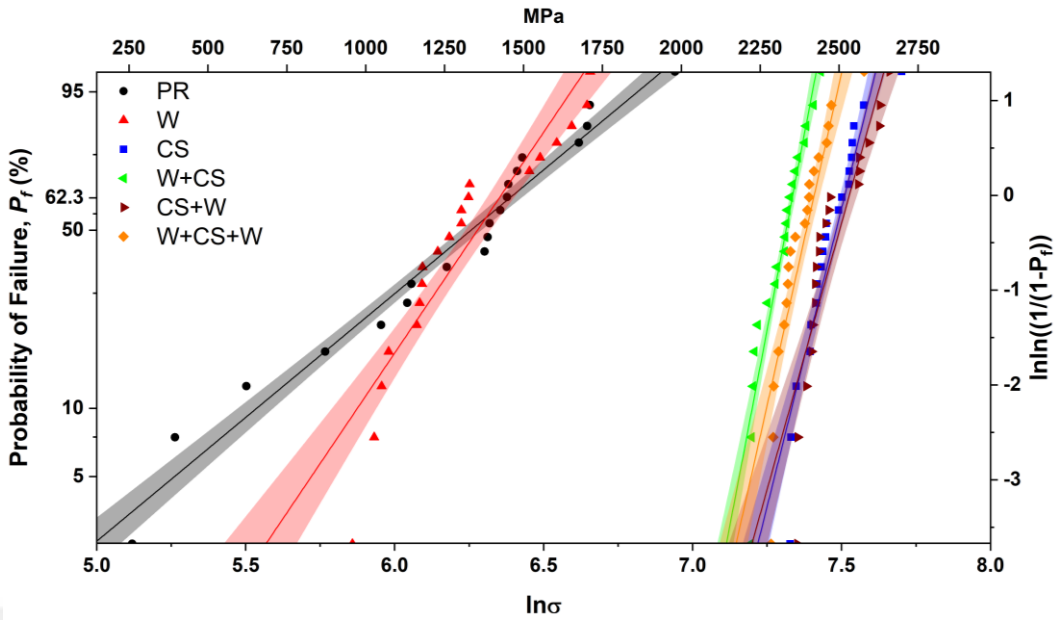


Figure 4.44 Weibull plot of AS glasses with different experimental conditions

It has already been pointed out that slope of each line is proportional to the reliability of the data series. Within this context, it is observed that chemically strengthened AS glasses exhibit significantly higher slopes than that of chemically strengthened L-SLS and H-SLS glasses. Higher reliability or higher accuracy in ring-on-ring test means that extremely low and extremely high fracture loads are absent for these data series. This indicates that crack propagation velocities of all conditions and each sample under applied load are uniform.

4.2.8 Determination of Surface Hardness

Figure 4.45 depicts the variation of Vickers hardness values of different glass samples under different experimental conditions. Pristine L-SLS, H-SLS and AS glasses have hardness values of 490±7 HV, 507±12 HV and 522±12 HV, respectively.

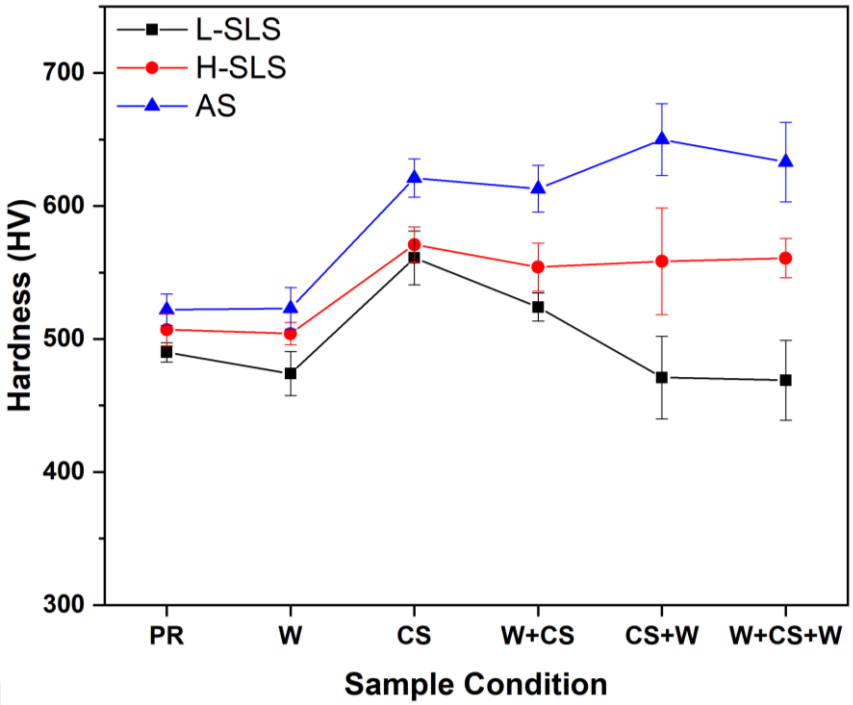


Figure 4.45 Comparison of surface hardness values for three different glass types under different experimental conditions

As the Al_2O_3 content increases in glass structure, network connectivity is promoted and thus hardness of the glass increases accordingly. Upon exposure to weathering, a slight decrease in hardness values is observed — reaching up to 20 HV for W condition of L-SLS glasses. Despite the decreasing effect of weathering on hardness, it is determined that generated compressive stress after chemical strengthening results an increase in the hardness values. Concerning W+CS condition, the increase in hardness is much limited compared to CS condition, especially for SLS glasses, because of lower compressive stress values (see Fig. 4.18). Generally, higher compressive stress results higher hardness values. Comparing compressive stresses, it is observed for SLS glasses that CS+W samples have higher compressive stress on the surface than W+CS and W+CS+W samples (see Fig. 4.18 and Fig. 4.19). However, this trend seems to be violated for chemically strengthened L-SLS glasses when weathering process is introduced. Although the compressive stress values of CS+W samples are higher than W+CS samples, surface hardness values are found to show an opposite trend. In weathered glasses, the altered layers are known to be mainly composed of carbonate and sulphate structures [14], [84] which have lower hardness values than glass surface — especially lower than chemically strengthened

glass surface. Formation of these alteration layers are observed both for L-SLS and H-SLS glasses. Influence of alteration layers on surface hardness is found to be the most intense for CS+W and W+S+W conditions of L-SLS samples, mainly caused by the great amount of layer formation. Contrarily, chemically strengthened H-SLS and AS glasses have not experienced a decrease in hardness after exposure to weathering thanks to improved network connectivity by higher Al_2O_3 content.

4.2.9 Determination of Cracking Probability

Post-contact indentation crack formation probabilities are determined by monitoring Vickers hardness measurements and crack formation behavior of chemically strengthened samples are compared in Figure 4.46, Figure 4.47 and Figure 4.48 for 500g, 1000g and 2000g of loads, respectively.

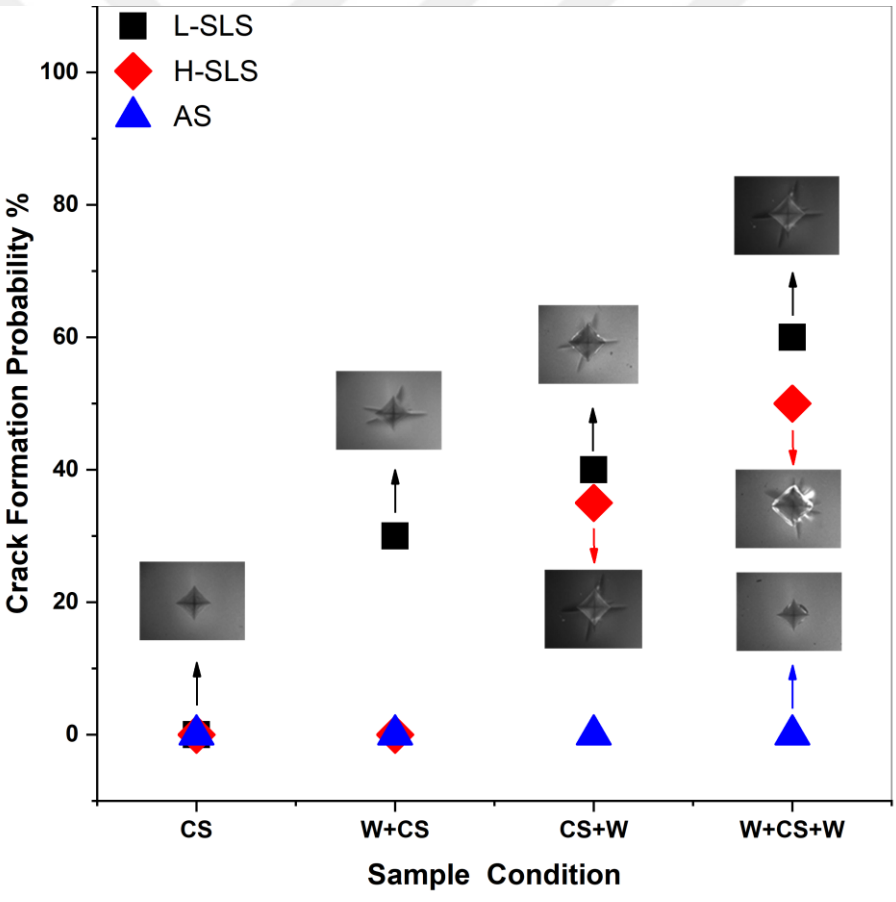


Figure 4.46 Crack formation probability of chemically strengthened glasses under 500g of load

In general, the plots illustrate that AS glasses show the lowest crack formation probability, while L-SLS glasses exhibit the highest probability of cracking. On the other hand, H-SLS glasses are found to be rather resistant to cracking compared to L-SLS glasses. Under 500 g indentation load (see Figure 4.46), for all glass compositions CS samples are the most resistant to cracking. Moreover, for L-SLS and H-SLS glasses cracking probability of samples processed by applying weathering in combination with chemical strengthening (W+CS, CS+W and W+CS+W) shows an increase, while no significant change is observed for AS glasses. In addition, if weathering is to be applied after chemical strengthening (for CS+W and W+CS+W) increase of cracking probability is more pronounced. Therefore, 500g is determined as the threshold load for crack formation of L-SLS and H-SLS glasses.

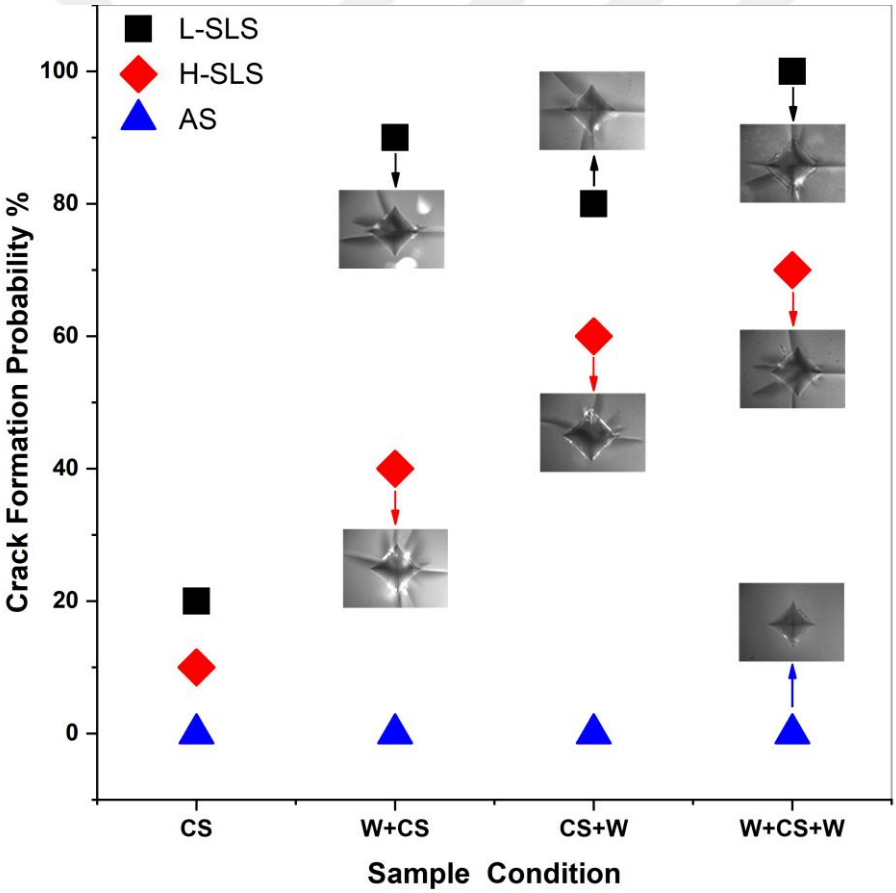


Figure 4.47 Crack formation probability of chemically strengthened glasses under 1000g of load

A similar behavior is observed for 1000 g indentation load (see Figure 4.47). Under 1000 g load CS samples are the most resistant to cracking for SLS compositions,

while AS glasses show no cracking for all conditions. It is also observed that, for CS and W+CS conditions of L-SLS glasses crack lengths show an average value of 125±15 μm, while for CS+W and W+CS+W samples these values reach up to 200±10 μm. This implies that for chemically strengthened L-SLS glasses as a consequence of exposure to weathering, water penetration into glass surface introduces flaws and facilitates the crack propagation as also reported by Gross et al [116]. Additionally, measured average crack lengths of H-SLS samples are in the level of 120±5 μm and found to be similar for all conditions. Under 2000 g indentation load, chemically strengthened L-SLS glasses show100% of cracking probability for all conditions (see Figure 4.48). H-SLS glasses, on the other hand, exhibit much higher crack resistance. However, exposure of H-SLS glasses to weathering results a decrease in this resistance. Indentation tests reveal that chemically strengthened AS glasses can withstand up to 2000g without cracking even if the glass is exposed to weathering.

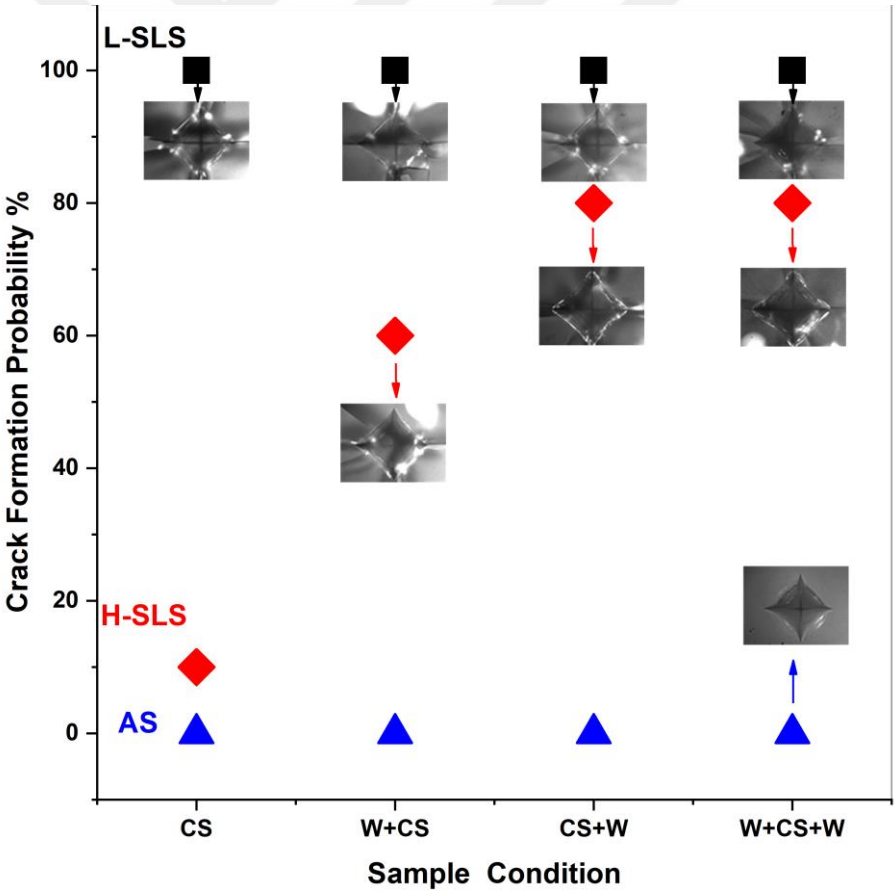


Figure 4.48 Crack formation probability of chemically strengthened glasses under 2000g of load

Significant difference in the crack formation probabilities of glasses are attributed to composition dependent mechanical properties. A material's response to the sharp contact is strongly influenced by the deformation mechanism. Rouxel et al. [81] indicated that indentation driven displacement of the material with a definite volume should be accommodated by the vicinity of indentation which results with densification, shear flow or phase transformation. Gross [117] reported that NBOs in the glass structure decreases free volume that favors shear flow mechanism under sharp contact loading. Since Al_2O_3 promotes network connectivity in silicate glasses, NBOs are eliminated and deformation mechanism is shifted to densification for AS glasses which prevents the formation of subsurface cracks and thus reduces the crack formation probability.

Examination of the representative images of indentations given as inset in Figure 4.48 reveal that despite an increase in the cracking resistance, a tendency to formation of chippings on the indentation edges is observed as the Al_2O_3 content of the glass composition increases. It is reported that cracking system shifts from median cracks to lateral cracks in the case of presence of compressive stress on the glass surface [118]. It is also known that intersection of lateral cracks with surface results chipping. For chemically strengthened glasses, the compressive stress generated on glass surface exerts a force against the volume of displaced material causing a mass repulsion towards the surface, consequently higher compressive stress values mean higher repulsive force. Therefore, it is noted that probability of chipping formation after cracking is higher for chemically strengthened H-SLS glasses than chemically strengthened L-SLS glasses. Chemically strengthened AS glasses exhibit great amount of compressive stress (>900 MPa) which results in material loss as edge chipping at the surface level of the indentation where the compressive stress reaches its maximum value.

4.3 General Results and Future Outlook

In this dissertation study, three different silica-based thin flat glasses with chemical compositions differing in Al_2O_3 content are processed with chemical strengthening and exposed to weathering. Subsequently, surface analytical techniques and mechanical testings are applied to the obtained samples for investigating the weathering behavior of chemically strengthened glasses with respect to glass composition and processing sequence of chemical strengthening and weathering.

1. Glass samples are chemically strengthened in KNO_3 salt bath at 425°C for 4 hours.
    - After chemical strengthening, the generated compressive stress values on the surface are measured as 600 MPa for L-SLS glasses, 680 MPa for H-SLS glasses and 900 MPa for AS glasses.
    - Depth of generated compression layer measured as 6.7 μm for L-SLS glasses, 9.5 μm for H-SLS glasses and 40 μm for AS glasses. It is observed that higher Al_2O_3 content in the composition has a positive influence on the efficiency of chemical strengthening process by increasing mobility of alkali ions.
2. Chemical strengthening process increases the modulus of rupture values from 452 MPa to 1315 MPa for L-SLS glasses, from 495 MPa to 1327 MPa for H-SLS glasses and from 619 MPa to 1735 MPa for AS glasses. Since the main mechanism which increases the modulus of rupture is magnitude of generated compressive stress, higher compressive stress ultimately results higher strength increase.
3. Surface hardness values increase from 490±7 HV to 561±20 HV for L-SLS glasses, from 507±12V to 571±13 HV for H-SLS glasses and from 522±13 HV to 621±14 HV for AS glasses after chemical strengthening process.
4. Decrease in subsurface crack formation under sharp contact indentation is observed as the Al_2O_3 content increases, since deformation mechanism is shifted from shear flow to densification accordingly.
5. Weathering process is applied to glasses before and/or after chemical strengthening process and its effect on surface properties are evaluated.

6. In the macro scale, weathering causes an iridescence appearance for soda-lime silicate glasses when it is applied after chemical strengthening. However, such an effect is not observed when weathering is applied before chemical strengthening.
7. Topographical investigations reveal that iridescence pattern is caused by formation of alteration layers which is accompanied by significant increase in surface roughness by means of weathering induced corrosion reactions.
8. Depth profiling results show that altered layers are depleted in alkali and alkali earth ions.
9. Infrared spectroscopy analysis proves that for chemically strengthened soda-lime silicate glasses, leaching and dissolution mechanisms occur anomalously faster and more intense compared to pristine state of the glass. Breakage of network forming Si–O–Si bonds are detected in the spectra of these conditions. This is due to the domination of glass surface by larger K^+ ions following the chemical strengthening process which facilitates the water diffusion and corrosion reactions.
10. Mechanical properties of chemically strengthened soda-lime silicate glasses are selectively affected from weathering with respect to processing sequence.
    - In case of prior exposure to weathering before chemical strengthening, strength increase is suppressed by the already grown and propagated surface flaws as well as hardness increase suppressed due to confined stress generation as a consequence of water entry into network structure.
    - On the other hand, exposure to weathering after chemical strengthening process has lesser impact on strength values because introduced compressive stress prevents the growth and propagation of flaws by dissolution reactions. However, hardness and cracking resistance of glasses decrease since the alteration layer's structure is different than that of glass surface.
11. Experimental results revealed that soda-lime silicate glasses are more prone to corrosion than aluminosilicate glasses, especially when weathering takes place

after chemical strengthening due to formation of alteration layers. On the other hand, for aluminosilicate glasses, no meaningful change in topographical, optical, structural and mechanical features are detected since these glasses are chemically more stable and does not undergo leaching and dissolution reactions.

12. Higher Al_2O_3 content in the glass composition is beneficial for both for process efficiency of chemical strengthening and increasing the chemical and mechanical durability of the strengthened glass against weathering conditions.
13. Considering the experimental findings, in order to prevent deterioration and minimize the risk of formation of alteration layers for maintaining the quality of a glass product, storage and usage conditions should be well adjusted. Exposure to high temperatures and humidity should be avoided to suppress leaching and dissolution reactions.

5
REFERENCES

[1] S. S. Kistler, "Stresses in Glass Produced by Nonuniform Exchange of Monovalent Ions," *J. Am. Ceram. Soc.*, vol. 45, no. 2, pp. 59–68, 1962.

[2] K. Cummings, W. A. Lanford, and M. Feldmann, "Weathering of glass in moist and polluted air," *Nucl. Instruments Methods Phys. Res. B*, vol. 136–138, pp. 858–862, 1998.

[3] S. Djanarthany and P. Trocellier, "IBA and SIMS coupling to study glass alteration mechanisms," *J. Non. Cryst. Solids*, vol. 353, pp. 4830–4838, 2007.

[4] M. Collin, S. Gin, P. Jollivet, L. Dupuy, V. Dauvois, and L. Duffours, "ToF-SIMS depth profiling of altered glass," *npj Mater. Degrad.*, vol. 3, no. 14, pp. 1–10, 2019.

[5] M. De Bardi, H. Hutter, M. Schreiner, and R. Bertoncello, "Potash-lime-silica glass: Protection from weathering," *Herit. Sci.*, vol. 3, no. 22, pp. 1–9, 2015.

[6] K. Bange, O. Anderson, and F. Rauch, "Multi-method characterization of soda-lime glass corrosion Part 2. Corrosion in humidity," *Glas. Sci. Technol.*, vol. 75, no. 1, pp. 20–33, 2002.

[7] M. De Bardi, H. Hutter, and M. Schreiner, "ToF-SIMS analysis for leaching studies of potash – lime – silica glass," *Appl. Surf. Sci.*, vol. 282, pp. 195–201, 2013.

[8] T. Lombardo, A. Chabas, and R. Lefèvre, "Weathering of float glass exposed outdoors in an urban area," *Glas. Technol.*, vol. 46, no. 3, pp. 271–276, 2005.

[9] M. E. Lynch, D. C. Folz, and D. E. Clark, "Use of FTIR reflectance spectroscopy to monitor corrosion mechanisms on glass surfaces," *J. Non. Cryst. Solids*, vol. 353, no. 27, pp. 2667–2674, 2007.

[10] S. M. Wiederhorn, "Influence of Water Vapor on Crack Propagation in Soda-Lime Glass," *J. Am. Ceram. Soc.*, vol. 50, no. 8, 1967.

[11] S. M. Wiederhorn, T. Fett, G. Rizzi, M. J. Hoffmann, and J. Guin, "Water Penetration—Its Effect on the Strength and Toughness of Silica Glass," *Metall. Mater. Trans. A*, vol. 44, no. 3, pp. 1164–1174, Mar. 2013.

[12] W. Vogel, *Glass Chemistry*, 2nd ed. Springer-Verlag, 1994.

[13] W. Vogel, *Structure and Crystallization of Glasses*. Pergamon Press, 1971.

[14] A. K. Varshneya, *Fundamentals of Inorganic Glasses*. 1993.

[15] E. D. Zanotto and J. C. Mauro, "The glassy state of matter: Its definition and ultimate fate," *J. Non. Cryst. Solids*, vol. 471, no. April, pp. 490–495, 2017.

[16] V. M. Sglavo, Ed., *Advances in Glass Science and Technology*. InTech, 2018.

[17] S. Napolitano, E. Glynos, and N. B. Tito, “Glass transition of polymers in bulk, confined geometries, and near interfaces,” *Reports Prog. Phys.*, vol. 80, no. 3, 2017.

[18] C. Barry Carter and M. Grant Norton, *Ceramic materials: Science and engineering*. 2007.

[19] E. Donth, *The Glass Transition - Relaxation Dynamics in Liquids and Disordered Materials*. Springer, 2001.

[20] J. W. P. Schmelzer and I. S. Gutzow, *Glasses and the Glass Transition*. Wiley-Vch, 2011.

[21] O. Laurent, B. Mantisi, and M. Micoulaut, “Structure and Topology of Soda-Lime Silicate Glasses : Implications for Window Glass,” *J. Phys. Chem.*, vol. 118, no. 44, pp. 12750–12762, 2014.

[22] B. Mysen and P. Richet, *Silicate Glasses and Melts, Volume 10*. Elsevier, 2005.

[23] J. E. Shelby, *Introduction to Glass Science and Technology*, 2nd ed. Cambridge: Royal Society of Chemistry, 2005.

[24] Mattias Edén, “27Al NMR Studies of Aluminosilicate Glasses,” *Annu. Reports NMR Spectrosc.*, vol. 86, pp. 237–331, 2015.

[25] H. Scholze, *Glass - Nature, Structure, and Properties*, 1st ed. Springer-Verlag New York, 1991.

[26] G. Macrelli, “Chemical Strengthening of Glass by Ion-Exchange,” *Work. 2017 ICG Annu. Meet.*

[27] H. G. Pfaender, *Schott Guide to Glass*. 1996.

[28] A. Macfarlane and G. Martin, *Glass a World History*. .

[29] “A Guide to Historical Glass,” *Roger Mayers Architects*, 2020. [Online]. Available: http://www.rmears.co.uk/our-publications/glass-and-glazing/. [Accessed: 05-May-2020].

[30] L. C. Glass, “History of Window Glass Manufacture,” 2020. [Online]. Available: http://www.londoncrownglass.f9.co.uk/History.html.

[31] Martin Rehor, “Diffuse interface models in theory of interacting continua,” Charles University Czech Republic, 2018.

[32] “How Glass Is Made,” 2020. [Online]. Available: https://www.guardianglass.com/mx/en/tools-and-resources/resources/glass-basics. [Accessed: 05-Mar-2020].

[33] G. R. Trott and A. Shorey, “Fusion Draw Process,” *Corning, New York*. [Online]. Available: https://www.corning.com/media/worldwide/global/documents/semi Glass_Wafer_Mechanical_Properties_A_Comparison_to_Silicon.pdf. [Accessed: 05-Apr-2020].

[34] H.-J. Lin and W.-K. Chang, “Design of a sheet forming apparatus for overflow fusion process by numerical simulation,” *J. Non. Cryst. Solids*, vol. 353, pp.

2817–2825, 2007.

[35] J. D. Musgraves, J. Hu, and L. Calvez, *Springer Handbook of Glass*. 2019.

[36] D. C. Allan, Bradley F. Bowden, X. Guo, J. C. Mauro, and M. Potuzak, "Method for fusion drawing ion-exchangeable glass," US 2013 0255314A1, 2013.

[37] P. Shou, R. Hongcan, C. Xin, and Y. Yong, "Continuous forming of ultrathin glass by float process," *Int. J. Appl. Glas. Sci.*, vol. 10, no. January, pp. 275–286, 2019.

[38] M. H. Krohn, J. R. Hellmann, D. L. Shelleman, C. G. Pantano, and G. E. Sakoske, "Biaxial Flexure Strength and Dynamic Fatigue of Soda-Lime-Silica Float Glass," *J. Am. Ceram. Soc.*, vol. 85, no. 7, pp. 1777–1782, 2004.

[39] T. A. Michalske, "A Molecular Mechanism for Stress Corrosion in Vitreous Silica," *J. Am. Ceram. Soc.*, vol. 66, pp. 284–288, 1983.

[40] J. R. Varner and H. J. Oel, "Surface Defects: Their Origin, Characterization and Effects on Strength," *J. Non. Cryst. Solids*, vol. 19, pp. 321–333, 1975.

[41] H. K. Pulker, *Coatings on Glass*, 2nd ed. Elsevier, 1999.

[42] S. Robert, H. Building, and M. Street, "Stress intensity factors for surface flaws in toughened glasses," no. July 1999, pp. 73–80, 2000.

[43] J. H. Nielsen, J. F. Olesen, P. N. Poulsen, and H. Stang, "Finite element implementation of a glass tempering model in three dimensions," *Comput. Struct.*, vol. 88, no. 17–18, pp. 963–972, 2010.

[44] H. D. Weymann, "A Thermoviscoelastic Description of the Tempering of Glass," *J. Am. Ceram. Soc.*, vol. 45, no. 11, pp. 517–522, 1962.

[45] A. K. Varshneya, "The physics of chemical strengthening of glass : Room for a new view," *J. Non. Cryst. Solids*, vol. 356, no. 44–49, pp. 2289–2294, 2010.

[46] A. K. Varshneya, "Chemical Strengthening of Glass : Lessons Learned and Yet To Be Learned," *Appl. Glas. Sci.*, vol. 142, pp. 131–142, 2010.

[47] S. Karlsson and B. Jonson, "The Technology of Chemical Glass Strengthening – A Review," no. March, 2010.

[48] R. Gy, "Ion exchange for glass strengthening," *Mater. Sci. Eng. B*, vol. 149, pp. 159–165, 2008.

[49] A. Tandia, K. D. Vargheese, J. C. Mauro, and A. K. Varshneya, "Atomistic understanding of the network dilation anomaly in ion-exchanged glass," *J. Non. Cryst. Solids*, vol. 358, no. 2, pp. 316–320, 2012.

[50] K. D. Vargheese, A. Tandia, and J. C. Mauro, "Molecular dynamics simulations of ion-exchanged glass," *J. Non. Cryst. Solids*, vol. 403, pp. 107–112, 2014.

[51] C. Ragoen, S. Sen, T. Lambricht, and S. Godet, "Effect of Al2O3 content on the mechanical and interdiffusional properties of ion-exchanged Na-aluminosilicate glasses," *J. Non. Cryst. Solids*, vol. 458, pp. 129–136, 2017.

[52] C. W. Sinton, W. C. Lacourse, and M. J. O. Connell, "Variations in K-Na Ion Exchange Depth in Commercial and Experimental Float Glass Compositions," *Mater. Res. Bull.*, vol. 34, pp. 2351–2359, 1999.

[53] H. Morozumi, S. Yoshida, and J. Matsuoka, “Composition dependence of crack formation probability in aluminoborosilicate glass,” *J. Non. Cryst. Solids*, vol. 444, pp. 31–37, 2016.

[54] V. M. Sglavo, “Chemical Strengthening of Soda Lime Silicate Float Glass : Effect of Small Differences in the KNO3 Bath,” *Int. J. Appl. Glas. Sci.*, vol. 6, no. 1, pp. 72–82, 2015.

[55] H. Hassani and V. M. Sglavo, “Effect of Na contamination on the chemical strengthening of soda-lime silicate float glass by ion-exchange in molten potassium nitrate,” *J. Non. Cryst. Solids*, vol. 515, pp. 143–148, 2019.

[56] A. Talimian and V. M. Sglavo, “Ion-exchange strengthening of borosilicate glass : Influence of salt impurities and treatment temperature,” *J. Non. Cryst. Solids*, vol. 456, pp. 12–21, 2017.

[57] L. Jiang, X. Guo, X. Li, L. Li, G. Zhang, and Y. Yan, “Different K – Na inter-diffusion kinetics between the air side and tin side of an ion-exchanged float aluminosilicate glass,” *Appl. Surf. Sci.*, vol. 265, pp. 889–894, 2013.

[58] X. Li, L. Jiang, X. Zhang, and Y. Yan, “Influence of residual compressive stress on nanoindentation response of ion-exchanged aluminosilicate float glass on air and tin sides,” *J. Non. Cryst. Solids*, vol. 385, pp. 1–8, 2014.

[59] V. Tyagi and A. K. Varshneya, “Measurement of progressive stress buildup during ion exchange in alkali aluminosilicate glass,” vol. 238, pp. 186–192, 1998.

[60] J. Isard and A. R. Patel, “A comparison between weathering and water leaching tests on glasses of simple composition,” *Glas. Technol.*, vol. 22, no. 6, pp. 247–250, 1981.

[61] H. V. Walters and P. B. Adams, “Effects of Humidity on the Weathering of Glass,” *J. Non. Cryst. Solids*, vol. 19, pp. 183–199, 1975.

[62] N. Papadopoulos and C. A. Drosou, “Influence of Weather Conditions on Glass Properties,” *J. Univ. Chem. Technol. Metall.*, vol. 47, no. 4, pp. 429–438, 2012.

[63] C. G. Pantano, “Effects of glass structure on the corrosion behavior of sodium-aluminosilicate glasses,” *J. Non. Cryst. Solids*, vol. 222, pp. 167–174, 1997.

[64] B. C. Bunker, “Molecular mechanisms for corrosion of silica and silicate glasses,” vol. 179, no. 1, pp. 300–308, 1994.

[65] F. Alloteau *et al.*, “New insight into atmospheric alteration of alkali-lime silicate glasses,” *Corros. Sci.*, vol. 122, pp. 12–25, 2017.

[66] J. Du and J. M. Rimsza, “Atomistic computer simulations of water interactions and dissolution of inorganic glasses,” *npj Mater. Degrad.*, vol. 1, pp. 1–16, 2017.

[67] S. M. Wiederhorn and L. H. Bolz, “Stress Corrosion and Static Fatigue of Glass,” *J. Am. Ceram. Soc.*, vol. 53, no. 10, pp. 543–548, 1970.

[68] R. Gy, “Stress corrosion of silicate glass : a review,” *J. Non. Cryst. Solids*, vol. 316, pp. 1–11, 2003.

[69] M. Ciccotti and L. Collo, “Stress-corrosion mechanisms in silicate glasses,” *J.*

Phys. D Appl. Phys., vol. 42, 2009.

[70] M. Tomozawa and W.-T. Han, "Water Entry into Silica Glass During Slow Crack Growth," *J. Am. Ceram. Soc.*, vol. 74, no. 10, pp. 2573–76, 1991.

[71] T. I. Suratwala and R. A. Steele, "Anomalous temperature dependence of sub-critical crack growth in silica glass," *J. Non. Cryst. Solids*, vol. 316, no. 1, pp. 174–182, 2003.

[72] "Economic Commission for Europe of the United Nations, Uniform provisions concerning the approval of safety glazing materials and their installation on vehicles," *Regulation*, no. 43 Rev 4, 2017.

[73] T. Kishii, "Surface Stress Meters Utilising the Optical Waveguide Effect of Chemically Tempered Glasses," *Opt. Lasers Eng.*, vol. 4, pp. 25–38, 1983.

[74] S. G. Reid, "Effects of spatial variability of glass strength in ring-on-ring tests," *Civ. Eng. Environ. Syst.*, vol. 24, no. 2, pp. 139–148, Jun. 2007.

[75] "Glass in building- Determination of the bending strength of glass - Part 5: Coaxial double ring test on flat specimens with small test surface areas, Turkish Standards Institution, TS EN 1288-5, 2003, Ankara, Turkey."

[76] W. Weibull, "A Statistical Distribution Function of Wide Applicability," *J. Appl. Mech.*, vol. 18, pp. 293–305, 1951.

[77] C. A. Klein, "Characteristic strength, Weibull modulus, and failure probability of fused silica glass Claude," *Opt. Eng.*, vol. 48, no. 11, pp. 1–10, 2009.

[78] S. Kirtay and D. Dispinar, "Effect of Ranking Selection on the Weibull Modulus Estimation," *Gazi Univ. J. Sci.*, vol. 25, no. 1, pp. 175–187, 2012.

[79] J. B. Quinn and G. D. Quinn, "A practical and systematic review of Weibull statistics for reporting strength of dental materials A practical and systematic review of Weibull statistics for reporting strengths of dental materials," *Dent. Mater.*, vol. 26, no. 2, pp. 135–147, 2010.

[80] A. Mohajerani and J. W. Zwanziger, "Mixed alkali effect on Vickers hardness and cracking," *J. Non. Cryst. Solids*, vol. 358, no. 12–13, pp. 1474–1479, 2012.

[81] T. Rouxel, U. D. R. I, and D. Beaulieu, "Driving force for indentation cracking in glass: composition, pressure and temperature dependence," *Philos. Trans. A*, vol. 373, no. 2038, pp. 1–26, 2015.

[82] T. K. Bechgaard, J. C. Mauro, and M. M. Smedskjaer, "Time and humidity dependence of indentation cracking in aluminosilicate glasses," *J. Non. Cryst. Solids*, vol. 491, no. February, pp. 64–70, 2018.

[83] A. Koike, S. Akiba, T. Sakagami, K. Hayashi, and S. Ito, "Difference of cracking behavior due to Vickers indentation between physically and chemically tempered glasses," *J. Non. Cryst. Solids*, vol. 358, pp. 3438–3444, 2012.

[84] I. Papucova, A. Plsko, and J. Pagacova, "Corrosion layers on the glass surface," *Procedia Eng.*, vol. 136, pp. 287–293, 2016.

[85] L. Dohmen *et al.*, "Pattern Formation in Silicate Glass Corrosion Zones," *Int. J. Appl. Glas. Sci.*, vol. 4, no. 4, pp. 357–370, 2013.

[86] D. De Fuente, M. Morcillo, M. A. De Buergo, and M. Vilarigues, “Early stages of glass alteration in the coastal atmosphere Teresa Palomar,” *Build. Environ.*, vol. 147, pp. 305–313, 2019.

[87] M. Emami, S. Nekouei, H. Ahmadi, Department, C. Pritzel, and R. Trettin, “Iridescence in Ancient Glass : A Morphological and Chemical Investigation,” *Int. J. Appl. Glas. Sci.*, vol. 7, no. 1, pp. 59–68, 2016.

[88] A. W. Laubengayer, “The Weathering and Iridescence of Some Ancient Roman Glass Found in Cyprus,” *J. Am. Ceram. Soc.*, vol. 14, no. 11, pp. 833–836, 1931.

[89] N. P. Mellott and C. G. Pantano, “A Mechanism of Corrosion-Induced Roughening of Glass Surfaces,” *Int. J. Appl. Glas. Sci.*, vol. 4, no. 3, pp. 274–279, 2013.

[90] S. Reiß, S. Krischok, and E. Rädlein, “Comparative study of weather induced corrosion mechanisms of toughened and normal float glasses,” *Glas. Technol. Eur. J. Glas. Sci. Technol. A*, vol. 60, no. 2, pp. 33–44, 2019.

[91] M. Feldmann, “Initial stages of float glass corrosion,” *J. Non. Cryst. Solids*, vol. 218, pp. 205–209, 1997.

[92] D. Ngo *et al.*, “Spectroscopic ellipsometry study of thickness and porosity of the alteration layer formed on international simple glass surface in aqueous corrosion conditions,” *npj Mater. Degrad.*, no. February, pp. 1–9, 2018.

[93] C. Kaspar, J. T. Reiser, J. V Ryan, and N. A. Wall, “Non-destructive characterization of corroded glass surfaces by spectroscopic ellipsometry,” *J. Non. Cryst. Solids*, vol. 481, pp. 260–266, 2018.

[94] B. C. Bunker, “Molecular mechanisms for corrosion of silica and silicate glasses,” *J. Non. Cryst. Solids*, vol. 179, no. 1, pp. 300–308, 1994.

[95] L. L. Hench, “Characterization of Glass Corrosion and Durability,” *J. Non. Cryst. Solids*, vol. 19, pp. 27–39, 1975.

[96] C. I. Merzbacher and W. B. White, “The structure of alkaline earth aluminosilicate glasses as determined by vibrational spectroscopy,” *J. Non. Cryst. Solids*, vol. 130, pp. 18–34, 1991.

[97] G. Spiekermann, M. Steele-macinnis, C. Schmidt, and S. Jahn, “Vibrational mode frequencies of silica species in SiO2 -H2O liquids and glasses from ab initio molecular dynamics,” *J. Chem. Phsics*, vol. 136, 2012.

[98] S. Amma, J. Luo, S. H. Kim, and C. G. Pantano, “Effects of fictive temperature on the leaching of soda lime silica glass surfaces,” *J. Am. Ceram. Soc.*, vol. 100, no. 4, pp. 1424–1431, 2017.

[99] N. Sheth, J. Luo, J. Banerjee, C. G. Pantano, and S. H. Kim, “Characterization of surface structures of dealkalized soda lime silica glass using X-ray photoelectron , specular reflection infrared , attenuated total reflection infrared and sum frequency generation spectroscopies,” *J. Non. Cryst. Solids*, vol. 474, pp. 24–31, 2017.

[100] A. M. Efimov and V. G. Pogareva, “IR absorption spectra of vitreous silica and silicate glasses : The nature of bands in the 1300 to 5000 cm − 1 region,” vol.

229, pp. 198–217, 2006.

[101] Y. L. P. Yong-Keun Lee and M. Tomozawa, “IR reflection spectroscopy of a soda-lime glass surface during ion-exchange,” *J. Non. Cryst. Solids*, vol. 222, pp. 125–130, 1997.

[102] J. Luo, Y. Zhou, S. T. Milner, C. G. Pantano, and S. H. Kim, “Molecular dynamics study of correlations between IR peak position and bond parameters of silica and silicate glasses : Effects of temperature and stress,” *J. Am. Ceram. Soc.*, vol. 101, no. 1, pp. 178–188, 2018.

[103] M. Tomozawa, “Stress corrosion reaction of silica glass and water,” *Phys. Chem. Glas.*, vol. 39, no. 2, pp. 65–69, 1998.

[104] D. E. Clark, M. F. Dilmore, E. C. Ethridget, and L. L. Hench, “Aqueous Corrosion of Soda-Silica and Soda-Lime-Silica Glass,” *J. Am. Ceram. Soc.*, vol. 59, no. 1–2, pp. 62–65, 1976.

[105] C. J. Simmons and S. W. Freiman, “Effect of Corrosion Processes on Subcritical Crack Growth in Glass,” Washington, D.C., 1981.

[106] S. Fearn, D. S. Mcphail, R. J. H. Morris, and M. G. Dowsett, “Sodium and hydrogen analysis of room temperature glass corrosion using low energy Cs SIMS,” *Appl. Surf. Sci.*, vol. 252, pp. 7070–7073, 2006.

[107] B. C. Bunker, G. W. Arnold, and E. K. Beauchamp, “Mechanisms for alkali leaching in mixed-Na-K silicate glasses,” *J. Non. Cryst. Solids*, vol. 58, pp. 295–322, 1983.

[108] A. Agarwal and M. Tomozawa, “Correlation of silica glass properties with the infrared spectra,” *J. Non. Cryst. Solids*, vol. 209, no. 1–2, pp. 166–174, 1997.

[109] L. L. Hench and D. E. Clark, “Physical Chemistry of Glass Surfaces,” *J. Non. Cryst. Solids*, vol. 28, pp. 83–105, 1978.

[110] T. Palomar, P. Redol, I. Cruz Almeida, E. Pereira da Silva, and M. Vilarigues, “The Influence of Environment in the Alteration of the Stained-Glass Windows in Portuguese Monuments,” *Heritage*, vol. 1. pp. 365–376, 2018.

[111] B. M. J. Smets and T. P. A. Lommen, “The leaching of sodium containing glasses: Ion exchange or diffusion of molecular water?,” *Le J. Phys. Colloq.*, vol. 43, no. C9, pp. 649–652, Dec. 1982.

[112] C. W. Sinton and W. C. LaCourse, “Experimental survey of the chemical durability of commercial soda-lime-silicate glasses,” *Mater. Res. Bull.*, vol. 36, pp. 2471–2479, 2001.

[113] M. Wang *et al.*, “Ion exchange strengthening and thermal expansion of glasses : Common origin and critical role of network connectivity,” *J. Non. Cryst. Solids*, vol. 455, pp. 70–74, 2017.

[114] A. I. Fu and J. C. Mauro, “Mutual diffusivity, network dilation, and salt bath poisoning effects in ion-exchanged glass,” *J. Non. Cryst. Solids*, vol. 363, pp. 199–204, 2013.

[115] S. Amma, S. H. Kim, and C. G. Pantano, “Analysis of Water and Hydroxyl Species

in Soda Lime Glass Surfaces Using Attenuated Total Reflection (ATR)-IR Spectroscopy," *J. Am. Ceram. Soc.*, vol. 99, no. 1, pp. 128–134, 2016.

[116] T. M. Gross and M. Tomozawa, "Crack-free high load Vickers indentation of silica glass," *J. Non. Cryst. Solids*, vol. 354, pp. 5567–5569, 2008.

[117] T. M. Gross and J. J. Price, "Vickers Indentation Cracking of Ion-Exchanged Glasses: Quasi-Static vs. Dynamic Contact," *Front. Mater.*, vol. 4, no. 2017, pp. 1–14, 2017.

[118] T. M. Gross, "Scratch Damage in Ion-Exchanged Alkali Aluminosilicate Glass: Crack Evolution and the Dependence of Lateral Cracking Threshold on Contact Geometry," in *Fractography of Glasses and Ceramics VI: Ceramic Transactions, Volume 230*, 2012, pp. 113–122.

6
PUBLICATIONS FROM THE THESIS

Contact information: atesgosterislioglu@gmail.com

Papers:

1. Y. A. Gosterislioglu, A. E. Ersundu, M. Celikbilek Ersundu, I. Sokmen, Investigation the Effect of Weathering on Chemically Strengthened Flat Glasses, Journal of Non-Crystalline Solids, 544, 15 September 2020, 120192

Conference Papers:

1. Gosterislioglu Y.A., Guldali, B., Terzi, G., Kacar, E., Simurka, L., Ersundu, M. C., Ersundu, A. E., Sokmen. I, "The Effect of Weathering on Chemical Strengthened Thin Glasses", 25th Internation Congres on Glass (ICG 2019), 9-14 June, Boston, Massachusettes

Projects:

1. YTU Scientific ResearchProject (BAP) No: FYL-2019-3577 "Investigation the Effect of Weathering on Chemically Strengthened Thin Flat Glasses", Researcher, (2019-2020).